PALACKÝ UNIVERSITY IN OLOMOUC

Faculty of Science

Department of Biophysics

Polarization of monocyte to macrophages: NADPH expression and protein modification

DOCTORAL THESIS

Author: **M.Sc. Deepak RATHI**

Study programme: P0533D11000

Branch of study: Biophysics

Form: Full-time

Supervisor: **doc. M.Sc. Ankush Prasad, Ph.D.**

Year: 2024

Bibliographical identification

Name of the author: Deepak Rathi

Title of thesis: Polarization of monocyte to macrophages: NADPH expression and protein modification

Type of thesis: Ph.D. thesis

Department: Department of Biophysics

Duration of doctoral study: 2020-2024

Supervisor: doc. M.Sc. Ankush Prasad, Ph.D.

Year of defense: 2024

Abstract:

Monocytes are the essential component of the immune system, which polarizes to macrophages-a pivotal facet of immune modulation characterized by discrete functional phenotypes, including the pro-inflammatory M1 and anti-inflammatory M2 macrophages. This process depends on multifaceted molecular mechanisms, prominently with the expression of Nicotinamide Adenine Dinucleotide Phosphate (NADPH) oxidases, post-translational protein modifications, and the regulatory influence of extracellular vesicles (EVs). NADPH oxidases, also called NOX, are a diverse enzyme family with seven (7) isoforms, playing a central role in intracellular reactive oxygen species (ROS) production from molecular oxygen (O_2). The molecular mechanisms of activation and assembly of NADPH oxidase underlying the assembly of the NADPH oxidase complex consist of multiple subunits including gp91phox, p22phox, p47phox, p67phox, and Rac. NADPH oxidase assembly includes phosphorylation events, protein-protein interactions, and the role of small GTPases such as Rac. Activation of NOX enzymes is associated with ROS release, thereby modulating intricate signaling cascades crucial in macrophage polarization. The production of ROS predominantly superoxide anion radical ($O_2^{\bullet-}$), and subsequently hydroxyl radical ($HO^{\bullet}$), hydrogen peroxide (H_2O_2), and singlet oxygen ($^1O_2$)] is necessary for our body, but if produced in higher amounts, they can cause the oxidation of biomolecules within the cell.

In the present study, we investigated the polarization of monocytes to macrophages, ROS generation during the transition, and mediated protein modifications under the influence of different differentiation inducers. Morphological changes in monocytes in the presence of a differentiation inducer were studied using Confocal Laser Scanning Microscopy (CLSM), and NADPH oxidase expression was studied using Immunoblotting. The regulation of the enzyme complex was studied in both monocytes and macrophages, and the role of EVs secreted from monocytes and their effect on differentiating monocytes as messengers or antioxidant cargo was also studied. Our results showed that monocytes turn into macrophages when they encounter inflammation or differentiation and produce ROS. Polyunsaturated fatty acids (PUFA) are easily damaged by these reactive molecules and can lead to reactive intermediates

or products such as aldehydes. Malondialdehyde (MDA), which is one of the final products of polyunsaturated fatty acids peroxidation led to protein modification.

Furthermore, the involvement of EVs derived from monocytes and their co-culture with non-differentiating/differentiating cells showed that EVs through their cargo of regulatory molecules, potentially NOX isotypes contributed to the modulation of polarization of monocytes to distinct macrophage phenotypes. We studied the effect of selected exogenous antioxidant/bioactive compounds isolated from industrial waste to understand their efficacy in protecting the cells against oxidative damage. The intricate equilibrium and transition between the pro-oxidant and antioxidant effects of antioxidants were also investigated.

Number of pages including references: 41

Number of appendices: 2

Language: English

Declaration

I hereby declare that I wrote this Doctoral thesis separately showing all the sources and authorship. I agree with the publication of the thesis by Act no. 111/1998 Coll., about universities, as amended. I was fully aware of the rights and obligations arising from Act no. 121/2000 Coll., the Copyright Act, as amended, is applied to my work.

In Olomouc, 29.04.2024   Signature

TABLE OF CONTENTS

List of Publications

This thesis is based on the following four research papers. These research papers are referred to in the text in **bold** and blue letters and are enclosed at the end of the thesis.

1. **Deepak Rathi**, Claudio Rossi, Pavel Pospíšil, Renuka Ramalingam Manoharan, Luigi Talarico, Agnese Magnani, Ankush Prasad. NOX2 and NOX4 expression in monocytes and macrophages extracellular vesicles in signaling and therapeutics. Frontiers in Cell and Developmental Biology 2024, 12: 1342227.

2. Ankush Prasad, **Deepak Rathi**, Michaela Sedlářová, Renuka Ramalingam Manoharan, Eliška Průdková, Pavel Pospíšil. Differential effects of ascorbic acid on monocytic cell morphology and protein modification: Shifting from pro-oxidative to antioxidant properties. Biochemistry and Biophysics Reports 2024, 37: 101622.

3. Ankush Prasad, Claudio Rossi, Renuka Ramalingam Manoharan, Michaela Sedlářová, Lorenzo Cangeloni, **Deepak Rathi**, Gabriella Tamasi, Pavel Pospíšil, Marco Consumi. Bioactive compounds: its characterization and impact on protein modification in differentiating human cells. International Journal of Molecular Sciences 2022, 23 (13): 7424.

4. Ankush Prasad, Hana Duchová, Renuka Ramalingam Manoharan, **Deepak Rathi**, Pavel Pospíšil. Imaging and Characterization of Oxidative Protein Modifications in Skin. International Journal of Molecular Sciences 2023, 24(4): 3981.

Abbreviations

AA	- ascorbic acid
AMP	- adenosine monophosphate
BCA	- bicinchoninic acid
CGD	- chronic granulomatous diseases
DHA	- dehydroascorbic acid
DHR	- dehydrogenase region
DLS	- dynamic light scattering
DMPO	- 5,5-dimethyl-1-pyrroline N-oxide
DNPH	- 2,4 Dinitrophenylhydrazine
DTT	- dithiothreitol
Duox	- dual oxidase
EB	- extracellular buffer
EVs	- extracellular vesicles
FAD	- flavin adenine dinucleotide
FBS	- fetal bovine serum
H_2O_2	- hydrogen peroxide
$HO^{\bullet}$	- hydroxyl radical
ILVs	- intraluminal vesicles
MVBs	- multi-vesicular bodies
MVs	- microvesicles
NADPH oxidase	- Nicotinamide adenine dinucleotide phosphate oxidase
O_2	- molecular oxygen
$O_2^{\bullet-}$	- superoxide anion radical
PEG	- polyethylene Glycol
PI_3P	- phosphatidylinositol 3-phosphate
PKC	- protein kinase C
PMA	- phorbol-12-Myristate-13-Acetate
ROS	- reactive oxygen species
SLE	- systemic lupus erythematosus
SNPs	- specific genetic variations
TBS	- tris-buffered saline

Curriculum Vitae

<u>M.Sc. Deepak Rathi</u>

Personal information

Date and place of birth: May 11, 1990 in Uttar Pradesh, India

Country of current residence: Czech Republic

Contact: +420-720611977 (M), +420 585 634 844 (O)

Email: deepak.rathi01@upol.cz

Affiliation: Department of Biophysics, Faculty of Sciences, Palacký University Šlechtitelů 27, 783 71 Olomouc, Czech Republic

Professional/work experience

- 2019-2020: Senior Research Fellow, Department of Gastroenterology, All India Institute of Medical Sciences, New Delhi, India.
- 2018-2019: Senior Research Fellow, Department of Medical Genetics, Sanjay Gandhi Post Graduate Institute of Medical Sciences, Lucknow, India.
- 2012-2016: Junior Research Fellow, Department of Pediatric Oncology, All India Institute of Medical Sciences, New Delhi, India.

Education

- 2020-current: PhD, Department of Biophysics, Faculty of Science, Palacký University, Olomouc, Czech Republic.
- 2010-2012: Master of Science (specialization: Biotechnology), Chaudhary Charan Singh University, Meerut, India.
- 2007-2010: Bachelor of Science (specialization: Biotechnology), Chaudhary Charan Singh University, Meerut, India.

Research interests: biochemistry, oxidative processes, oncology, animal physiology, extracellular vesicle, antioxidants.

Conference and seminar presentations

- IHC & IF Workshop by Proteintech (Online Mode), October 2023
- 12th International Human Peroxidase Meeting held on August 30 - September 2, 2023, in Budapest, Hungary (Seminar Presentation)
- SYSCON 2016, All India Institute of Medical Sciences, New Delhi, India
- "7th Annual the Cytometry Society Meeting & 15th Indo-US Clinical Cytometry Workshop 2014"
- National Symposium on Modern Approaches and Innovations in the College of Applied Education and Health Sciences of Biotechnology, Meerut, India
- Bio innovation in Disease Diagnosis at Auro-probe Laboratories, Modinagar, India

Awards and Recognitions

- Qualified National Eligibility Test (NET) conducted by Council of Scientific and Industrial Research - University Grant Commission (CSIR-UGC), All India Rank-42
- Qualified combined eligibility test (CET) for Ph.D. conducted by Dr. RML Awadh University, India

- Topper of the class of master's course (M.Sc. Biotechnology), College of Applied Education and Health Sciences, Chaudhary Charan Singh University, Meerut India
- First prize in a quiz competition on Recent Trends in Bioscience during B.Sc conducted by College of Applied Education and Health Sciences, Chaudhary Charan Singh University, Meerut, India

Acknowledgments

1. INTRODUCTION

Nicotinamide Adenine Dinucleotide Phosphate (NADPH) oxidase (also known as NOX) serves as pivotal sources of cellular reactive oxygen species (ROS). These ROS play crucial roles in various cellular processes, including the synthesis of hormones, remodeling of the extracellular matrix, host defense mechanisms, and redox signaling pathways [1]. However, ROS mediated by NOX, termed oxidative burst, primarily helps eradicate invading microorganisms in macrophages and neutrophils, thus acting as an inflammatory mediator [2]. Initially, it was believed that the generation of superoxide anion radical ($O_2^{\bullet-}$) through NOX occurred solely in phagocytes. However, recent revelations have unveiled several enzymes responsible for ROS production in diverse tissues, each exhibiting molecular differences. These enzymes share similarities with NOX2 (phagocytic NOX) and are collectively referred to as the NOX family [3]. Within the human genome, seven NOX homologs are present: NOX1 to NOX5 and Duox1 and Duox2, each differing in expression levels, regulatory mechanisms, tissue-specific expression patterns, types of ROS generated, and mechanisms governing their activity. In particular, control of their activity is of significant importance concerning the acute regulation of ROS formation and their participation in signaling cascades.

The common functionalities of NOX proteins are attributed to their conserved structural characteristics, including the NADPH-binding site situated at the C-terminus, the flavin adenine dinucleotide (FAD)-binding area adjacent to the C-terminal transmembrane domain, six preserved transmembrane domains, and four conserved heme-binding histidine [4]. NOX1, initially identified as a homolog of NOX2, exhibits pronounced expression in various tissues, such as the colonic epithelium, smooth muscle cells, endothelial cells, uterus, placenta, osteoclasts, retinal pericytes, neurons, astrocytes, and microglia [5]. The NOX1 complex comprises the catalytic subunit NOX1 (a gp91phox homolog), NADPH oxidase organizer 1 subunit (NOXO1, similar to p47phox), NADPH oxidase activator 1 subunit (NOXA1, similar to p67phox), the p22phox subunit, and the small GTPase Rac1 subunit. NOX1 interacts with the transmembrane subunit p22phox, preserving its stability and enzymatic efficacy. NOX1 activation involves complex formation with the activators NOXA1, NOXO1, and Rac1 GTPase, culminating in the conversion of molecular oxygen (O_2) to $O_2^{\bullet-}$ [6]. NOX2 expression is

prominent in inflammatory cells like monocytes, macrophages, and neutrophils, as well as in various tissues including the brain, neurons, microglia, heart, kidney, gastrointestinal tract, liver, and pancreas. Numerous studies have elucidated NOX2 signaling pathways, particularly in neutrophils [7].

NOX3 shares structural similarities with NOX1 and NOX2. It can be activated by regulatory subunits (such as p47phox and p67phox) or by NOXO1 and NOXA1. Recent investigations underscore the essential role of p22phox in NOX3 activation and $O_2^{\bullet-}$ production. NOX3 exhibits notable expressions in the inner ear, contributing to the formation of otoconia crystals in the vestibular system. In addition, it exhibits lower expression levels in the liver, lung, spleen, and fetal kidney [8]. NOX4 has distinct characteristics that separate it apart from other NOX proteins, since it relies exclusively on the p22phox subunit for ROS production. Unlike its counterparts, NOX4 exhibits constant activity and operates independently of cytosolic subunits. It is highly prevalent in the kidneys and various cell populations, such as mesangial cells, smooth muscle cells, fibroblasts, osteoclasts, endothelial cells, neurons, and hepatocytes [9].

NOX5 presents a unique N-terminal domain containing four Ca^{2+} binding sites crucial for its activation, facilitated by additional elongation factor (EF)-hand motifs (helix-loop-helix motifs). Recent investigations suggest that NOX5 becomes active in response to an elevation in intracellular calcium levels, triggered by calcium/calmodulin-dependent kinase signaling and various post-translational modifications including phosphorylation, S-nitrosylation, SUMOylation, and oxidation. Upon stimulation, calcium binds to the C-terminal NADPH domain, facilitating electron transfer to FAD and heme molecules, ultimately resulting in the generation of $O_2^{\bullet-}$. NOX5 is detectable in the spleen, testes, and endothelial cells [6].

DUOX1/2 stands apart from other NOX isoforms due to its possession of an additional N-terminal domain that exhibits peroxidase activity and contains intracellular EF (α-helix "E," and a second α-helix "F") hand-type Ca^{2+}-binding pockets. Both DUOX1 and DUOX2 exhibit different N-glycosylation states: a highly glycosylated mannose form observed in the endoplasmic reticulum (ER) and a fully glycosylated form present at the plasma membrane [1]. Like NOX5, DUOX1 and DUOX2 rely on calcium for activation and are prominently expressed

in the thyroid, respiratory system, and gastrointestinal tract [10]. In addition to its involvement in the oxidation of iodide by thyroid peroxidase (TPO), DUOX1/2 plays a vital role in host defense mechanisms [11]. Different NOX isoforms and their subunits are presented in Figure 1.
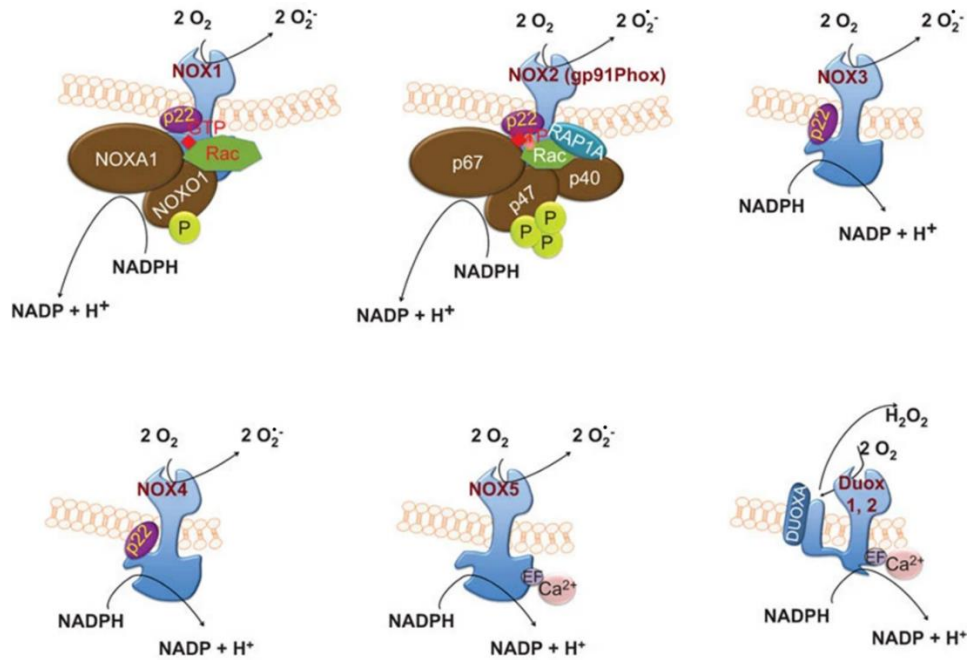
Figure 1: Different NOX enzymes and the mechanisms of their activation. NOX1 and NOX2 undergo activation through the phosphorylation of NOXO1 and p47phox, respectively, which includes the relocation of the multidomain complex (containing p40phox, p67phox, and Rac) from the cytoplasm to the membrane, together with the transfer of electrons from the substrate to O_2. NOX3 activation is solely on p22phox, excluding Rac binding. Activation of NOX4 requires the involvement of both p22phox and Poldip2, while the activation of NOX5 and Duox activation depends on Ca^{2+} binding (adopted from Pandey et al., 2014 doi:10.1038/cmi.2014.89).

The thesis is written in the form of a mini-review, briefing the current knowledge related to NADPH oxidases, monocyte-to-macrophage polarization, NOX2 and NOX4 expression, extracellular vesicles (EVs) mediated ROS/NOX regulation, and oxidative damage. The results of my research, published in Rathi et al. (2024), Prasad et al. (2024), Prasad et al. (2023), and Prasad et al. (2022), are discussed in the context of up-to-date findings and are

referred to in the text by bold and blue letters. These publications are enclosed in Appendix 2 of the thesis.

1.1 Nicotinamide Adenine Dinucleotide Phosphate (NADPH) oxidases and its relation to diseases

Out of seven ROS producing NOX, NOX2 is the most well-studied oxidase complex. Several diseases, as comorbidities, are caused by mutations in different subunits of the NADPH oxidase enzyme. The parts of the NADPH oxidase 2 (NOX2) complex, usually found in certain immune cells, are also found in other cells and tissues throughout the body. If these parts (gp91phox, p22phox, p47phox, and p67phox) have mutations or are deleted, they can cause several health conditions due to weakened immune systems. In mice lacking the CYBB gene (which encodes the NOX2/gp91phox protein) or NCF1 (which encodes the p47-phox protein), problems linked to a deficiency in the NOX2 complex have been reported [12]. It has been known that the $O_2^{\bullet-}$ produced by NOX2 helps regulate how tight or relaxed our arteries are by breaking down nitric oxide ($NO^{\bullet}$), it is known for making blood vessels wider. Studies with mice lacking NOX1 and NOX2 suggest that these substances affect the function of our blood vessels. [13]. Having fewer NCF1 gene copies increases the likelihood of developing rheumatoid arthritis. This link has been observed in mice with modified p47phox. Successful arthritis treatment has involved using substances that enhance oxidative bursts. In systemic lupus erythematosus (SLE), specific genetic variations (SNPs) in NCF2 (which encode the p67phox protein) are strongly associated with the risk of the disease. One of these variations (rs17849502, p67phox H389Q) is also associated with a higher risk of very early-onset inflammatory bowel disease (VEOIBD), as mentioned earlier. Like p67phox H389Q, some other variations associated with lupus (rs13306575, p67phox R395W; rs35937854, p67phox A297V) are positioned in parts where proteins intermingle, possibly affecting how the oxidase subunits interact [12].

1.2 Activation of NADPH oxidase

Phagocytic cells, particularly neutrophils and macrophages, employ various effector mechanisms to eliminate engulfed bacterial, fungal, and protozoal pathogens. A central player in these defense mechanisms is $O_2^{\bullet-}$ which is derived from O_2. The controlled generation of $O_2^{\bullet-}$ occurs in response to the appropriate activation of membrane receptors through a tightly regulated enzyme complex. The oxidase helps create $O_2^{\bullet-}$ by using NADPH to reduce O_2 through a one-electron process. In the cell membrane, the working oxidase complex includes a cytochrome b558, made up of two subunits (NOX2 or gp91phox, and p22phox), and four components inside the cell: p47phox, p67phox, p40phox, and a small GTPase Rac1/2 [14].

The key player in NADPH oxidase is gp91phox, a protein with 570 amino acids. It has six α-helical structures in the cell membrane, linked by 3 external and 2 cytosolic loops, and a unit inside the cell called the dehydrogenase region (DHR). NOX2 accomplishes all the steps for moving electrons from NADPH to O_2, including holding NADPH and FAD in the DHR and two hemes (interacting with the second and fifth transmembrane helices) in the cell membrane. When the phagocytes are at rest, the oxidase components are separated. Activation occurs when cytochrome b558 (large glycosylated β subunit gp91phox + small non-glycosylated α subunit p22phox) interacts with cytosolic components, which requires that these components (p67phox, p47phox and Rac) move to the membrane where cytochrome b558 is located (Figure 2). This whole progression is complete with protein and lipid interactions, which are important for the assembly of oxidase [15]. In the principal model of oxidase assembly, the pivotal event is the interaction between p67phox and the DHR of NOX2. This interaction induces a conformational change in NOX2, which serves as the starting point for electron flow [16]. As p67phox lacks its own domain of intrinsic membrane attachment, it depends on the association of p47phox and Rac for proper positioning and contact with NOX2 [17]. The roles of p47phox and Rac in helping p67phox interact with NOX2 are different and cannot be substituted. Under controlled conditions (cell free system), the oxidase can become active without p47phox, but Rac is necessary for the activation of the oxidase. These processes lead to oxidase modification and conformational changes [17].
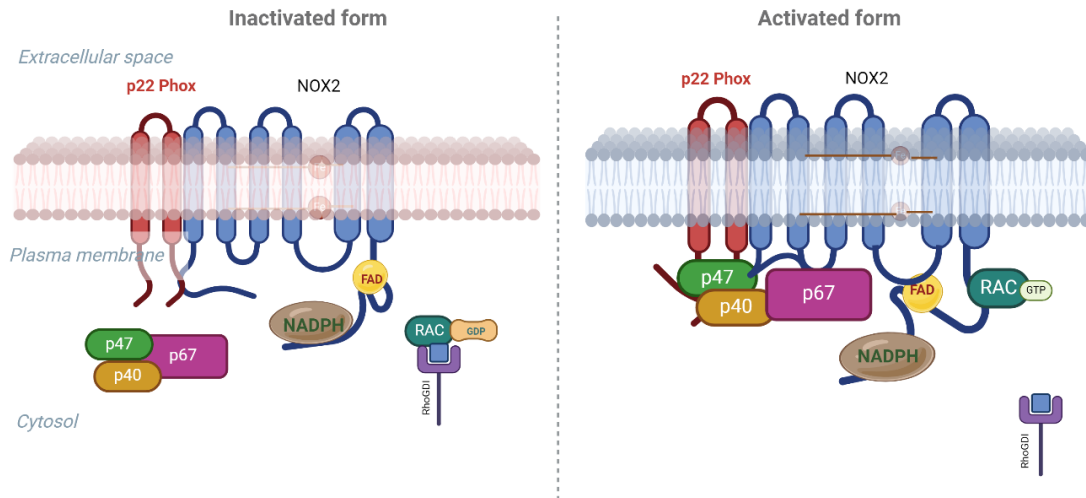
Figure 2: The image depicts the inactive (left) and active (right) form of NOX2, illustrating distinct subunits and their arrangement within the enzyme complex. This image was created using biorender.com.

In NADPH oxidase complex, a cytochrome b558 heterodimer, which consists of two integral membrane proteins [gp91phox (NOX2) and p22phox], NADPH donates electrons to FAD in the presence of the cytosolic subunit p67phox. Subsequently, electrons are relayed from FAD to the heme group of gp91phox (NOX2). Molecular oxygen is then reduced by the transferred electrons, leading to the formation $O_2^{\bullet-}$ (Figure 3).
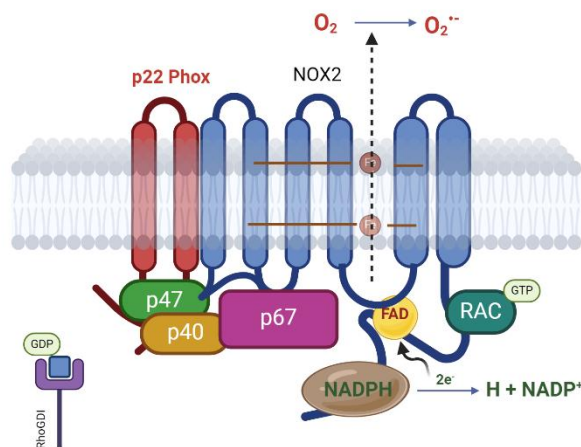
Figure 3: The schematic diagrams depict the electron flow from NADPH to FAD, from FAD to heme, and from heme to O_2 in the NADPH oxidase enzyme complex, resulting in the formation of $O_2^{\bullet-}$ (image created using biorender.com).

NADPH oxidase-mediated ROS generation plays a critical role in cell fate. These can activate cells and can lead to oxidation and damage in the cell. Reactive oxygen species produced in mitochondria can activate several immune pathways involves TLR signaling adapter, tumor necrosis factor receptor-associated factor 6 (TRAF6), resulting in more production of mitochondrial and cellular ROS [18]. Another group of cytosolic multiprotein proteins complex called inflammasome contains a sensor protein NOD-like receptor (NLR) family, ASC (an adaptor protein), and effector caspase-1 [19] also activated by ROS [20]. The inflammasome complex bounded with the nucleotide-binding domain and the leucine-rich repeat-containing protein (NLR), this NLR regulates the secretion of pro-inflammatory interleukin (IL)-1β and IL-18 cytokines.

Monocytes and macrophages, the main carriers of inflammasome genes, adjust to their surroundings by polarizing into the pro-inflammatory M1 phenotype, promoting inflammation, or the anti-inflammatory M2 phenotype [21]. On the other hand, research findings show that Phorbol-12-Myristate-13-Acetate (PMA) can increase the expression of NLRP3, which can facilitate the differentiation and maturation processes of leukemia cells. Moreover, it directly impacts the apoptosis of leukemia cells and their transition into cells resembling monocytes / macrophages [22]. In systemic sclerosis, the ROS-mediated feedback loop appears to sustain the expression of NOX-2 and NOX-4 [23].

1.3 Cell differentiation- monocytes to macrophage polarization

Monocyte differentiation/ polarization involves the transformation into specialized cell types, including macrophages, dendritic cells, and osteoclasts in response to specific signals (summarized in Figure 4). Macrophages with pronounced pro-inflammatory and bactericidal attributes are categorized under the designation of M1 macrophages. Conversely, M2 macrophages assume a role in inflammation resolution, contribute significantly to wound healing processes, facilitate tumor growth, and are instrumental in generating anti-inflammatory mediators as well as growth factors (Figure 4) [24].

When cells such as U-937 and THP-1 encounter differentiation inducers such as PMA and ascorbic acid, their proliferation rate undergoes a noticeable slowdown, thus initiating the

differentiation process. Consequently, these monocytes assume a morphology suggestive of macrophages, owing to structural modifications. However, the precise characteristics of the resultant cell line remain somewhat mysterious, depending on the specific dose and duration of exposure to inducers. Previous investigations have elucidated that cells treated with various inducers exhibit increased expressions of CD11b and CD14, concomitant with the onset of adhesion and subsequent arrest of the cell cycle, which also agrees with our published results **(Figure 3, Article 2)**. Furthermore, it is recognized that cell differentiation triggers the activation of Ca^{2+} and phospholipid-dependent isoforms of protein kinase C (PKC), thus promoting adenosine monophosphate (AMP) metabolism, thus facilitating the maturation of these cells into macrophages.
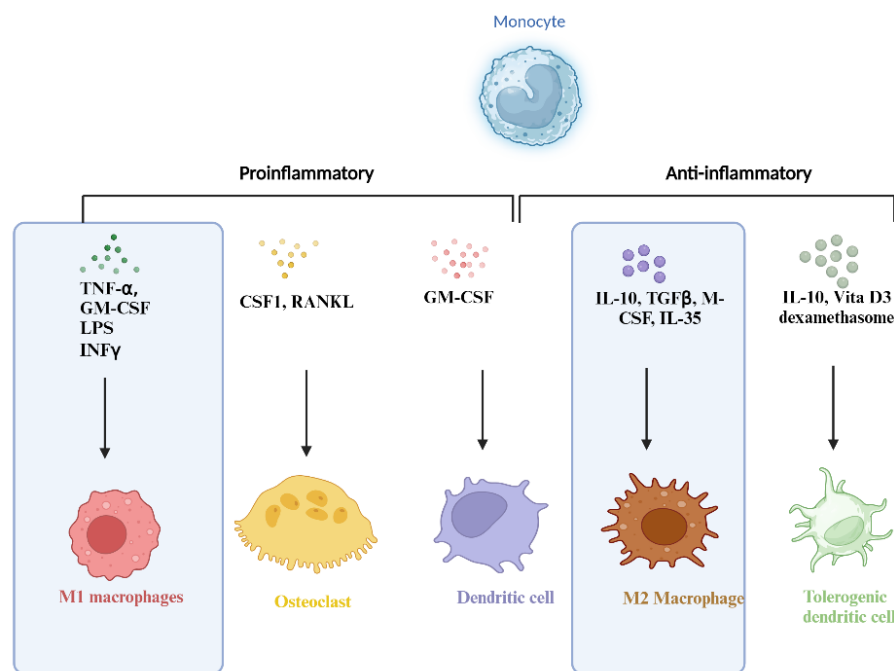
Figure 4: Monocyte polarization and differentiation with different stimuli (image created using biorender.com)

In our study, after 72 hours (h) of treatment with ascorbic acid and PMA, cells were visualized by confocal laser scanning microscope and morphological alteration of cells was observed. Significant differentiation was observed in U-937 cells treated with PMA concentrations at 250 nM and 150 nM, respectively (Figure 5; **Figures 4 and 5, Article 3**). For

the observation of the integrity of the cellular plasma membrane and nucleus, FM4-64 and Hoechst 33342 stains, respectively, were used. We did not observe damage to the nucleus (blue fluorescence) or plasma membrane (red fluorescence) of the cell at the concentrations of PMA and ascorbic acid. Differentiated monocytes showed dendrite types of structure, and non-differentiated monocytes (control) exhibit a spherical type of structure.
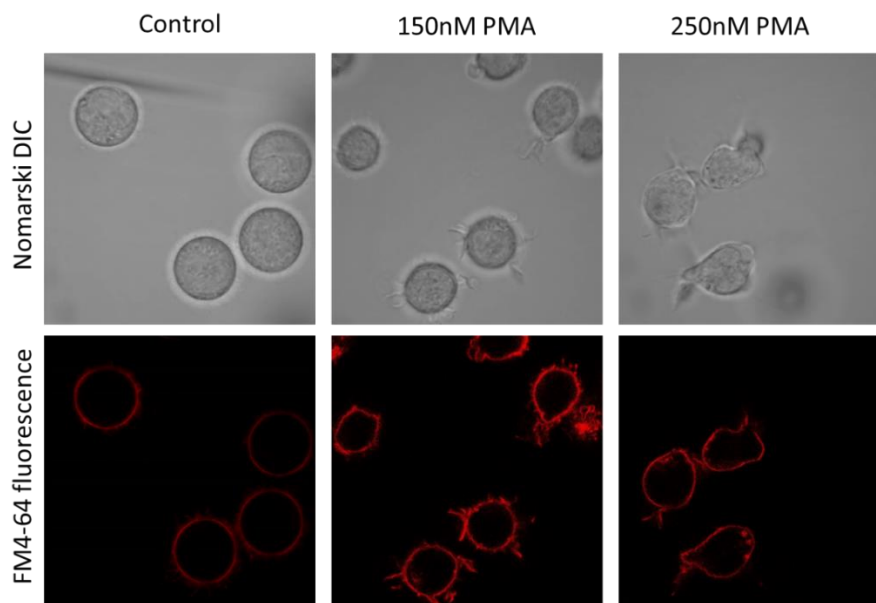
Figure 5: Monocyte cell plasma membrane integrity and differentiation with 150 and 250 nM PMA*:* Staining was performed using FM4-64 in non-differentiated and 72 h differentiated U-937 cells incubated for 5 min. The images were taken in two channels (Nomarski DIC and FM4-64).

1.4 Ascorbic acid as antioxidant and pro-oxidant

Ascorbic acid (vitamin C) and vitamin E, functioning as antioxidants, have significantly influenced our understanding, highlighting the vital role of antioxidants in the biochemistry of living organisms. Vitamin E stands out for its ability to impede the lipid peroxidation process. This underscores antioxidants as crucial agents that counteract oxidation reactions, frequently scavenging ROS before they inflict damage on cells [25]. Treatment with ascorbic acid after stress has been observed to be more effective than vitamin A in enhancing glutathione and catalase levels and reducing lipid peroxidation. [26]. Vitamins are molecules either occurring naturally or synthesized chemically, indispensable for sustaining the human body in minimal quantities. These essential nutrients, beyond the body's endogenous synthesis capabilities,

serve as viable supplements through dietary intake. They intricately contribute to diverse physiological functions vital for maintaining optimal metabolic processes. For instance, vitamin D functions akin to hormones, regulating mineral metabolism; vitamin A governs cellular and tissue growth, while vitamins E, C, and A exert antioxidant properties. Furthermore, the vitamin B complex group operates as essential enzyme cofactors and precursors. Excessive amounts of these vitamins primarily undergo storage in the hepatic and adipose tissues, obviating the necessity for daily dietary incorporation. However, supplementation with elevated doses of these vitamins can induce toxicity, thereby posing potential health hazards [27]. Notably, certain cell types, including muscle cells, exhibit reduced absorption of dehydroascorbic acid (DHA) under conditions of elevated glucose concentration, a phenomenon attributed to the competitive interaction between glucose and ascorbate for GLUT-1 transporters (Glucose transporter) [28].

Ascorbic acid has dual roles as both an antioxidant and a pro-oxidant depending on the different environmental conditions [29]. The antioxidative characteristic of ascorbic acid originates from the creation of a stable ascorbic acid radical, facilitated by the donation of a hydrogen atom to ROS [30]. This process involves the utilization and neutralization of ROS, which serves as the fundamental mechanism that underpins the antioxidant property of ascorbic acid. Essential conditions for optimal antioxidant efficacy include a low concentration of ascorbic acid (<0.1 mM) and a pH of 7.0. Subsequently, the ascorbic acid radical has the potential to revert to its unaltered state (ascorbic acid), facilitated by cellular enzymatic processes, or undergo transformation into oxidized ascorbic acid through a disproportionation reaction [31].

The pro-oxidant propensity of ascorbic acid manifests under different conditions. First, it occurs during the auto-oxidation process at elevated concentrations (>4 mM) and pH of an alkaline solution pH (>7). This involves the reaction between the ascorbic acid dianion and O_2, resulting in the formation of an ascorbic acid radical and $O_2^{\bullet-}$ (Figure 6). Given the physiological concentration range of ascorbic acid on the micromolar scale and the physiological pH maintaining around 7.0, the kinetics of this auto-oxidation process exhibit notable kinetics (10^{-6} to 10^{-7} s^{-1}), diminishing its biological relevance under typical conditions. In the initial step,

ascorbic acid undergoes oxidation, resulting in the formation of the ascorbic acid radical concomitant with the reduction of a metal ion. Subsequently, the ascorbic acid radical undergoes conversion to oxidized ascorbic acid through the disproportionation reaction. Reduced metal ions then readily engage with oxygen, yielding an $O_2^{\bullet-}$ that eventually generates hydrogen peroxide (H_2O_2) [29] (Figure 6). The H_2O_2 produced undergoes the classic Fenton reaction in the presence of metal ions. Oxidized ascorbic acid can be restored to its original form, ascorbic acid, through the consumption of cellular glutathione or other cellular processes. Given that these reactions can occur at lower ascorbic acid concentrations (<0.1 mM) and under near neutral pH conditions, their physiological relevance is considerable [29].
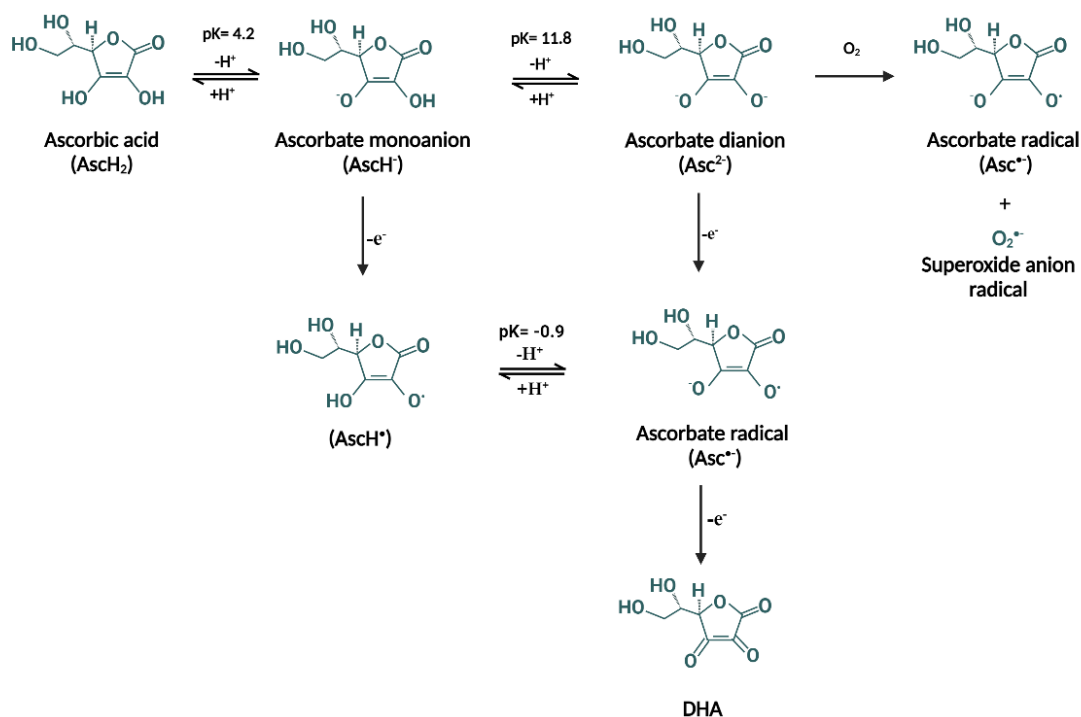
Figure 6: Structures of the chemical species associated with ascorbic acid and its oxidation (adopted with modification from Du *et al.*, 2012 [29] (image created using biorender.com).

In our recent study (**Article 2**), which deals with the antioxidant and pro-oxidant activity of ascorbic acid in U-937 cells, it has been concluded that proteins undergo changes in response to the influence of ascorbic acid on U-937 cells when subjected to transformation into macrophages. This transformation involves the production of ROS (pro-oxidative

behavior) at lower concentration (below 5μM) and a switch exhibiting antioxidant properties (at 10μM or above) (**Figure 5, Article 2**). Essentially, this study indicates that the role of ascorbic acid is not only as an antioxidant but also in promoting the differentiation of monocytes into macrophages, emphasizing its involvement in the immune response via ROS formation.

Ascorbic acid enters most cells through specific transporters called sodium-dependent vitamin C Transporter 1 (SVCT1) and Sodium-dependent Vitamin C transporter 2 (SVCT2) [32] In some of the research studies in U-937 cells, it is evident that SVCT2 expression is in mitochondria [33]. An additional important observation refers to the susceptibility of both plasma membrane and mitochondrial SVCT2 activity to inhibition by low micromolar concentrations of the oxidized form of ascorbic acid, that is, DHA [34]. The above findings explain a particular approach adopted by U-937 cells for the transportation of ascorbic acid across both the plasma and mitochondrial membranes. Importantly, this mechanism appears amenable to alteration influenced by factors associated with their differentiation into monocytes [35]. The investigation revealed that the differentiation of U-937 cells is linked to a decrease in SVCT2 mRNA expression, without inducing significant effects on SVCT1 mRNA. Importantly, this observation was discerned in cells cultured without ascorbic acid, strongly indicating that the identified inhibitory response holds specific biological relevance, and the same study indicates that the transition of pro-monocytes to monocytes is accompanied by a notable reduction in the expression of SVCT2. Interestingly, a distinct scenario is anticipated during the recruitment of monocytes to inflamed tissues. It is therefore postulated that subsequent differentiation of these recruited monocytes into macrophages might produce a different pattern or response with respect to SVCT2 expression [36].

1.5 ROS signalling and monocyte differentiation

At the levels of signal transduction and molecular phenotypes, M1 macrophages exhibit distinct characteristics, including activation of transcription factors such as Signal Transducer and Transcription Activator 1 (STAT1) and Nuclear Factor Kappa B (NFκB). Furthermore, these macrophages exhibit increased production of pro-inflammatory cytokines,

encompassing TNFα, IL-1β, IL-6, IL-12, and various others [37]. In contrast, M2 macrophages are distinguished by the activation of the transcription factor STAT6, heightened expression of the mannose receptor (CD206), and the synthesis of cytokines including transforming growth factor-beta (TGF-β), chemokine (C-C motif) ligand 18 (CCL18), and interleukin-1 receptor antagonist (IL-1Ra). Numerous investigations have elucidated the contribution of ROS in the initiation of signaling pathways, specifically nuclear factor Kappa B (NFκB) and p38 Mitogen-Activated Protein Kinase (MAPK). These intricate pathways, upon ROS activation, orchestrate the upregulation of pro-inflammatory gene expression within macrophages. A hypothesized mechanism centers on the initiation of NOX and superoxide dismutase (SOD) activation, leading to the generation of H_2O_2 in response to stimulation by Toll-Like Receptor 4 (TLR4) stimulation. This sequence of events is postulated to play a role in cellular processes associated with oxidative stress and immune responses.

In the complex realm of macrophage regulation, the intricate interaction of ROS, particularly those stemming from NOX, in shaping macrophage activation and function remains a puzzle yet to be fully unraveled. Despite its apparent significance, the influence of NOX-derived ROS on macrophage behavior remains elusive. Notably, the suppression of M2-associated marker expression follows the inhibition of NOX-derived $O_2^{\bullet-}$, a phenomenon that adds a layer of complexity to understanding NOX-mediated effects on macrophage dynamics. Paradoxically, in NOX-deficient non-obese diabetic (NOD) mice, an unexpected increase in M2 markers occurs, further complicating the understanding of NOX-derived ROS impact on macrophage activation pathways. This unexpected outcomes adds uncertainty to the intricate web of interactions between NOX-derived ROS and macrophage behavior [38].

Disagreements in findings may arise from variations in the experimental methodologies employed to inhibit ROS production. In a comprehensive perspective, both macrophage phenotypes M1 and M2 are influenced by NOX-derived ROS and mitochondrial ROS (mtROS), affecting the underlying signaling pathways. It is postulated that the stage of cell differentiation and intracellular and mtROS likely play a crucial role in determining the induction of M1 or M2 polarization [39].
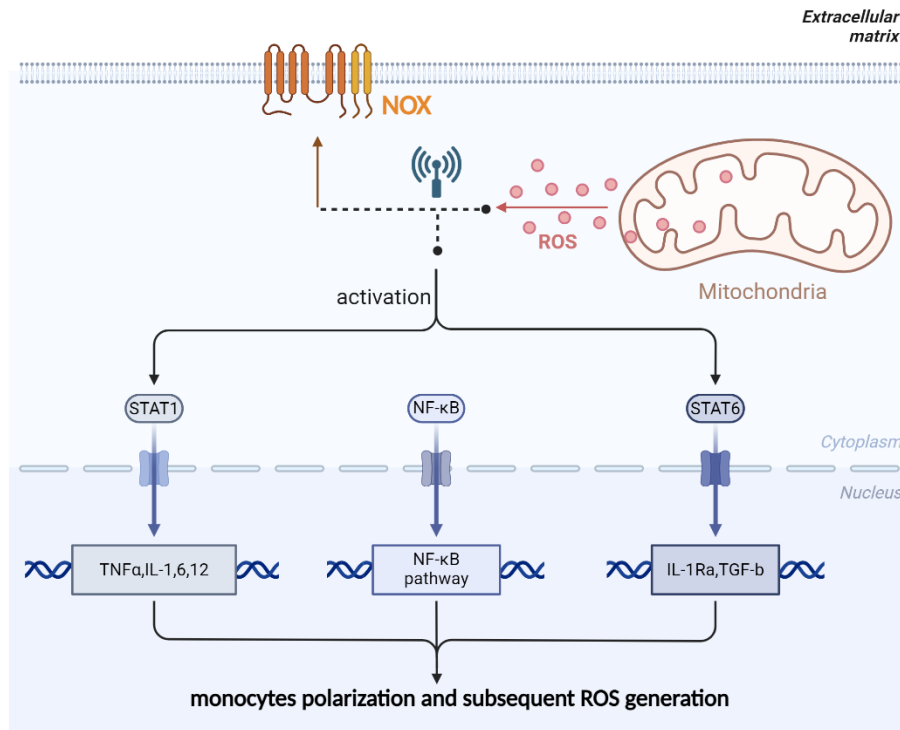
Figure 7: Current state of understanding on "ROS and regulation of cell differentiation'' (image created using biorender.com).

1.6 Extracellular vesicles (EVs), its biogenesis pathway and ROS regulation

Typically, when macrophages are activated, they interact with a variety of target cells to achieve their immunomodulatory effects. This interaction may involve direct contact between cells or the discharge of a secretome, encompassing cytokines and Extracellular vesicles (EVs). In the core, when activated, macrophages communicate with different cells by making direct contact or by releasing substances such as cytokines and EVs, influencing the immune response [40]. Extracellular vesicles constitute naturally occurring, minute lipid vesicles released by nearly all mammalian cells, permeating various body fluids such as plasma, serum, breast milk, cerebrospinal fluid, and serum. The EVs include microvesicles (MVs) and exosomes, each distinguished by their origin and structural characteristics. Microvesicles, spanning a size range of 150 to 1000 nm, materialize through the direct outward budding of

the plasma membrane. On the contrary, exosomes, of a smaller size ranging from 30 to 100 nm, trace their origin to endosomes and are discharged by fusion of multi-vesicular bodies (MVBs) with the plasma membrane [41] (Figure 8).
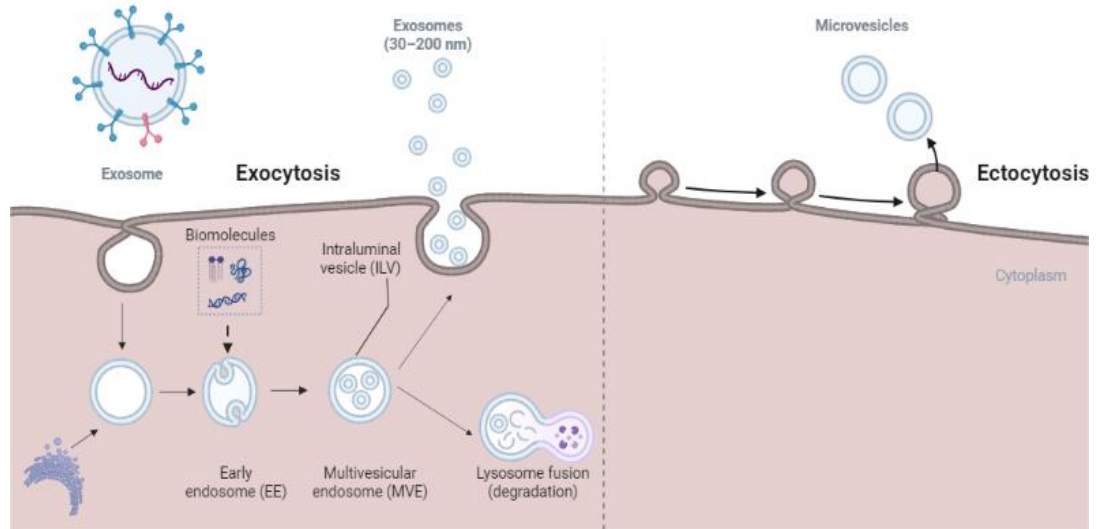
Figure 8: Extracellular vesicle biogenesis pathway. Small EVs begin with early endosome formation triggered by ligand-receptor interactions, followed by the emergence of early endosomes. These endosomes generate ILVs through ligand-mediated membrane invagination. Subsequently, they mature into MVBs. Multi-vascular bodies can undergo either fusion with lysosomes for degradation or fusion with the cellular membrane, releasing small EVs into extracellular spaces (image created using biorender.com).

Extracellular vesicles secretion has been observed in both the eukaryotic and prokaryotic domains, indicative of a conserved biological process in evolutionary timelines [42]. Extracellular vesicles encompass a diverse array of cellular components, including proteins, lipids, mRNA, and miRNA, originating from the interior of the cell. When internalized by recipient cells, these EVs actively participate in a multitude of biological processes. A noteworthy aspect of the function of EVs is their ability to protect their cargo from potential enzymatic degradation within the extracellular location, ensuring the preservation and effective delivery of the encapsulated molecular content [43]. Inside cells, there are special compartments called multivesicular bodies (MVBs) and late endosomes. These compartments have small vesicles inside them, known as intraluminal vesicles (ILVs), that hold specific

proteins, lipids, and other materials. When these ILVs are released, they become exosomes. The creation of ILVs happens as the cell membranes fold inward, a discovery made while studying how the transferrin receptor (TfR) is released in small vesicles by mature reticulocytes.

The movement of MVB's towards the cell's outer membrane is facilitated by the cellular infrastructure, utilizing the cytoskeletal framework and microtubule network. Following the fusion of MVBs with the cell surface in a process known as exocytosis, the internal vesicles within MVBs, known as ILVs, are released into the extracellular environment as exosomes. This intricate cellular mechanism ensures the transport and secretion of ILVs through a regulated and orchestrated process that involves MVB and the cell surface [44]. Multivesicular bodies represent a diverse and varied group within cellular structures [45]. The composition of MVBs is diverse, prompting ongoing inquiries into the possible divergence of pathways for secretion and degradation within these structures. The question of whether specific markers or cargoes influence these distinct pathways remains unanswered. Numerous mechanisms have been identified in the intricate process of exosome biogenesis. A pivotal participant in this process is the Endosomal Sorting Complex Required for Transport (ESCRT) machinery, complemented by the vital involvement of Soluble N-ethylmaleimide-sensitive factor activating protein receptor (SNARE) proteins and their effectors, including RAB GTPases, in orchestrating the intricate secretion of exosomes [46].

In our study, we characterized EVs isolated from U-937 and THP-1 cells, subsequently identifying NOX isoforms within them, and whether EVs can modulate NOX4 and NOX2 expression in monocytes and macrophages (**Article 1**). For the isolation of EVs, different approaches such as filtration, centrifugation, and polyethylene glycol (PEG) enrichment were applied. For the isolation of EV, the supernatant was collected and filtered through a 0.2 μm polyether sulfone membrane syringe filter (explained in detail in section 2.3 of **Article 1**). Polyethylene glycol enrichment and high-speed centrifugation were also utilized following filtration, and the outcomes from both methods were comparable (**Figure 1, Article 1**). Characterization of EVs was carried out by differential light scattering (DLS), transmission electron microscopy (TEM) and immunoblotting (Figure 9; **Figure 2 and Supplementary data**

2, Article 1). In transmission electron microscopy (TEM) at various magnifications, the size of EVs was confirmed (Figure 9). Subsequently, the isolated vesicles were measured using dynamic light scattering (DLS), yielding a mean Z-average diameter of approximately 134 nm with a standard deviation of about 8.64 nm and a polydispersity index of 0.278. Following size measurement, immunoblotting was conducted for anti-CD63.
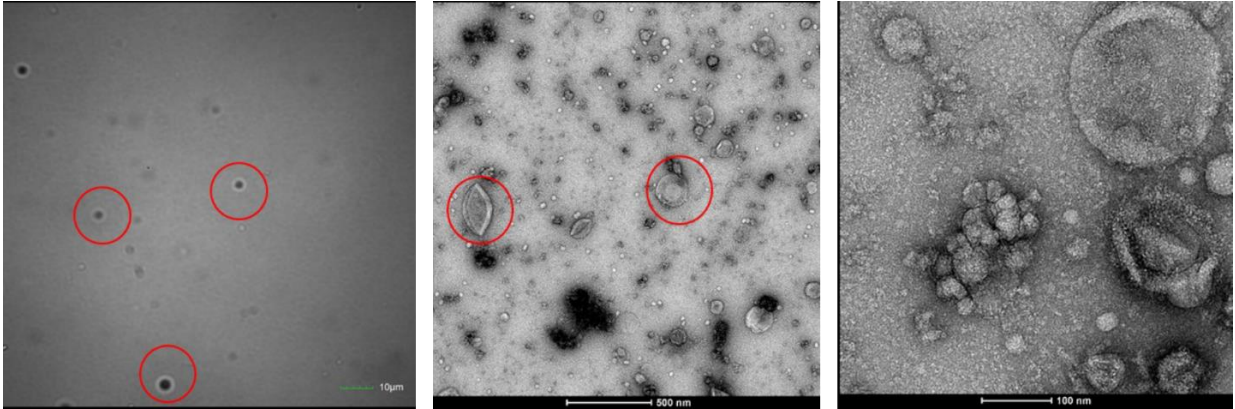
Figure 9: Extracellular vesicles at different magnification measured using TEM.

CD63 is a lysosomal membrane protein ranging from 30 to 60 kDa, characterized by its structure consisting of four alpha-helical transmembrane domains with two extracellular loops. Both the N- and C-terminals of CD63 are oriented inward within exosomes. During the past two decades, various tetraspanins, including CD63, CD81, and CD9, have been established as markers of EV/exosomes. In our investigation, we used endogenous CD63 as a surface marker for EV. Our immunoblot analysis of the isolated protein revealed a distinctive band at approximately 63kDa (**Figure 2, Article 1**). This CD63 protein, which likely underwent post-translational modifications such as glycosylation, confirms the presence of EVs. In similar studies, multiple bands within the range of 30 to 85 kDa have been observed, which could be attributed to various factors, including, but not limited to, post-translational modifications, proteolytic cleavage, and other experimental variables [47].

1.7 Extracellular vesicle and NOX regulation

In recent reports, the impact of ROS on nerve fibers (axons) regeneration after being injured has been studied [48]. In the study, the authors focused on the involvement of tiny structures called exosomes (EV of intraluminal origin), which release complexes containing an active form of NOX2 when axonal injury occurs. NOX2 is known for its role in generating ROS, molecules known to be involved in various cellular processes. The main breakthrough of this study was that the release of these exosomal NOX2 complexes was found to extremely important in controlling axon regeneration. Reactive oxygen species produced by NOX2 appeared to influence specific pathways within cells that are crucial for axon growth. Essentially, this research provided a deeper understanding of the complex molecular mechanisms that govern the regeneration of injured nerve fibers. The authors emphasized the significant role that ROS-mediated processes play in this context. In simpler terms, the study helped to understand how certain molecules, specifically those involved in oxidative stress, affect the ability of nerve fibers to heal and grow after being injured [48].

Inspired by the study, we designed a co-culture experiment of EVs isolated from monocytes (U-937 and THP-1) with monocytes treated with differentiation inducers (PMA and ascorbic acid). We then investigated the expression of NOX2 and NOX4 enzymes in control, differentiated and differentiated cell co-cultured with exosomes.

To confirm the additional effect of differentiation inducers or EV on monocytes, cell viability test using trypan blue in control (no differentiation agent + no exosomes) and all treated samples with ascorbic acid, PMA and EV, the viability percentage of the cells was greater than 80% at 24 h and 72 h. Within the control group (without differentiation agents or exosomes), viability percentages of 90% and 80% were observed at 24 h and 72 h, respectively. Samples subjected to PMA-induced differentiation exhibited a viability of 86.5% at 24 h, increasing to 95% at 72 h. Similarly, samples treated with viability maintained with ascorbic acid within the same range, consistently exceeding 80%, at various concentrations (5μM and 10μM). Upon treatment with EVs and differentiation using PMA, viability reached 88% at 24 h and 94% at 72 h. Likewise, samples differentiated with ascorbic acid exhibited viability within the same range, consistently exceeding 80% at different concentrations (5μM and 10μM).

Consequently, it was concluded that neither external administration of differentiation agents (PMA or ascorbic acid) nor supplementation of EVs induced any stress that led to changes in cell proliferation and viability (**Figure 3, Article 1**).

In the results of this study based on immunoblotting, EVs treatment was found to suppress the expression of NADPH oxidases in cells treated with differentiation inducer. Immunoblot results for anti-NOX4 antibody, showed NOX4 expression at 67kDa. In differentiated cells [(PMA, 150 nM and 250nM) or ascorbic acid (5 µM and 10 µM)], the expression of NOX4 was slightly suppressed, except for cells treated with 10 µM ascorbic acid. However, co-culture of EV along with cells demonstrated no apparent influence on NOX4 expression compared to the control. Interestingly, in 72 h differentiated cell co-cultured with EV, a pronounced down-regulation of NOX4 expression was observed, particularly in cells treated with ascorbic acid (**Figure 4, Article 1**). This observation may lead to a hypothesis regarding the potential regulatory role of microRNAs in NOX4 expression during the transition from monocytes to macrophages.

NOX2 expression was found to be only suppressed in co-cultured macrophages specifically in U-937, while no significant suppression was observed in THP-1 cells (**Figure 5, Article 1**). In THP-1 cells, immunoprecipitation was performed using NOX2 antibodies and protein A agarose beads. In the differentiation induced and EVs co-cultured cells, the immunoblots on NOX2 showed significant suppression in EV co-cultured conditions (**Supplementary data S7, Article 1**).

The formation of MDA-protein adduct was investigated using anti-malondialdehyde (anti-MDA) polyclonal antibody. anti-MDA blotting showed suppression of the level of MDA-protein adduct formation under the EV treated conditions. The obtained results have been summarized in Figure 10. For the validation of this experiment, H_2O_2 treated cells were also used as positive controls. Additionally, we measured the suppression of ROS on chemically generated HO$^\bullet$ (using Fenton reagent) under the exogenous addition of EVs using electron paramagnetic resonance (EPR) spin-trapping spectroscopy. The formation of α-hydroxyethyl radical adducts of POBN [POBN-CH(CH$_3$)OH adduct] was found to be significantly suppressed with the exogenous addition of EVs in a dose-dependent manner (**Figure 7, Article 1**).
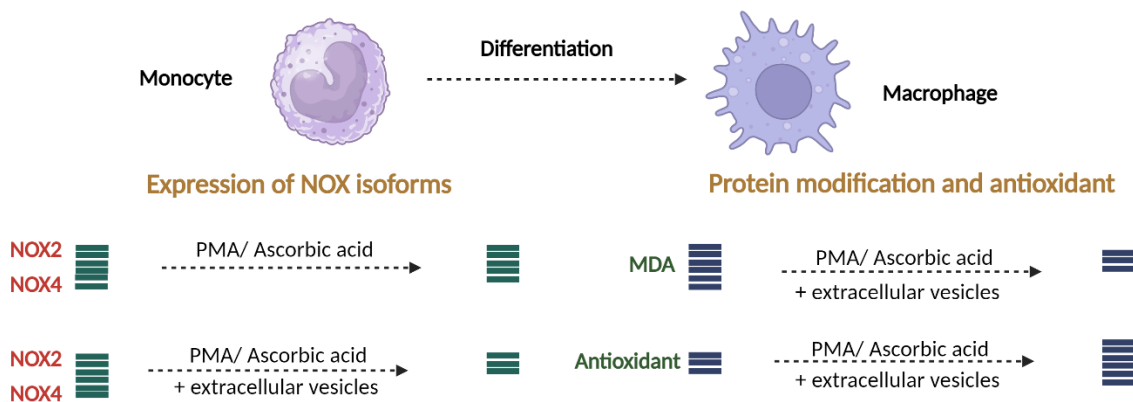
Figure 10: Summary on NOX4, NOX2, MDA and antioxidant level in non-differentiated, differentiated, and co-cultured (cells+ EVs) conditions (image created using biorender.com).

Extracellular vesicles, particularly exosomes, play a vital role in reducing oxidative stress within recipient cells by directly transporting enzymatic antioxidants such as glutathione (GSH), superoxide dismutase 1 (SOD1), thioredoxin reductase 1 (TrxR1), methioredoxin reductase (TrxR2), glutathione peroxidase, in addition to mRNA of antioxidative enzyme which later translates [49, 50]. Consequently, EV therapy emerges as a promising frontier in regenerative medicine [51, 52]. The therapeutic potential of EVs lies in their ability to modulate cellular functions by transporting cargo to recipient cells. EVs derived from various sources can be selectively utilized to target specific therapeutic applications, and this technology has found applications in regenerative medicine to enhance tissue repair, address neurological disorders such as Alzheimer's and Parkinson's disease, and contribute to cancer therapy, among other areas [53, 54].

1.8 Antioxidant activity of bioactive compounds

Bioactive compounds are molecules found in natural sources that can have specific physiological effects on cells and the body in general. These compounds can influence various biological processes, and a large percentage of bioactive compounds are known to possess antioxidant properties. Bioactive compounds play a pivotal role in cellular homeostasis,

countering oxidative stress induced by dietary insults like alcohol and high-fat intake. Their antioxidative capabilities involve scavenging ROS, therefore safeguarding cellular integrity.

Bioactive compounds in addition can exhibit anti-inflammatory properties, modulating signaling pathways to mitigate inflammatory responses. In the realm of oncology, bioactive compounds showcase anti-cancer attributes through intricate regulation of cellular processes. Their influence extends to epigenetic control, particularly in histone acetylation, contributing to gene expression modulation. In essence, bioactive compounds serve as molecular sentinels, orchestrating a finely tuned response to dietary challenges, ensuring cellular resilience and maintaining physiological equilibrium [55]. Dietary stress triggers a shift in the cellular redox state, culminating in a profoundly oxidative environment characterized by the overproduction and buildup of ROS. This imbalance results in oxidative stress, instigating inflammatory responses and disrupting metabolic functions. The heightened presence of ROS induces a cascade of detrimental effects, impacting cellular processes and contributing to the deleterious consequences associated with dietary stress, including oxidative stress-induced damage, inflammatory reactions, and compromised metabolic homeostasis. In principle, the perturbation in redox equilibrium serves as a key instigator of pathological conditions linked to dietary stress [56].

Under normal physiological conditions, the body's defense mechanisms, including enzymes like catalase, SOD, and the glutathione, work synergistically to convert ROS and reactive nitrogen species (RNS) into less harmful substances. However, during pathological states, an excess production of ROS/RNS overwhelms these defenses or disrupts their normal functioning. This imbalance results in oxidative stress, a condition where the body's antioxidant capacity falls short of counteracting the heightened oxidant levels. Prolonged oxidative stress evolves into chronic inflammation, contributing to the development of various diseases such as diabetes, cardiovascular disorders, arthritis, and cancer. The disturbance in redox equilibrium becomes a pivotal factor in the pathogenesis of these health issues [57]. Phytochemicals, comprising polyphenols, flavonoids, steroids, organosulfur compounds, and vitamins, constitute plant-derived metabolites widely dispersed across different plant organs, playing integral roles in plant growth and developmental processes. Beyond their botanical

significance, these phytochemicals have garnered attention for their therapeutic potential. Currently, they are harnessed for the prevention and management of a spectrum of diseases, including diabetes, cardiovascular disorders, and cancer. Exploiting the health-promoting attributes of these botanical compounds has become a focal point in medical investigations, underscoring their diverse applications in enhancing human well-being and providing a natural strategy to counteract various pathological conditions [58].

Phytochemicals demonstrate antioxidant capabilities, as evidenced by findings from both laboratory (*in vitro*) and live organism (*in vivo*) studies. These compounds are observed to directly counteract ROS and elevate the expression of cellular antioxidant enzymes. By scavenging ROS and bolstering the activity of intrinsic antioxidant defenses, phytochemicals play a crucial role in shielding cells from oxidative stress-induced damage. This dual action, underscores the protective effects of phytochemicals against cellular injuries caused by oxidative stress [59]. In recent study, it has been studied that exposing Drosophila flies to environmental toxins increased oxidative stress, resulting in neurotoxicity. However, when Drosophila flies were given a diet enriched with phytochemicals before being exposed to paraquat, a protective effect was observed. The dietary inclusion of phytochemicals displayed neuroprotective properties, alleviating the harmful effects of oxidative stress and serving as antioxidants. This implies that incorporating phytochemicals into the diet before exposure to toxins could be advantageous in preventing neurotoxicity. It highlights the potential of these compounds in mitigating the detrimental impact of environmental toxins on the nervous system in Drosophila flies [60].

Our study (**Article 3**) related to bioactive compounds and their impact on protein modifications concludes that the activation or differentiation of monocytes into macrophages is orchestrated by the induction of diverse pro-inflammatory mediators and the generation of $O_2^{\bullet-}$. Notably, lipids, particularly polyunsaturated fatty acids (PUFA's), exhibit heightened susceptibility to oxidative stress. The evaluated compounds [four (4) bioactive compounds (chlorogenic acid, oleuropein, tomatine and tyrosol; oleuropein and tomatine extract were prepared from the leaves of olives and tomato [61-63] and other were acquired commercially)] chosen based on pilot experiments] demonstrated no cytotoxicity and did not impede the

differentiation of U-937 cells into monocytic lineages, as validated through confocal laser scanning microscopic analysis. Tomatine and tyrosol, among the tested compounds, displayed augmented antioxidant activity compared to chlorogenic acid and oleuropein, as evidenced by immunoblotting analysis utilizing an anti-MDA antibody (**Figure 6, Article 3**). The question of whether foods or supplements abundant in antioxidants confer anti-disease efficacy remains a subject of substantial debate. Indeed, there are varying viewpoints on the hypothesis proposing that antioxidant vitamins possess the capability to prevent chronic diseases [64].

1.9 Oxidative damage and skin health

Skin aging involves the gradual loss of structural and functional traits. It is influenced by intrinsic factors and external elements like infections and diseases, including autoimmune conditions and skin cancers. Reactive oxygen species play a crucial role in both natural and external aging, causing chronic disturbances in skin equilibrium, leading to senescence and persistent inflammation. Understanding ROS mechanisms is vital to prevent age-related signs and address premature skin aging [65]. Ultraviolet radiation serves as the primary catalyst for the production of ROS in the skin. The generation of ROS following UVA and UVB irradiation relies on the absorption of photons by intrinsic photosensitizer molecules like cytochromes, riboflavin, heme, and porphyrin [66]. Subsequently, these excited photosensitizers can lead to the generation of ROS, including the $O_2^{\bullet-}$ and $^1O_2$ [67, 68]. Superoxide dismutase transforms $O_2^{\bullet-}$ into H_2O_2, which, in concert with transitional metals like Fe(II) or Cu(II), facilitates the formation of the highly harmful $HO^{\bullet}$ [66].

In **Article 4**, we attempted to address the direct correlation of ROS formation and mediated biomolecule oxidation. In our study, we measured spontaneous ultra-weak photon emission from porcine ears and after applying the Fenton reagent topically. Different concentrations of H_2O_2 (0, 2.5 mM, 5 mM, and 10 mM) and $FeSO_4$ were applied to skin biopsies, and images of the resulting ultra-weak photon emission were taken. The results showed a direct correlation of ultra-weak photon emission and concentration of the Fenton reagent applied topical to skin biopsies (**Figure 1, Article 4**). With the addition of sodium ascorbate (10mM) prior to application of oxidant on porcine skin, the ultra-weak photon

emission was found to be significantly suppressed which indicated a direct participation of $^1O_2$ in overall ultra-weak photon emission (**Figure 2, Article 4**). Under circumstances such as lack to scavenger or uncontrolled production of ROS, radical reactions in cells can occur leading to modifications of various cellular components, including DNA, proteins, lipids, and carbohydrates. In **Article 4**, we performed an immunoblotting study to identify proteins undergoing modification. Stress induction was specifically induced by H_2O_2 treatment, as extreme oxidative damage was not necessary for studying protein modification using western blotting and the presence of endogenous transition metal ions was deemed sufficient for mediating this process.

For protein modification, focusing on protein carboxylation and protein carbonylation, we utilized anti-MDA and anti-2,4 dinitrophenylhydrazone (anti-DNP) immunoblotting, respectively. Skin biopsies treated with H_2O_2 (10 mM) and control non-treated samples were subjected to sodium dodecyl-sulfate polyacrylamide gel electrophoresis (SDS-PAGE). The use of anti-MDA antibodies allowed us to detect MDA-modified proteins, revealing the formation of MDA-protein adducts around 15 kDa, 45 kDa, 50 kDa, 65 kDa, 130 kDa, and 250 kDa. Notably, the band density of proteins at 65 kDa, 130 kDa, and 250 kDa was found to be increased compared to the control un-treated groups (**Figure 5, Article 4**). To investigate the formation of protein carbonyls, a process called derivatization was employed (section 3.4, **Article 4**). The western blot analysis of skin biopsies, both untreated (control) and those treated with H_2O_2, provided insights into the levels of carbonylated proteins. Notably, a distinctive band at 130 kDa appeared in both groups, exhibiting varied patterns. The proteins subjected to carbonylation processes in the control group were markedly less prevalent than those in the treatment group, as indicated by the distinct band observed at 130 kDa. This observation suggests a significant impact of H_2O_2 on the formation of carbonylated proteins in comparison to the untreated control samples (**Article 4**).

Reactive oxygen species oxidize proteins, causing both structural and functional impairments, alongside the formation of protein aggregates and cross-links. These changes can disrupt the typical folding and conformation of proteins, thereby hindering protein-protein interactions and enzymatic activities. Amino acids, such as cysteine, methionine, and histidine,

are recognized as particularly susceptible targets of ROS generation. Moreover, lipids, notably due to the presence of PUFA's, are prone to peroxidation, resulting in the generation of lipid hydroperoxides and various other reactive lipid species. Within our investigation, MDA, emerging as a by-product of lipid peroxidation, arises through a series of reactions involving the cleavage of peroxide bonds and the subsequent rearrangement of resultant radicals. Furthermore, ROS can inflict considerable damage on DNA and Ribonucleic acid (RNA) by oxidizing their bases, ultimately leading to the formation of DNA adducts, breaks, and cross-links. These modifications can culminate in mutations and genomic instability, potentially contributing to the onset of diseases.

2. AIMS OF THE STUDY

During cellular metabolic processes or in response to biotic or abiotic stress, various reactive species are generated. NADPH oxidases are recognized as key enzymes in this process and are distributed across various cellular locations. In addition to directly studying their formation, researchers often employ indirect methods such as examining modified products and their influence on synthesis and biomolecule oxidation pathways. All things considered; we have aimed our study as follows:

i.   Explore the involvement of NADPH oxidases in ROS generation and NOX expression in monocytes and macrophages.

ii. Investigate the influence of EVs on NADPH oxidase expression during monocyte differentiation.

iii. Examine how EVs co-culture affects the alteration of NOX2 and NOX4 expression during differentiation.

iv. Analyze the pro-oxidant and antioxidant effects of ascorbic acid on cellular polarization and protein oxidation during differentiation.

v.   Conduct a detailed investigation into the antioxidant properties of exosomes, ascorbic acid, and selected bioactive compounds.

vi. Discuss ROS and oxidative stress in skin health.

3. EXPERIMENTAL METHODOLOGY

3.1 Cell lines

U-937 and THP-1 cells which are male human pro-monocytic myeloid leukemia cell lines were purchased from American Type Culture Collection (ATCC; Rockville, MD, USA) [69]. U-937 leukemia cells carry the t(10; 11)(p13; q14) translocation, resulting in a fusion between the MLLT10 (myeloid/lymphoid or mixed-lineage leukemia) gene and the Ap-3-like clathrin assembly protein PICALM (clathrin assembly lymphoid myeloid leukemia), which contributes to the tumorous nature of the cell line [70].

3.2 Cell seeding and growing condition

Cells were cultured in a 6-well CELLSTAR cell culture multiwell microplates (Greiner Bio-One, Kremsmünster, Austria) for experiments with initial seeding of 10^5 cells/ mL of medium and incubated for 72 h at 37 ° C with 5% CO_2. To growth medium (RPMI-1640) pre-supplemented with 0.05 mM L-glutamine were added 10% fetal bovine serum (FBS) and 1% antibiotics (penicillin and streptomycin) in the *v/v* ratio. The experiments were carried out when viability was above 70%.

3.3 Cell differentiation

The differentiation inducers, ascorbic acid at concentrations ranging from 0 to 10 µM, and PMA dissolved in DMSO at concentrations of 150 nM for THP-1 cells and 250 nM for U-937 cells, were employed. As PMA is light-sensitive, precautions were taken during handling. The cultures were seeded with a total of $1x10^6$ live cells/mL for either 48h or 72 h as specified in **Articles 1-3**. Ascorbic acid was dissolved in extracellular buffer (EB) consisting of HEPES (15 mM), NaCl (135 mM), KCl (5 mM), $CaCl_2$ (1.8 mM), $MgCl_2$ (0.8 mM), pH 7.4.

3.4 Trypan blue assay for cell proliferation and viability

Cellular proliferation and viability were measured using trypan blue at 0, 24 h and 72 h of treatment or as specified in **Articles 1-3**. Trypan blue concentration was kept at 0.05%, viability of cells was measured after 2 min of incubation using a TC20 automated cell counter (Bio-Rad Laboratories, Hercules, CA, United States). TC20 automated cell counter was used to determine cell density. For a detailed protocol, please refer to Section 2.8 of **Article 1.**

3.5 Cell proliferation assay

Cell proliferation was assayed by measuring the metabolism of a tetrazolium substrate [3-(4,5-Dimethylthiazol-2-yl)-2,5-Diphenyltetrazolium Bromide] (MTT). The effect of DMSO used to dissolve PMA and EB used to dissolve ascorbic acid on U-937 cell proliferation was determined following the method of the cell proliferation assay kit (ab211091). For the test, cells were seeded in triplicates. Cells cultured in the absence or presence of PMA and ascorbic acid were incubated for 72 h at 37 ° C. Following the desired treatments, the medium was discarded and serum-free RPMI-1640 media along with MTT reagent was incubated for 4 h at 37 ° C. To avoid interference by the MTT reagent, MTT solvent was added and the 96-well microplate was kept on shaker for 15 min. The absorbance was recorded at 590 nm using Microplate Readers (Agilent Scientific Instruments, Santa Clara, CA, United States).

3.6 Harvesting of cells

After differentiation, RPMI-1640 media was replaced (carefully without disturbing the cells) with serum free RPMI-1640 media and incubated for 24 h for providing resting period to the cells. After 96 h in total, cells were collected in different tubes and centrifuged at 300xg for 10 min (**Article 2**). In **Article 1 and 3**, cells were harvested after 72h of differentiation. Cell pellets were collected and washed (2x) with phosphate buffer saline (PBS) (speed and time as above).

3.7 Confocal laser scanning microscopy

The Fluorview 1000 confocal unit attached to the IX80 microscope was used to visualize cells on slides or 6-well plates (Olympus Czech Group, Prague, Czech Republic). FM4-64 (15µM, 5 min, RT) was used to staining of cells for monitoring the integrity of cell plasma membrane, Hoechst 33342 (2µM) for nuclear integrity and CD11b FITC fluorescence labeled antibody (dilution 1:2500) for surface marker (differentiation marker) under different experimental conditions as specified in **Articles 1-3**. The He–Ne laser was used for excitation of FM4-64 at 543 nm and its emission was recorded in the range 655-755 nm. FM4-64 (Sigma Aldrich GmbH, Germany) is a lipophilic dye used to stain the plasma membrane. Hoechst 33342 (Sigma Aldrich GmbH, Germany) (membrane-permeant stain) binds to AT-rich regions of double-stranded DNA for which excitation was achieved at 405 nm diode laser and emission was recorded at 430-470 nm bandpass filter. For CD11b FITC, excitation was achieved using a 488-nm argon laser, and emission was recorded in the range of 505-550 nm.

3.8 Transmission electron microscopy

For visualization of EVs at different magnification, a transmission electron microscope (TEM) Jeol 2010F, which works in the range of 80-200kV, equipped with a LaB6 cathode and a Keenview G2 CCD camera, was used. Images are presented at the scale of 500 and 100 nm (Figure 9).

3.9 Preparation of EVs free fetal bovine serum (FBS)

Extracellular vesicle-free FBS was used for cell culture, prepared by filtration through a 0.2 µm polyether sulfone membrane syringe filter (VWR International, Puerto Rico, United States of America), followed by centrifugation at 21,000 × g for 3 h to remove components smaller than 0.2 µm. The resulting supernatant was collected and used for preparing complete media.

3.10 Isolation of EVs from culture media

Extracellular vesicles were isolated from cultured media after 5 days of cell seeding in EV-free FBS-complemented media. 20 mL of media were collected from the flask and centrifuged at 300 × g for 10 min at 4 °C to remove cells. The supernatant was then collected and filtered through a 0.2 µM polyether sulfone membrane syringe filter. This step was followed by centrifugation for 3 h at 21,000 × g at 4 °C. After this centrifugation step, pellets were collected and washed with ice-cooled PBS (2x) for 3 h at 21,000 × g at 4 °C. Pellets containing EVs were collected and re-suspended in 250 µl of HPLC-grade water and stored at -20 °C for further use. For co-culture experiments, freshly isolated EVs were used.
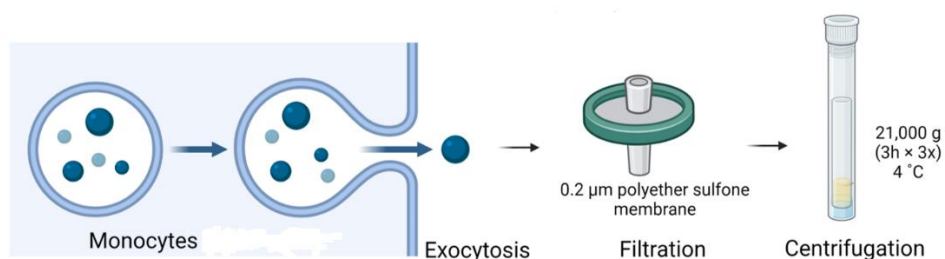

Figure 11: Isolation step of EV from monocytes (image created using biorender.com).

Another method for the isolation of EVs was also attempted using polyethylene glycol (PEG)-mediated precipitation. Following filtration of the media through a 0.2 µM polyether sulfone filter, the filtrate was mixed in a ratio of 1:2.5 and incubated overnight at 4 °C with 50% PEG6000 prepared in d/w. Following this step, the mixture was centrifuged at 13,000×g for 60 min at 4 °C, and the pellet was washed twice with chilled PBS (13,000×g, 60 min at 4 °C). EVs were collected and stored for further use.

3.11 Characterization of EVs using dynamic light scattering (DLS) spectroscopy

Dynamic light scattering measurements of isolated EVs were performed to determine the size distribution using the Malvern Zetasizer RED Pro with a detector angle of 173˚ (backscatter) at a temperature of 25 °C. For the measurement, 25 µL of isolated particles were diluted in 975 µL of d/w, and particle size analysis was conducted for both EVs isolated using centrifugation and PEG enrichment.

3.12 Co-culture experiment of EV with monocytes and differentiating agents

The 6-well plate was used for a co-culture experiment, in which PMA was added at a final concentration of 250nM for U-937 cells and 150nM for THP-1 cells. For ascorbic acid, final concentrations of 5µM and 10 µM was used for differentiating the cells. In each well, cells were seeded at a density of $1*10^5$ cells/mL. For controls, cells in the absence of differentiating agents and/or with EV (20µL) were added. The cells were then incubated for 72 h at 37 °C, and trypan blue assays were performed at 24 h and 72 h in U-937 cells (**Figure 3, Article 1**). After 72 h, cells were harvested, and protein isolation was performed.

3.13 Protein isolation from cells and EVs

For protein isolation from cells, pellets generated during cell harvesting (Section 3.6) was resuspended in 200-250 µl (depending on cell density) of RIPA buffer [150 mM NaCl, 50mM Tris (pH 8.0), 0.5 % sodium deoxycholate, 0.1 % SDS, 1 % NP-40] and 1% protease and phosphatase inhibitor were supplemented. For the protein isolation from EV, the EV obtained in Section 3.10 was used except the step in which resuspension was done in HPLC grade water, RIPA buffer was used. After adding RIPA buffers, cells and EV were kept on ice for 5 min. Following this step, sonication was carried out at 40% amplitude (1 cycle, 30 s each, 6x). After each cycle of sonication, cells/EVs were transferred to the ice (to avoid protein damage and degradation). After completing the sonication, the samples were centrifuged at 18,400 × g for 30 min at 4 ° C. Centrifugation leads to pelleting of the cell debris at the bottom of the centrifuge tube, and protein-containing supernatant was collected carefully without disturbing the pellets. For details on protocol, please refer to Section 2.6 of **Article 1**.

3.14 Estimation of isolated proteins

The isolated protein samples were kept on ice for further steps. Protein estimation was performed using the Pierce bicinchoninic acid (BCA) protein estimation kit (Thermo Fisher Scientific, Paisley, UK). 10 µl of isolated protein samples and 10 µl of protein standards provided with the BCA assay kit (concentrations 125 µg/mL, 250 µg/mL, 500 µg/mL, 750

µg/mL, 1,000 µg/mL, 1,500 µg/mL and 2,000 µg/mL) were added to a 96-well plate. The RIPA buffer served as the control sample. In all wells, 200 µl of the solution mixture (working solution prepared using solution A and B in the 50:1 ratio) were added and plate was covered with an aluminum foil and incubated at 37 °C for 30 min. The 96-well plate was taken, and the absorbance was recorded at 562 nm. The concentration was calculated according to the protein standard and by plotting the calibration curve. The protein sample was stored at -80 ° C for further use. The procedure was used in studies presented in **Articles 1-3**.

3.15 Immunoprecipitation

For immunoprecipitation, 10 µg of protein lysate was used from each sample variant followed by incubation with primary antibody (0.25µg, anti-NOX2 antibody). Incubation of the mixture was followed by gentle rocking at 4° C overnight. The protein bound to primary antibody was precipitated with protein A bound to beads (50 µl/mL of cell lysate) with incubation for 2 h at 4 ° C with gentle shaking. This step was followed by washing of the beads at 3,000 g for 2 min at 4 ° C with 1 mL of precooled TBS to remove excess beads, unbounded antibodies, and impurities (3x) and pellet was collected. They were resuspended in 75µL tris-buffer saline. 25 µL SDS sample buffer was added, vortexed, and then centrifuged for 30 s (5000 rpm). The samples were heated at 100 ° C for 5 min followed by centrifugation at 10,000 rpm for 2 min. Supernatants containing the protein of interest followed by SDS-PAGE and western blotting (**Supplementary data 7, Article 1**).

3.16 Tricine SDS-PAGE electrophoresis

The isolated protein was mixed with 5x Laemmli sample buffer along with 100 mM dithiothreitol (DTT) and incubated at 70℃ for 10 min in a dry bath. 10 µg/lane of protein sample were loaded into the well (1.5 mm polyacrylamide gel containing 4% stacking gel and 10% resolving gel). For the visualization of molecular weight of proteins, the pre-stained protein ladder was loaded (for details, please refer to the **Supplementary data 9, Article 1**).

For the identification of protein carbonyls (**Article 4**), the free carbonyl group of the isolated protein sample was derivatized with 2,4 dinitrophenylhydrazine (DNPH) which results

in the formation of a 2,4 dinitrophenylhydrazone (DNP) derivative. For derivatization, the protein sample was mixed with an equal amount of 12% SDS and 1X DNPH solution (50 mM DNPH in 50% sulfuric acid). Following this step, it was incubated for 30 min at RT for the derivatization reaction to occur. 30% glycerol and 2M Tris base (0.75x v/v of DNPH solution) were added for the neutralization of the derivatization reaction. Subsequently, the mixture was centrifuged at 14, 000 rpm for 10 min and the supernatant was collected and processed further for SDS-PAGE gel.

3.17 Transfer of the proteins from SDS gel

The proteins from the SDS gels were transferred to polyvinylidene difluoride (PVDF) or nitrocellulose membrane (Bio-Rad, California, USA). Protein transfer to membranes was achieved using the Trans-Blot Turbo transfer system (Bio-Rad, California, USA), and the transfer time ranged from 7-30 mins (depending on the gel thickness). For confirmation of protein transfer, membranes were incubated in Ponceau staining (0.1% ponceau S: 1% acetic acid, *w:v;* diluted to 100 mL of d/w) for 5-10 minutes, followed by washing and visualization of stained protein bands. This step was taken in all cases to assure proper loading of samples (**Supplementary data, Article 1**)

3.18 Immunoblotting

After protein transfer, the membranes were blocked with 5% BSA in tris buffered saline (TBS) (pH 7.4) and 0.1% Tween 20 (referred to as TBST) on a shaker at 15 rpm (the incubation time varied from 1.5-12h depending on experiments; shorter incubation was done at RT and overnight incubation were done at 4 ° C). Following blocking, it was then incubated with primary antibodies prepared in 5% BSA in TBST for 1.5 h at RT for anti-NOX2, anti-NOX4, anti-CD63 and anti-DNP while for anti-MDA, it was incubated between 1.5 and 12 h (**Articles 1-4**). Please refer to Figure 12 for antibodies used in the **Articles 1-3**. After primary antibody incubation, washing (3x, 10 min each) on a shaker was done using TBST. For primary antibodies, a dilution of 1:5000 in most cases, if otherwise indicated.
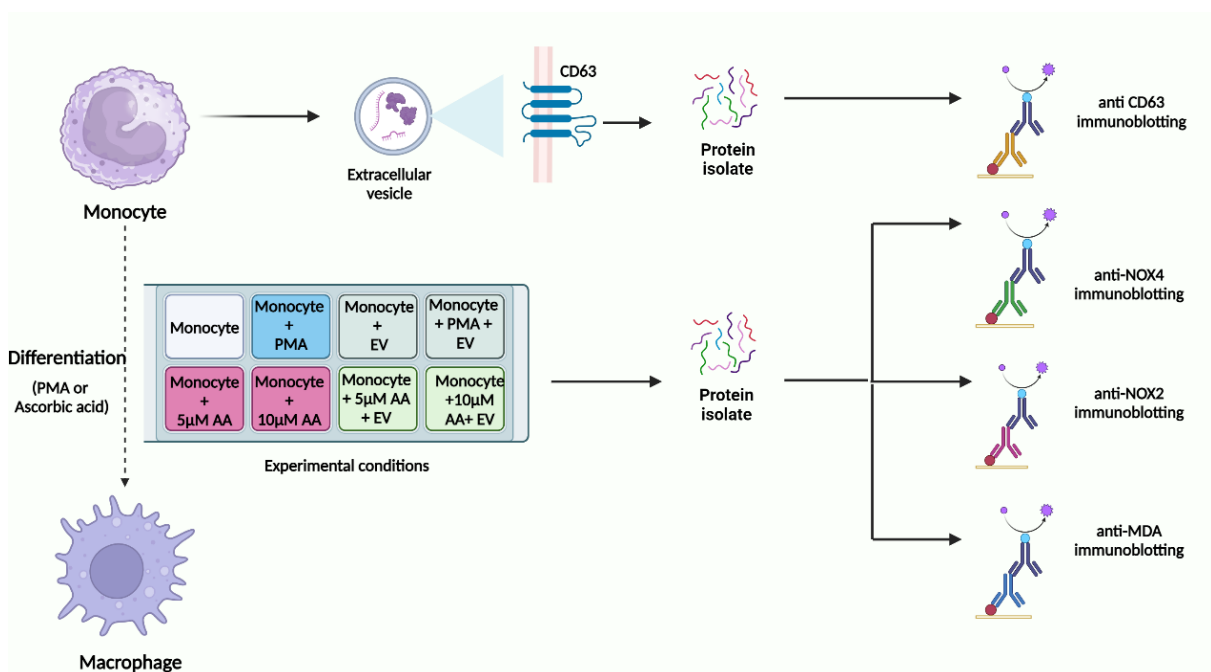
Figure 12: Schematic representation showing the experimental setup for immunoblotting for monocytes with non-differentiating and differentiating controls along with the co-culture experiment with EVs (image created using biorender.com).

The membranes were then incubated for another 1-2h at RT with goat anti-rabbit IgG HRP conjugated or Affinipure goat anti-mouse IgG HRP conjugated secondary antibody (dilution 1:10000, 5% BSA in TBST) followed by 3x washing (10 min each) with TBST and gentle shaking. After the final wash, the immunocomplexes were developed using Immobilon Western Chemiluminescent HRP substrate (Sigma Aldrich, GmbH, Germany) and imaged using the Amersham 600 imager (GE Healthcare, United Kingdom).

3.19 Validation of experiments (EPR spin-trapping spectroscopy and high-performance liquid chromatography)

Spin-trapping was performed using an electron paramagnetic resonance (EPR) spectrometer (MiniScope MS400, Magnettech GmbH, Berlin, Germany) with 10 mM POBN (4-pyridyl-1-oxide-N-tert-butylnitrone). EPR spectra were recorded under the following parameters: microwave power (10 mW), modulation amplitude (1 G), modulation frequency

34

(100 kHz), sweep width (100 G), scan rate (1.62 G s^{-1}). These experiments were carried out to confirm the antioxidant capacity of EVs (**Figure 7, Article 1**).

To validate the immunoblot results on MDA-protein adduct, estimation of total MDA using HPLC was performed according to Pilz et al. (2000) [71]. Please refer to **Supplementary data 2, Article 2** for detailed protocol on sample preparation.

4. CONCLUSIONS AND FUTURE PERSPECTIVES

Based on the findings presented in this thesis, our conclusions are as follows:

- Our research demonstrated the correlation between monocyte differentiation into macrophages and the protein modifications induced by ROS generation.

- Monocyte-derived EVs downregulated the expression of NOX4 and NOX2 in differentiated macrophages, suggesting a possible modulation of NADPH oxidase expression at the transcriptional or translational level.

- EVs resulted in inhibition of lipid peroxidation and subsequently reduced protein modification, supporting recent findings suggesting EVs as carriers of antioxidants. This study confirms EVs as promising candidates for therapeutic use in conditions linked to oxidative stress.

- Unlike traditional antioxidant delivery through liposomes, EV therapy can offer improved efficiency in cellular uptake, presenting a viable solution to the challenges associated with antioxidant administration, especially spontaneous uptake by cells.

- We demonstrated the dual nature of ascorbic acid, transitioning from a pro-oxidative to an antioxidant property.

- Our immunoblotting analysis using anti-MDA antibody revealed that bioactive compounds derived from food industrial waste, specifically tomato and olive leaves, displayed antioxidant effects, suggesting their potential for food supplementation. Notably, tomatine and tyrosol exhibited robust effects when tested on human cell lines, while chlorogenic acid and oleuropein demonstrated moderate effects.

- We investigated the immediate impact of ROS via topical application on a human skin model. Our findings revealed an increase in ultra-weak photon emission in skin samples under oxidative stress. Furthermore, we elucidated the underlying mechanism that leads to the formation of oxidatively modified proteins and protein carbonyls.

- The results of our study expand our comprehension of the mechanism underlying ROS generation within the skin layers, along with its implications and potential preventive measures. These insights facilitate the development and implementation of preventive strategies to manage ROS-related skin issues.

REFERENCES

[1] K. Bedard, K.-H. Krause, The NOX family of ROS-generating NADPH oxidases: Physiology and pathophysiology, Physiological Reviews 87(1) (2007) 245-313.

[2] A.M. Franchini, D. Hunt, J.A. Melendez, J.R. Drake, FcγR-driven Release of IL-6 by Macrophages Requires NOX2-dependent Production of Reactive Oxygen Species, Journal of Biological Chemistry 288(35) (2013) 25098-25108.

[3] A.R. Cross, A.W. Segal, The NADPH oxidase of professional phagocytes - prototype of the NOX electron transport chain systems, Biochimica Et Biophysica Acta-Bioenergetics 1657(1) (2004) 1-22.

[4] R.M. Touyz, A.M. Briones, M. Sedeek, D. Burger, A.C. Montezano, NOX Isoforms and Reactive Oxygen Species in Vascular Health, Molecular Interventions 11(1) (2011) 27-35.

[5] M. Gimenez, B.M. Schickling, L.R. Lopes, F.J. Miller, Nox1 in cardiovascular diseases: regulation and pathophysiology, Clinical Science 130(3) (2016) 151-165.

[6] A. Parascandolo, M.O. Laukkanen, Carcinogenesis and Reactive Oxygen Species Signaling: Interaction of the NADPH Oxidase NOX1-5 and Superoxide Dismutase 1-3 Signal Transduction Pathways, Antioxidants & Redox Signaling 30(3) (2019) 443-486.

[7] R. Rastogi, X.K. Geng, F.W. Li, Y.C. Ding, NOX Activation by Subunit Interaction and Underlying Mechanisms in Disease, Frontiers in Cellular Neuroscience 10 (2017).

[8] K. Schröder, N. Weissmann, R.P. Brandes, Organizers and activators: Cytosolic Nox proteins impacting on vascular function, Free Radical Biology and Medicine 109 (2017) 22-32.

[9] G. Giardino, M.P. Cicalese, O. Delmonte, M. Migliavacca, B. Palterer, L. Loffredo, E. Cirillo, V. Gallo, F. Violi, C. Pignata, NADPH Oxidase Deficiency: A Multisystem Approach, Oxidative Medicine and Cellular Longevity 4590127 (2017).

[10] F. Magnani, S. Nenci, E.M. Fananas, M. Ceccon, E. Romero, M.W. Fraaije, A. Mattevi, Crystal structures and atomic model of NADPH oxidase, Proceedings of the National Academy of Sciences of the United States of America 114(26) (2017) 6764-6769.

[11] A. van der Vliet, K. Danyal, D.E. Heppner, Dual oxidase: a novel therapeutic target in allergic disease, British Journal of Pharmacology 175(9) (2018) 1401-1418.

[12] S. O'Neill, J. Brault, M.J. Stasia, U.G. Knaus, Genetic disorders coupled to ROS deficiency, Redox Biology 6 (2015) 135-156.

[13] K. Matsuno, H. Yamada, K. Iwata, D. Jin, M. Katsuyama, M. Matsuki, S. Takai, K. Yamanishi, M. Miyazaki, H. Matsubara, C. Yabe-Nishimura, Nox1 is involved in angiotensin II-mediated hypertension - A study in Nox1-deficient mice, Circulation 112(17) (2005) 2677-2685.

[14] E. Pick, Cell-Free NADPH Oxidase Activation Assays: A Triumph of Reductionism, Neutrophil: Methods and Protocols, 3rd Edition 2087 (2020) 325-411.

[15] E.V. Mikhalchik, V.A. Lipatova, L.Y. Basyreva, O.M. Panasenko, S.A. Gusev, V.I. Sergienko, Hyperglycemia and Some Aspects of Leukocyte Activation In Vitro, Bulletin of Experimental Biology and Medicine 170(6) (2021) 748-751.

[16] C.H. Han, J.L.R. Freeman, T.H. Lee, S.A. Motalebi, J.D. Lambeth, Regulation of the neutrophil respiratory burst oxidase -: Identification of an activation domain in p67phox, Journal of Biological Chemistry 273(27) (1998) 16663-16668.

[17] R. Sarfstein, Y. Gorzalczany, A. Mizrahi, Y. Berdichevsky, S. Molshanski-Mor, C. Weinbaum, M. Hirshberg, M.C. Dagher, E. Pick, Dual role of Rac in the assembly of NADPH oxidase, tethering to the membrane and activation of p67phox: A study based on mutagenesis of p67phox: Rac1 chimeras, Journal of Biological Chemistry 279(16) (2004) 16007-16016.

[18] A.P. West, I.E. Brodsky, C. Rahner, D.K. Woo, H. Erdjument-Bromage, P. Tempst, M.C. Walsh, Y. Choi, G.S. Shadel, S. Ghosh, TLR signalling augments macrophage bactericidal activity through mitochondrial ROS, Nature 472(7344) (2011) 476-U543.

[19] P.R. Vajjhala, R.E. Mirams, J.M. Hill, Multiple Binding Sites on the Pyrin Domain of ASC Protein Allow Self-association and Interaction with NLRP3 Protein, Journal of Biological Chemistry 287(50) (2012) 41732-41743.

[20] I.C. Allen, M.A. Scull, C.B. Moore, E.K. Holl, E. McElvania-TeKippe, D.J. Taxman, E.H. Guthrie, R.J. Pickles, J.P.Y. Ting, The NLRP3 Inflammasome Mediates In Vivo Innate Immunity to Influenza A Virus through Recognition of Viral RNA, Immunity 30(4) (2009) 556-565.

[21] F. Awad, E. Assrawi, C. Jumeau, S. Georgin-Lavialle, L. Cobret, P. Duquesnoy, W. Piterboth, L. Thomas, K. Stankovic-Stojanovic, C. Louvrier, I. Giurgea, G. Grateau, S. Amselem, S.A. Karabina, Impact of human monocyte and macrophage polarization on NLR expression and NLRP3 inflammasome activation, Plos One 12(4) (2017).

[22] Y.X. Wang, C.H. Xin, X.K. Li, X.X. Chang, R. Jiang, NLRP3 participates in the differentiation and apoptosis of PMA-treated leukemia cells, Molecular Medicine Reports 28(2) (2023).

[23] T. Spadoni, S.S. Baroni, D. Amico, L. Albani, G. Moroncini, E.V. Avvedimento, A. Gabrielli, A Reactive Oxygen Species-Mediated Loop Maintains Increased Expression of NADPH Oxidases 2 and 4 in Skin Fibroblasts From Patients With Systemic Sclerosis, Arthritis & Rheumatology 67(6) (2015) 1611-1622.

[24] A. Mantovani, S.K. Biswas, M.R. Galdiero, A. Sica, M. Locati, Macrophage plasticity and polarization in tissue repair and remodelling, Journal of Pathology 229(2) (2013) 176-185.

[25] J.A. Knight, Free radicals: Their history and current status in aging and disease, Annals of Clinical and Laboratory Science 28(6) (1998) 331-346.

[26] S. Zaidi, N. Banu, Antioxidant potential of vitamins A, E and C in modulating oxidative stress in rat brain, Clinica Chimica Acta 340(1-2) (2004) 229-233.

[27] B. Wansink, Position of the American Dietetic Association: Food and nutrition misinformation, Journal of the American Dietetic Association 106(4) (2006) 601-607.

[28] J. Korcok, S.J. Dixon, T.C.Y. Lo, J.X. Wilson, Differential effects of glucose on dehydroascorbic acid transport and intracellular ascorbate accumulation in astrocytes and skeletal myocytes, Brain Research 993(1-2) (2003) 201-207.

[29] J. Du, J.J. Cullen, G.R. Buettner, Ascorbic acid: Chemistry, biology and the treatment of cancer, Biochimica Et Biophysica Acta-Reviews on Cancer 1826(2) (2012) 443-457.

[30] S.B. Nimse, D. Pal, Free radicals, natural antioxidants, and their reaction mechanisms, Rsc Advances 5(35) (2015) 27986-28006.

[31] C.L. Linster, E. Van Schaftingen, Vitamin C - Biosynthesis, recycling and degradation in mammals, Febs Journal 274(1) (2007) 1-22.

[32] Y. Toyoda, H. Miyata, N. Uchida, K. Morimoto, R. Shigesawa, H. Kassai, K. Nakao, N.H. Tomioka, H. Matsuo, K. Ichida, M. Hosoyamada, A. Aiba, H. Suzuki, T. Takada, Vitamin C transporter SVCT1 serves a physiological role as a urate importer: functional analyses and in vivo investigations, Pflugers Archiv-European Journal of Physiology 475(4) (2023) 489-504.

[33] C. Azzolini, M. Fiorani, L. Cerioni, A. Guidarelli, O. Cantoni, Sodium-dependent transport of ascorbic acid in U937 cell mitochondria, Iubmb Life 65(2) (2013) 149-153.

[34] J.M. Cárcamo, A. Pedraza, O. Bórquez-Ojeda, D.W. Golde, Vitamin C suppresses TNFα-induced NFκB activation by inhibiting IκBα phosphorylation, Biochemistry 41(43) (2002) 12995-13002.

[35] I. Savini, A. Rossi, M.V. Catani, R. Ceci, L. Avigliano, Redox regulation of vitamin C transporter SVCT2 in C2C12 myotubes, Biochemical and Biophysical Research Communications 361(2) (2007) 385-390.

[36] M. Scotti, M. Fiorani, A. Guidarelli, O. Cantoni, Differentiation of Promonocytic U937 Cells to Monocytes Is Associated with Reduced Mitochondrial Transport of Ascorbic Acid, Oxidative Medicine and Cellular Longevity 4194502 (2018).

[37] J.A. Van Ginderachter, K. Movahedi, G.H. Ghassabeh, S. Meerschaut, A. Beschin, G. Raes, P. De Baetselier, Classical and alternative activation of mononuclear phagocytes: Picking the best of both worlds for tumor promotion, Immunobiology 211(6-8) (2006) 487-501.

[38] Y. Zhang, S. Choksi, K. Chen, Y. Pobezinskaya, I. Linnoila, Z.G. Liu, ROS play a critical role in the differentiation of alternatively activated macrophages and the occurrence of tumor-associated macrophages, Cell Research 23(7) (2013) 898-914.

[39] E. Rendra, V. Riabov, D.M. Mossel, T. Sevastyanova, M.C. Harmsen, J. Kzhyshkowska, Reactive oxygen species (ROS) in macrophage activation and function in diabetes, Immunobiology 224(2) (2019) 242-253.

[40] Y.Z. Wang, M. Zhao, S.Y. Liu, J. Guo, Y.R. Lu, J.Q. Cheng, J.P. Liu, Macrophage-derived extracellular vesicles: diverse mediators of pathology and therapeutics in multiple diseases, Cell Death & Disease 11(10) (2020).

[41] B. György, M.E. Hung, X.O. Breakefield, J.N. Leonard, Therapeutic Applications of Extracellular Vesicles: Clinical Promise and Open Questions, Annual Review of Pharmacology and Toxicology, Vol 55 55 (2015) 439-464.

[42] G. Raposo, W. Stoorvogel, Extracellular vesicles: Exosomes, microvesicles, and friends, Journal of Cell Biology 200(4) (2013) 373-383.

[43] L.A. Mulcahy, R.C. Pink, D.R.F. Carter, Routes and mechanisms of extracellular vesicle uptake, Journal of Extracellular Vesicles 3(1) (2014).

[44] M. Colombo, G. Raposo, C. Théry, Biogenesis, Secretion, and Intercellular Interactions of Exosomes and Other Extracellular Vesicles, Annual Review of Cell and Developmental Biology, Vol 30 30 (2014) 255-289.

[45] I.J. White, L.M. Bailey, M.R. Aghakhani, S.E. Moss, C.E. Futter, EGF stimulates annexin 1-dependent inward vesiculation in a multivesicular endosome subpopulation, Embo Journal 25(1) (2006) 1-12.

[46] L. Mashouri, H. Yousefi, A.R. Aref, A.M. Ahadi, F. Molaei, S.K. Alahari, Exosomes: composition, biogenesis, and mechanisms in cancer metastasis and drug resistance, Molecular Cancer 18 (2019).

[47] A. Engering, L. Kuhn, D. Fluitsma, E. Hoefsmit, J. Pieters, Differential post-translational modification of CD63 molecules during maturation of human dendritic cells, European Journal of Biochemistry 270(11) (2003) 2412-2420.

[48] A. Hervera, F. De Virgiliis, I. Palmisano, L.M. Zhou, E. Tantardini, G.P. Kong, T. Hutson, M.C. Danzi, R.B. Perry, C.X.C. Santos, A.N. Kapustin, R.A. Fleck, J.A. Del Río, T. Carroll, V. Lemmon, J.L. Bixby, A.M. Shah, M. Fainzilber, S. Di Giovanni, Reactive oxygen species regulate axonal regeneration through the release of exosomal NADPH oxidase 2 complexes into injured axons, Nature Cell Biology 20(3) (2018) 307.

[49] Y.M. Yan, W.Q. Jiang, Y.W. Tan, S.Q. Zou, H.G. Zhang, F. Mao, A.H. Gong, H. Qian, W.R. Xu, hucMSC Exosome-Derived GPX1 Is Required for the Recovery of Hepatic Oxidant Injury, Molecular Therapy 25(2) (2017) 465-479.

[50] T.Y. Lin, T.M. Chang, H.C. Huang, Extracellular Vesicles Derived from Human Umbilical Cord Mesenchymal Stem Cells Attenuate Mast Cell Activation, Antioxidants 11(11) (2022).

[51] S. Muthu, A. Bapat, R. Jain, N. Jeyaraman, M. Jeyaraman, Exosomal therapy-a new frontier in regenerative medicine, Stem cell investigation 8 (7) (2021).

[52] A. Thakur, D.C. Parra, P. Motallebnejad, M. Brocchi, H.J. Chen, Exosomes: Small vesicles with big roles in cancer, vaccine development, and therapeutics, Bioactive Materials 10 (2022) 281-294.

[53] P. Gao, X. Li, X. Du, S. Liu, Y. Xu, Diagnostic and Therapeutic Potential of Exosomes in Neurodegenerative Diseases, Frontiers in Aging Neuroscience 13 (2021).

[54] M. Zhang, S. Hu, L. Liu, P. Dang, Y. Liu, Z. Sun, B. Qiao, C. Wang, Engineered exosomes from different sources for cancer-targeted therapy, Signal Transduction and Targeted Therapy 8(1) (2023).

[55] H. Kang, B. Kim, Bioactive Compounds as Inhibitors of Inflammation, Oxidative Stress and Metabolic Dysfunctions via Regulation of Cellular Redox Balance and Histone Acetylation State, Foods 12(5) (2023).

[56] S. Falone, M.P. Lisanti, C. Domenicotti, Oxidative Stress and Reprogramming of Mitochondrial Function and Dynamics as Targets to Modulate Cancer Cell Behavior and Chemoresistance, Oxidative Medicine and Cellular Longevity 4647807 (2019).

[57] M. Thiruvengadam, B. Venkidasamy, U. Subramanian, R. Samynathan, M.A. Shariati, M. Rebezov, S. Girish, S. Thangavel, A.R. Dhanapal, N. Fedoseeva, J. Lee, I.M. Chung, Bioactive Compounds in Oxidative Stress-Mediated Diseases: Targeting the NRF2/ARE Signaling Pathway and Epigenetic Regulation, Antioxidants 10(12) (2021).

[58] Y.J. Zhang, R.Y. Gan, S. Li, Y. Zhou, A.N. Li, D.P. Xu, H.B. Li, Antioxidant Phytochemicals for the Prevention and Treatment of Chronic Diseases, Molecules 20(12) (2015) 21138-21156.

[59] J. Montonen, P. Knekt, R. Järvinen, A. Reunanen, Dietary antioxidant intake and risk of type 2 diabetes, Diabetes Care 27(2) (2004) 362-366.

[60] J.H. Park, J.W. Jung, Y.J. Ahn, H.W. Kwon, Neuroprotective properties of phytochemicals against paraquat-induced oxidative stress and neurotoxicity in *Drosophila melanogaster*, Pesticide Biochemistry and Physiology 104(2) (2012) 118-125.

[61] G. Tamasi, M.C. Baratto, C. Bonechi, A. Byelyakova, A. Pardini, A. Donati, G. Leone, M. Consumi, S. Lamponi, A. Magnani, C. Rossi, Chemical characterization and antioxidant properties of products and by-products from Olea europaea L, Food Science & Nutrition 7(9) (2019) 2907-2920.

[62] G. Tamasi, A. Pardini, C. Bonechi, A. Donati, F. Pessina, P. Marcolongo, A. Gamberucci, G. Leone, M. Consumi, A. Magnani, C. Rossi, Characterization of nutraceutical components in tomato pulp, skin and locular gel, European Food Research and Technology 245(4) (2019) 907-918.

[63] A. Pardini, M. Consumi, G. Leone, C. Bonechi, G. Tamasi, P. Sangiorgio, A. Verardi, C. Rossi, A. Magnani, Effect of different post-harvest storage conditions and heat treatment on tomatine content in commercial varieties of green tomatoes, Journal of Food Composition and Analysis 96 (2021).

[64] R.M. Ortega, Importance of functional foods in the Mediterranean diet, Public Health Nutrition 9(8A) (2006) 1136-1140.

[65] F. Papaccio, A. D'Arino, S. Caputo, B. Bellei, Focus on the Contribution of Oxidative Stress in Skin Aging, Antioxidants 11(6) (2022).

[66] K.M. Hanson, J.D. Simon, Epidermal *trans*-urocanic acid and the UV-A-induced photoaging of the skin, Proceedings of the National Academy of Sciences of the United States of America 95(18) (1998) 10576-10578.

[67] P. Pospíšil, A. Prasad, M. Rác, Role of reactive oxygen species in ultra-weak photon emission in biological systems, Journal of Photochemistry and Photobiology B: Biology 139 (2014) 11-23.

[68] P. Pospíšil, A. Prasad, M. Rác, Mechanism of the Formation of Electronically Excited Species by Oxidative Metabolic Processes: Role of Reactive Oxygen Species, Biomolecules 9(7) (2019).

[69] C. Sundstrom, K. Nilsson, Establishment and Characterization Of A Human Histiocytic Lymphoma Cell Line (U-937), International Journal of Cancer 17(5) (1976) 565-577.

[70] M.H. Dreyling, J.A. MartinezCliment, M. Zheng, J. Mao, J.D. Rowley, S.K. Bohlander, The t(10;11)(p13;q14) in the U937 cell line results in the fusion of the AF10 gene and CALM, encoding a new member of the AP-3 clathrin assembly protein family, Proceedings of the National Academy of Sciences of the United States of America 93(10) (1996) 4804-4809.

[71] J. Pilz, I. Meineke, C.H. Gleiter, Measurement of free and bound malondialdehyde in plasma by high-performance liquid chromatography as the 2,4-dinitrophenylhydrazine derivative, Journal of Chromatography B 742(2) (2000) 315-325.

Appendix 1: list of biological materials and chemicals

Biological material
- U-937 and THP-1 cell line (ATCC® CRL-1593.2™)

Used chemicals
- 10% NP-40, Detergent, 10% solution in water (abcam, # ab142227)
- Acetic Acid (Lach-Ner, # 607-002-00-6)
- Acrylamide (Sigma-Aldrich, # A8887)
- Albumin Fraction V, NZ-Origin (BSA) (Carl Roth, # 9048-46-8)
- Ammonium persulfate (APS) (Bio-Rad, # 161-0700)
- Anti-NADPH oxidase 4 antibody (anti-NOX4) (abcam, # ab133303)
- Anti- Malondialdehyde antibody (anti-MDA) (abcam, # ab27642)
- Bromphenol Blue (Sigma-Aldrich, # 93773)
- cOmpleteTM, Mini Protease Inhibitor Cocktail (Roche, # 4693124001)
- Coomassie® Brilliant Blue G-250 (CBB) (Bio-Rad, # 1610406)
- Dimethyl sulfoxide (DMSO) (Duchefa Biochemie, # D1370.1000)
- Di-sodium hydrogen phosphate dodecahydrate (Lach-Ner, #: 30061-CP0)
- DL- Dithiothreitol (DTT)(Sigma-Aldrich, # 43815)
- EIA Grade Affinity Purified Goat Anti-Rabbit IgG (H+L) Horseradish Peroxidase Conjugate (Bio-Rad, # 172-1019)
- Foetal bovine serum, Heat inactivated (FBS) (Biosera, # FB-1001H/500)
- FM™ 4-64 Dye (*N*-(3-Triethylammoniumpropyl)-4-(6-(4-(Diethylamino)Phenyl) Hexatrienyl) Pyridinium Dibromide) (ThermoScientific, # T3166)
- Glycerol anhydrous (Lach-Ner, #: 40058-AT0)
- Hoechst 33342, Trihydrochloride, Trihydrate (ThermoScientific, # H3570)
- N, N´-Methylene-Bis-Acrylamide (BIS) (Bio-Rad, # 1610200)
- N, N, N´, N´- Tetramethylenediamine (TEMED) (Sigma-Aldrich, # T7024)
- PageRuler Plus Prestained Protein Ladder (ThermoScientific, # 26625)
- PBS tablets (Gibco, # 18912-014)
- Polyethylene glycol 6000 (PEG)
- Penicillin Streptomycin (Gibco, # 15140-122)
- Phorbol 12-myristate 13-acetate (Sigma-Aldrich, # P1586)
- Phosphatase Inhibitor Cocktail (Sigma-Aldrich, # P0044)
- Ponceau S (Sigma-Aldrich, # P3504)
- Potassium chloride (Sigma-Aldrich, #: P9541)
- Potassium dihydrogen phosphate (Sigma-Aldrich, #: P0662)
- RPMI-1640 w/ stable Glutamine (Biosera, # LM-R1639/500)
- SDS (Bio-Rad, # 1610302)
- Sodium chloride (Lach-Ner, #: 30093-AP0)
- Transfer Turbo 5x Transfer buffer (Bio-Rad, # 10026938)
- Tricine (Sigma-Aldrich, # T0377)
- Tris (Roche, # 10708976001)

- Tween 20 (Sigma-Aldrich, # 93773)
- Trypan Blue cell culture tested (Sigma-Aldrich, # T6146)

Appendix 2: list of publications

1. **Deepak Rathi**, Claudio Rossi, Pavel Pospíšil, Renuka Ramalingam Manoharan, Luigi Talarico, Agnese Magnani, Ankush Prasad. NOX2 and NOX4 expression in monocytes and macrophages extracellular vesicles in signaling and therapeutics. Frontiers in Cell and Developmental Biology 2024, 12: 1342227.

2. Ankush Prasad, **Deepak Rathi**, Michaela Sedlářová, Renuka Ramalingam Manoharan, Eliška Průdková, Pavel Pospíšil. Differential effects of ascorbic acid on monocytic cell morphology and protein modification: Shifting from pro-oxidative to antioxidant properties. Biochemistry and Biophysics Reports 2024, 37: 101622.

3. Ankush Prasad, Claudio Rossi, Renuka Ramalingam Manoharan, Michaela Sedlářová, Lorenzo Cangeloni, **Deepak Rathi**, Gabriella Tamasi, Pavel Pospíšil, Marco Consumi. Bioactive compounds: its characterization and impact on protein modification in differentiating human cells. International Journal of Molecular Sciences 2022, 23 (13): 7424.

4. Ankush Prasad, Hana Duchová, Renuka Ramalingam Manoharan, **Deepak Rathi**, Pavel Pospíšil. Imaging and Characterization of Oxidative Protein Modifications in Skin. International Journal of Molecular Sciences 2023, 24(4): 3981.

NOX2 and NOX4 expression in monocytes and macrophages-extracellular vesicles in signalling and therapeutics

Deepak Rathi [1], Claudio Rossi [2,3], Pavel Pospíšil [1], Renuka Ramalingam Manoharan [1], Luigi Talarico [2,3], Agnese Magnani [2,3] and Ankush Prasad [1]*

[1]Department of Biophysics, Faculty of Science, Palacký University, Olomouc, Czechia, [2]Department of Biotechnology, Chemistry and Pharmacy, University of Siena, Siena, Italy, [3]Center for Colloid and Surface Science (CSGI), Florence, Italy

Extracellular vesicles (EVs) are a type of cytoplasmic vesicles secreted by a variety of cells. EVs originating from cells have been known to participate in cell communication, antigen presentation, immune cell activation, tolerance induction, etc. These EVs can also carry the active form of Nicotinamide Adenine Dinucleotide Phosphate Oxidase Hydrogen (NADPH) oxidase, which is very essential for the production of reactive oxygen species (ROS) and that can then modulate processes such as cell regeneration. The aim of this study is to characterize the EVs isolated from U-937 and THP-1 cells, identify the NADPH oxidase (NOX) isoforms, and to determine whether EVs can modulate NOX4 and NOX2 in monocytes and macrophages. In our study, isolated EVs of U-937 were characterized using dynamic light scattering (DLS) spectroscopy and immunoblotting. The results showed that the exogenous addition of differentiation agents (either phorbol 12-myristate 13-acetate (PMA) or ascorbic acid) or the supplementation of EVs used in the study did not cause any stress leading to alterations in cell proliferation and viability. In cells co-cultured with EVs for 72 h, strong suppression of NOX4 and NOX2 is evident when monocytes transform into macrophagic cells. We also observed lower levels of oxidative stress measured using immunoblotting and electron paramagnetic resonance spectroscopy under the EVs co-cultured condition, which also indicates that EVs might contribute significantly by acting as an antioxidant source, which agrees with previous studies that hypothesized the role of EVs in therapeutics. Therefore, our results provide evidence for NOX regulation by EVs in addition to its role as an antioxidant cargo.

KEYWORDS

extracellular vesicles, NADPH oxidase, NOX2, NOX4, monocytes, macrophages, reactive oxygen species, free radicals

1 Introduction

Cells (prokaryotes or eukaryotes) secrete lipid-bound vesicles that encapsulate nucleic acids and proteins into the extracellular space called EVs (Di Bella, 2022). The size ranges for these EVs are known to range from nanometres to micrometres. EVs are a broad term used to describe a heterogeneous group of vesicles that are released into the extracellular space by cells; these can be exosomes, microvesicles (also called exosomes or shedding vesicles), and apoptotic bodies (Johnson et al., 2020). Cells can secrete different types of vesicles that can be heterogenic in size and composition (Surman et al., 2017). The biogenesis pathways of these vesicles can vary. EVs can be isolated from different body fluids such as saliva, urine, plasma, lymph, synovial fluid, cerebrospinal fluid, amniotic fluid, breastmilk, tears, bile, gastric acid, etc. (Doyle and Wang, 2019). During the last two decades, research related to EVs has accelerated due to its supposed role in different physiological pathways, cell communication, drug delivery, and as a therapeutic compound (Nederveen et al., 2021).
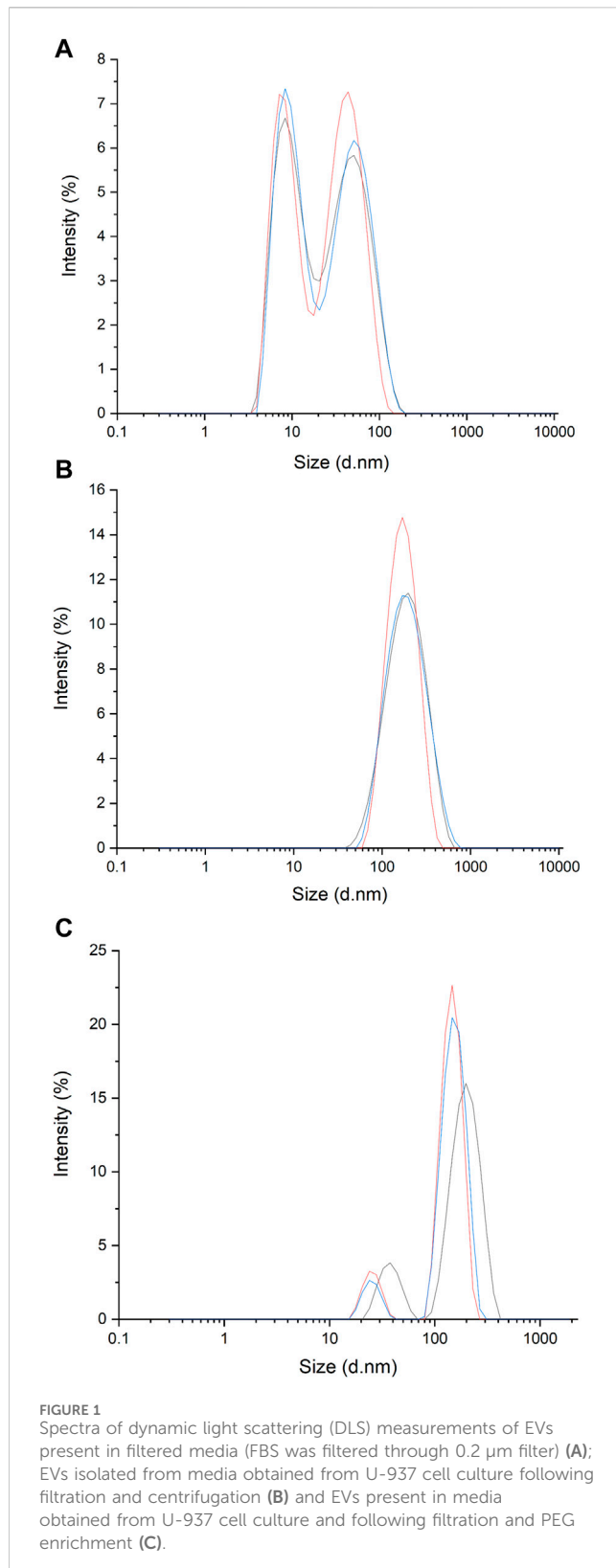
Biogenesis of EVs can be broadly classified into microvesicles or exosome biogenesis. Microvesicles, also known as exosomes or shredding vesicles, are formed by outward budding of the plasma membrane of the cells. The formation of microvesicles can be triggered by stressors or any change in the microenvironment. The change in lipid composition and the action of the cytoskeleton component results in outward budding and eventually scission through the formation of the neck-like structure. During the budding process, different components of the cell such as proteins, lipids, and nucleic acids can be loaded, referred to as cargo. The process of exosome biogenesis begins with endocytosis, in which extracellular components or materials internalize into the cells. Following this step, the structure is directed toward the lysosomes or the cell surface (van Niel et al., 2018; Kalluri and LeBleu, 2020; Lau and Yam, 2023). The biogenesis process is significant for the characterization of exosomes because some proteins are incorporated in exosomes, which include some tetraspanin, lipid bilayer tetraspanin proteins such as CD9, CD63 and CD81 along with the intraexosomal proteins tumour susceptibility gene 101 (TSG101) intraexosomal proteins, the ALG2 interacting protein X (ALIX); however, to date, no single specific marker that has been discovered that can define only exosomes and differentiate them from microvesicles (Barile and Vassalli, 2017). The biogenesis and secretion of intraluminal vesicles are determined by a multiunit cytoplasmic system called the endosomal sorting complex required for transport (ESCRT), which modulates the plasma membrane for vesicle budding and microvesicular cargo sorting.

In recent research, it has also been evident that exosomes produced by tumor cells can modulate the cancer's progression, and exosomes have also been shown to facilitate the metastasis of cancer to secondary organs (Chen et al., 2021). In lung cancer models, cancer cell exosomes can suppress the effect of innate immunity, resulting in suppression of immunity against virus infection (Gao et al., 2018). In this process of suppression of immunity against viral infection, the epidermal growth factor receptor (EGFR) carrying exosomes releases to host macrophages in which these EGFR carrying exosomes

suppress the expression of type 1 interferon and interferon regulatory transcription factor 3 (IRF3) expression. In human fibroblasts, exosomes play a crucial role in removing harmful cytosolic DNA to maintain cellular homeostasis. However, artificial inhibition of exosome secretion can lead to the accumulation of genomic DNA in the cytoplasm. Subsequently, DNA sensing proteins may activate the innate immune response, resulting in ROS-dependent DNA damage, which in turn can lead to cell cycle arrest or apoptosis (Takahashi et al., 2017).

NADPH oxidases are one of many sources of reactive oxygen species (ROS) in biological systems. There are seven isoforms (Nox1–5, Duox1, Duox2) that have different tissue distribution within the cell or organelles. (Bedard and Krause, 2007; Mittler et al., 2011; Landry and Cotter, 2014; Krishnamoorthy and Chang, 2018; Hahner et al., 2020; Prasad et al., 2021). This ROS generation, in addition to being involved in the elimination of the invading pathogen, is also known to regulate several signaling pathways. Under conditions where ROS, such as the superoxide anion radical ($O_2^{\bullet-}$) and hydroxyl radical ($HO^{\bullet}$), are formed above a certain threshold that cannot be scavenged by enzymatic and non-enzymatic antioxidants within the cells, peroxidation of polyunsaturated fatty acids (PUFA's) can occur. This can then lead to the generation of reactive intermediates and products such as malondialdehyde (MDA) (Ayala et al., 2014; Tsikas, 2017; Pospisil et al., 2019; Dalrymple et al., 2022). Generated MDA is a well-known marker of oxidative stress and lipid peroxidation; however, it can also be involved in the post-translational modification of proteins, through the addition of carbonyl groups (-CO) which is known as carbon carbonylation (Suzuki et al., 2010; Tola et al., 2021). Understanding the regulation and function of NADPH oxidase is an active area of research because of its potential therapeutic implications. In recent results presented by Hervera et al., it has been shown that NOX2 present in macrophage secreted exosomes was involved in the regulation of axonal regeneration of injured axons; therefore, NOX regulation may serve as potential factor in regenerative medicine (Hervera et al., 2018).

Our study aims to characterize EVs isolated from U-937 and THP-1 cells, identification of NOX isoforms, and whether EVs can modulate NOX4 and NOX2 expression in monocytes and macrophages. The motivation behind the study is based on the fact that NOX4 expression has been reported predominantly in monocytes, but it has been known to be present in M2 macrophages (post-inflammatory); the same is true for part of the population of M1 macrophages (pre-inflammatory) that express the NOX2 complex (Bermudez et al., 2016). M1 and M2 macrophages are two distinct phenotypes of macrophages, whose functional profiles represent different activation states and immune system functions. M1 can be activated by bacterial lipopolysaccharide and interferon γ. After activation, M1 macrophages produce ROS and nitric oxide (NO) that helps in innate immunity, whereas M2 macrophages are activated through certain cytokines that induce collagen production for wound healing or tissue repair. In a recent study, miRNAs have been hypothesized to inhibit the expression of divalent metal transporter 1 in cardiomyocytes, thus increasing glutathione (GSH) levels and depleting ROS and

FIGURE 1
Spectra of dynamic light scattering (DLS) measurements of EVs present in filtered media (FBS was filtered through 0.2 µm filter) **(A)**; EVs isolated from media obtained from U-937 cell culture following filtration and centrifugation **(B)** and EVs present in media obtained from U-937 cell culture and following filtration and PEG enrichment **(C)**.

TABLE 1 The table shows the size distribution of particles within the samples measured using DLS.

Sample name	Size (nm)	Pdi
Filtered and centrifuged FBS	15.7 ± 0.3	0.43 ± 0.01
Exosomes (centrifuged)	154.8 ± 15.2	0.308 ± 0.04

2 Materials and methods

2.1 Reagents and antibodies

Cell culture medium (RPMI-1640), fetal bovine serum, and antibiotics [antibiotic-antimycotic solution] were purchased from Biosera (Nuaille, France). Phorbol 12-myristate 13-acetate (PMA), ascorbic acid, and polyethylene glycol 6,000 and 4-pyridyl-1-oxide-N-tert-butylnitrone (POBN) were obtained from Sigma Aldrich (St. Louis, Missouri, United States of America). Rabbit polyclonal anti-malondialdehyde (MDA) antibody and anti-NADPH oxidase 4 (anti-NOX4), were purchased from Abcam (Cambridge, United Kingdom) and HRP-conjugated goat anti-rabbit antibody was purchased from BioRad. CD63 monoclonal antibodies, NOX2 polyclonal antibody, and secondary antibody (HRP-conjugated goat anti-mouse) were obtained from Proteintech (GmbH Germany). Protease and phosphatase inhibitors were purchased from Roche (Mannheim, Germany) and Protein A-Agarose (sc-2001) was purchased from Santa Cruz Biotechnology (Heidelberg, Germany). Please refer to the Supplementary Material for a catalog of reagents and clones of antibodies.

2.2 Cell line and growing condition

U-937 and THP-1 cells were purchased from the American Type Culture Collection (ATCC; Rockville, Maryland, United States) and cultured in RPMI 1640 medium containing 1% antibiotic v/v and 10% fetal bovine serum (FBS). To avoid contamination of EVs present in FBS, EV-depleted FBS was used. Using a 0.2 µm polyether sulfone membrane syringe filter (VWR International, Puerto Rico, United States of America), particles larger than 0.2 µm were removed (Shelke et al., 2014), and the filtrate was collected and measured (Shu et al., 2021) (Figure 1). Furthermore, to get rid of the smaller component <0.2 µm (Figure 1A), centrifugation was performed at 21,000 × g for 3 h and the supernatant was collected. Following this step, the obtained FBS was used for further cell culture.

2.3 Isolation of EVs from the media of cultured cells using centrifugation

From the media containing cultured cells (U-937) in the log phase (5 days after cell passage) and with viability ~90–95%, the cell products were harvested and subjected to centrifugation at 300 g for 10 min at 4°C for removal of cells from the harvested media. The supernatant was collected and filtered through a 0.2 µm polyether

MDA formation (Zhang et al., 2022). Therefore, in addition to NOX expression, we also focused on protein modification and ROS suppression in monocytes and macrophages by co-culture experiments in the absence and presence of EVs.
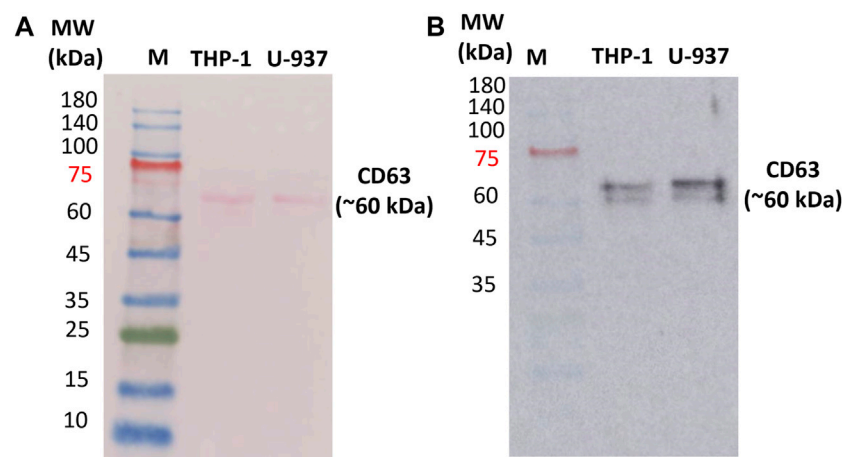
FIGURE 2
Ponceau staining of the nitrocellulose membrane to confirm the presence of proteins (A) and Western blot confirming the expression of transmembrane proteins CD63 in isolated EVs (B). 10 µg of protein isolated from exosomes (U-937 and THP-1) were loaded. 'M' indicates the prestained marker of which 5 µL was loaded. CD63 primary antibody (1: 2500) and HRP-conjugated Goat Anti-Mouse secondary antibody (1:10,000) were used.

sulfone membrane syringe filter and then centrifuged at $21,000 \times g$ for 3 h at 4°C. After this, the supernatants were discarded, and the pellet was washed again at $21,000 \times g$ (2X, 3 h) with ice-cold phosphate buffer saline (PBS, 1X). Subsequently, the pellet was suspended in 250 µL of HPLC grade water. The isolated EVs were stored at -20°C until further processing. The same procedure was followed for THP-1 cells.

2.4 Isolation of EVs by polyethylene glycol (PEG) precipitation

The medium containing cultured cells and cell products was harvested and then centrifugation was carried out at $300 \times g$ for 10 min at 4°C for cell removal from the harvested medium. The supernatant was collected and filtered through 0.2 µm polyether sulfone membrane syringe filter. 50% of the PEG6000 solution was prepared in d/w, after which the filtrate was mixed with the PEG: filtrate (1: 2.5) followed by a short vortex and incubated at 4°C overnight to form aggregates. After overnight incubation, the PEG mixture was centrifuged at $13,000\ g$ for 60 min at 4°C. The pellet was then washed twice with ice-cold PBS at $13,000 \times g$. The collected pellet was stored at -20°C until further processing.

2.5 Characterization of EVs using dynamic light scattering (DLS) spectroscopy

To determine the size distribution of isolated particles in the suspension, DLS measurements were performed using a Malvern Zetasizer RED Pro using a detector angle of 173° (backscatter) at a temperature of 25°C. For sampling, 25 µL of isolated vesicles were diluted in 975 mL of d/w and particle size analysis was carried out for both EVs isolated using centrifugation (as in Section 2.3) and PEG enrichment (as in Section 2.4). Control measurements were performed using EV -free FBS. To confirm that our isolate contains

an EV, we used a transmission electron microscope (TEM) to visualize the particles (data not shown).
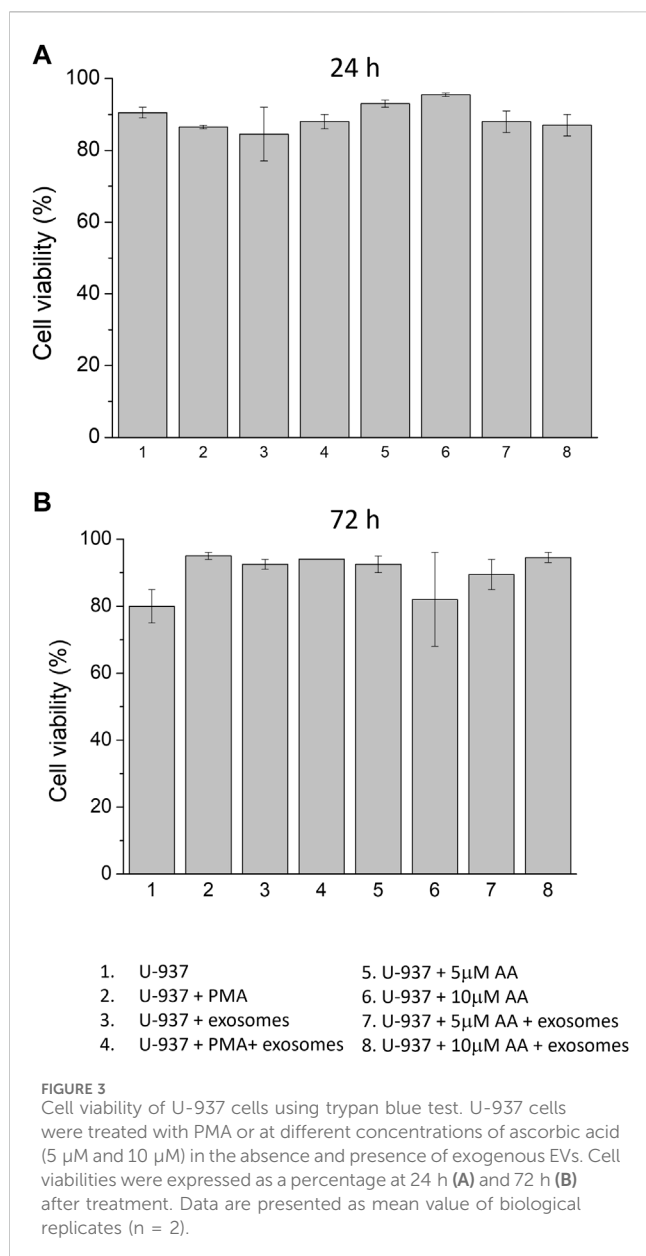
2.6 Protein isolation from EVs

Based on the results obtained from the basic characterization of the isolated EVs, since potential aggregation was observed in EVs prepared using PEG enrichment (Figure 1C), further studies were carried out using EVs isolated using centrifugation. For protein isolation, EVs (in d/w) were sonicated (40% amplitude; 1 cycle for 30 s) in ice-cold Radioimmunoprecipitation Assay (RIPA) buffer [150 mM NaCl, 50 mM Tris (pH 8.0), 0.5% sodium deoxycholate, 0.1% SDS, 1% NP-40] containing 1% protease inhibitor and phosphatase inhibitor. Sonication was repeated 6 times with a 30 s gap before the next sonication. EVs were kept on ice after each cycle of sonication. Following this step, centrifugation at $18,400 \times g$ was done for 30 min at 4°C to remove cell debris and to obtain proteins in the supernatant.

Estimation of protein was done using Pierce bicinchoninic (BCA) protein estimation kit (Thermo Fisher Scientific, Paisley, United Kingdom). The measurement procedure used is as outlined in the manufacturer's guidelines with minor modifications as described in our previous study (Manoharan et al., 2023; Prasad et al., 2023).

2.7 Anti-CD63 blotting (surface marker) for EVs confirmation

Immunoblotting was performed with CD63 surface markers on EVs. The samples were prepared with 5 × Laemmli sample buffer along with 100 mM Dithiothreitol (DTT) and a protein concentration of 10 µg was used for electrophoresis. Prior to loading the samples, the protein samples were incubated at 70°C for 10 min in a dry bath. Subsequently, the sample was loaded onto

A 24 h

B 72 h

1. U-937
2. U-937 + PMA
3. U-937 + exosomes
4. U-937 + PMA+ exosomes
5. U-937 + 5μM AA
6. U-937 + 10μM AA
7. U-937 + 5μM AA + exosomes
8. U-937 + 10μM AA + exosomes

FIGURE 3
Cell viability of U-937 cells using trypan blue test. U-937 cells were treated with PMA or at different concentrations of ascorbic acid (5 μM and 10 μM) in the absence and presence of exogenous EVs. Cell viabilities were expressed as a percentage at 24 h **(A)** and 72 h **(B)** after treatment. Data are presented as mean value of biological replicates (n = 2).

10% Tricine SDS-PAGE. The proteins were then transferred to either PVDF membrane (Bio-Rad, California, United States of America) which was charged prior with methanol or nitrocellulose membrane. The protein transfer to the membrane was achieved using the Trans-Blot Turbo transfer system (Bio-Rad, California, United States). Following the transfer, to ensure that the loading of protein samples is uniform (loading control), Ponceau staining (0.1% Ponceau S: 1% acetic acid, *w: v;* diluted to 100 mL d/w) was done. After washing, the membrane was blocked with 5% BSA in Tris-buffered saline (TBS) (pH 7.4) and 0.1% Tween 20 (referred to as TBST) for 90 min at room temperature (RT). After blocking, washing with TBST (3x) was done for 10 min each. The blocked membranes were then incubated for 90 min at RT with anti-CD63 mouse monoclonal antibody (dilution 1: 5000) followed by 3x washing (10 min each) with TBST. Subsequently, the membrane was incubated for another 90 min at RT with HRP-conjugated goat

anti-mouse secondary antibody (dilution 1:10,000) and washed with TBST (3x, 10 min each). Immunocomplexes were imaged using the Amersham imager 600 (GE Healthcare, United Kingdom) and Immobilon Western Chemiluminescent HRP Substrate (Sigma Aldrich, GmbH, Germany).

2.8 Co-culture of U-937 cells with differentiating agents and EVs

Co-culture experimental setups were made. For the setting of the plates, U-937 and THP-1 controls with differentiating agents [250 nM or 150 nM PMA and ascorbic acid (5 μM and 10 μM)] were prepared. For the experimental sample, cells (1×10^5/mL) under the above conditions (PMA or ascorbic acid) were cultured in the presence of exogenous EVs (20 μL, the same isolates were used for all experiments within the setup). Cells were treated with PMA/ascorbic acid for 72 h (for monocyte to macrophage differentiation) in a 6 well plate and isolated EVs (section 2.3) were added at the start of the treatment. Cell viability at 24h and 72 h were monitored using the trypan blue test to follow cell proliferation and effect of EVs and/or differentiating agents. For protein isolation, 5 mL of non-treated and treated cells were used, and quantification was done based on the method described in Section 2.6. Following quantification, 10 μg protein sample/lane was used for immunoblotting.
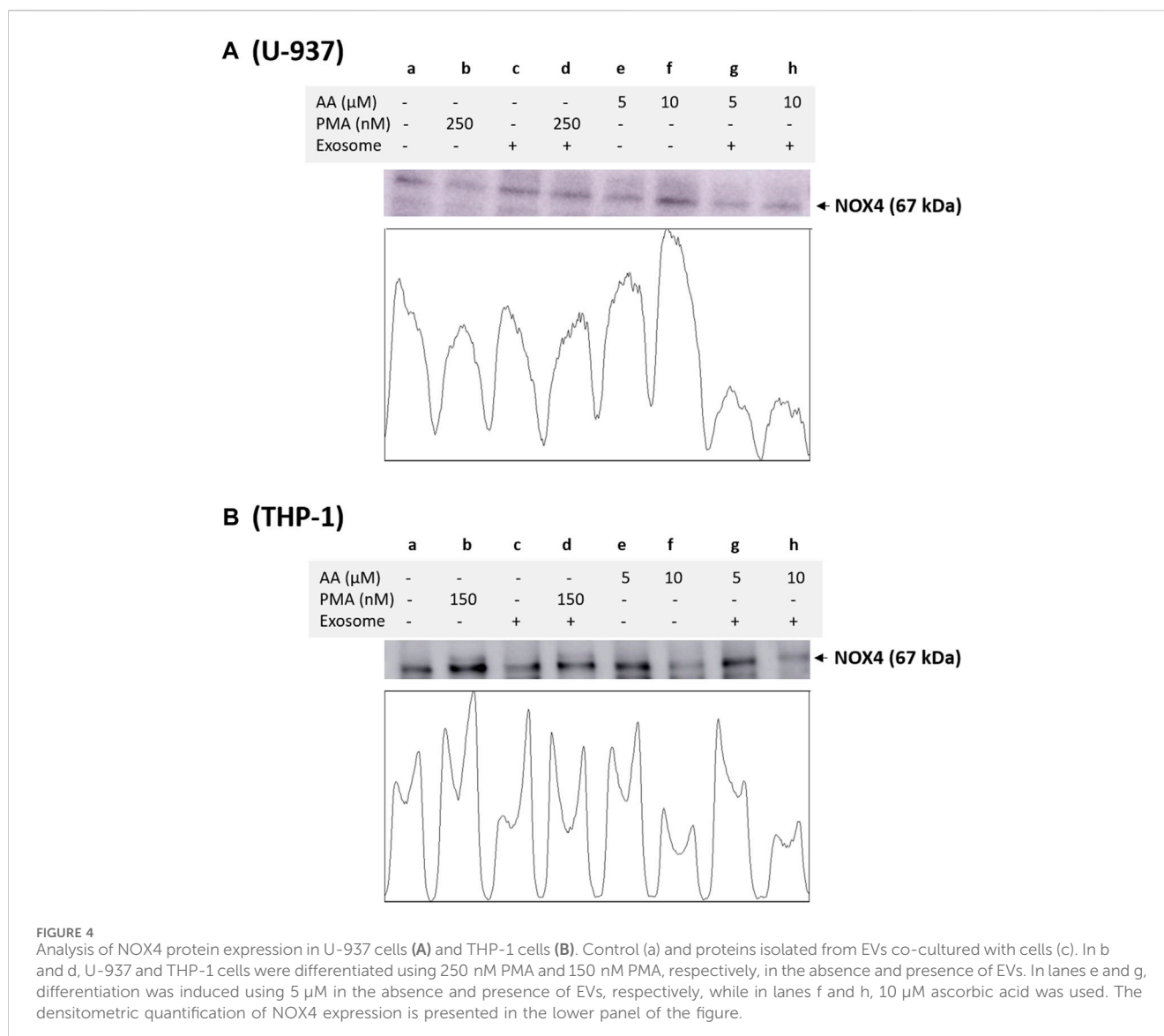
2.9 Western blot analysis

Immunoblotting was performed against NOX4 and NOX2. Until the blocking of membranes, the procedure as described in Section 2.8 was followed. The blocked membranes were then incubated for 90 min at room temperature (RT) with either anti-NOX4 rabbit monoclonal antibody (dilution 1:5000) or anti-NOX2 mice polyclonal antibody followed by 3x washing (10 min each) with TBST. Subsequently, the membranes were incubated for another 90 min at RT with HRP-conjugated goat anti-rabbit secondary antibody and HRP-conjugated goat anti-mice secondary antibody, respectively (dilution 1:10,000) and washed with TBST (3x, 10 min each). Immunocomplexes were imaged using the procedures described in Section 2.7.

To confirm MDA-protein adduct formation, nitrocellulose membranes transferred with MDA adduct proteins were incubated with rabbit polyclonal anti-malondialdehyde antibody prepared at a dilution of 1:5000 in TBST and incubated for 90 min at RT. Following three washes with TBST, the membranes were incubated with horseradish peroxidase (HRP) conjugated anti-rabbit secondary antibody (1:10,000) for 90 min at RT. The blots were imaged as described above.

2.10 EPR spin-trapping spectroscopy

Chemically generated HO$^\bullet$ using Fenton reagent was detected by spin-trapping with 10 mM POBN (4-pyridyl-1-oxide-N-tert-butylnitrone) containing 170 mM ethanol. The measurements were performed using an electron paramagnetic resonance

FIGURE 4
Analysis of NOX4 protein expression in U-937 cells **(A)** and THP-1 cells **(B)**. Control (a) and proteins isolated from EVs co-cultured with cells (c). In b and d, U-937 and THP-1 cells were differentiated using 250 nM PMA and 150 nM PMA, respectively, in the absence and presence of EVs. In lanes e and g, differentiation was induced using 5 µM in the absence and presence of EVs, respectively, while in lanes f and h, 10 µM ascorbic acid was used. The densitometric quantification of NOX4 expression is presented in the lower panel of the figure.

spectrometer (MiniScope MS400, Magnettech GmbH, Berlin, Germany) (Pou et al., 1994). Experiments were carried out in the absence and presence of different concentrations of EVs isolated from U-937 cells resuspended in HPLC grade water. EPR spectra were recorded under the following parameters: microwave power (10 mW), modulation amplitude (1 G), modulation frequency (100 kHz), sweep width (100 G), scan rate (1.62 G s^{-1}).
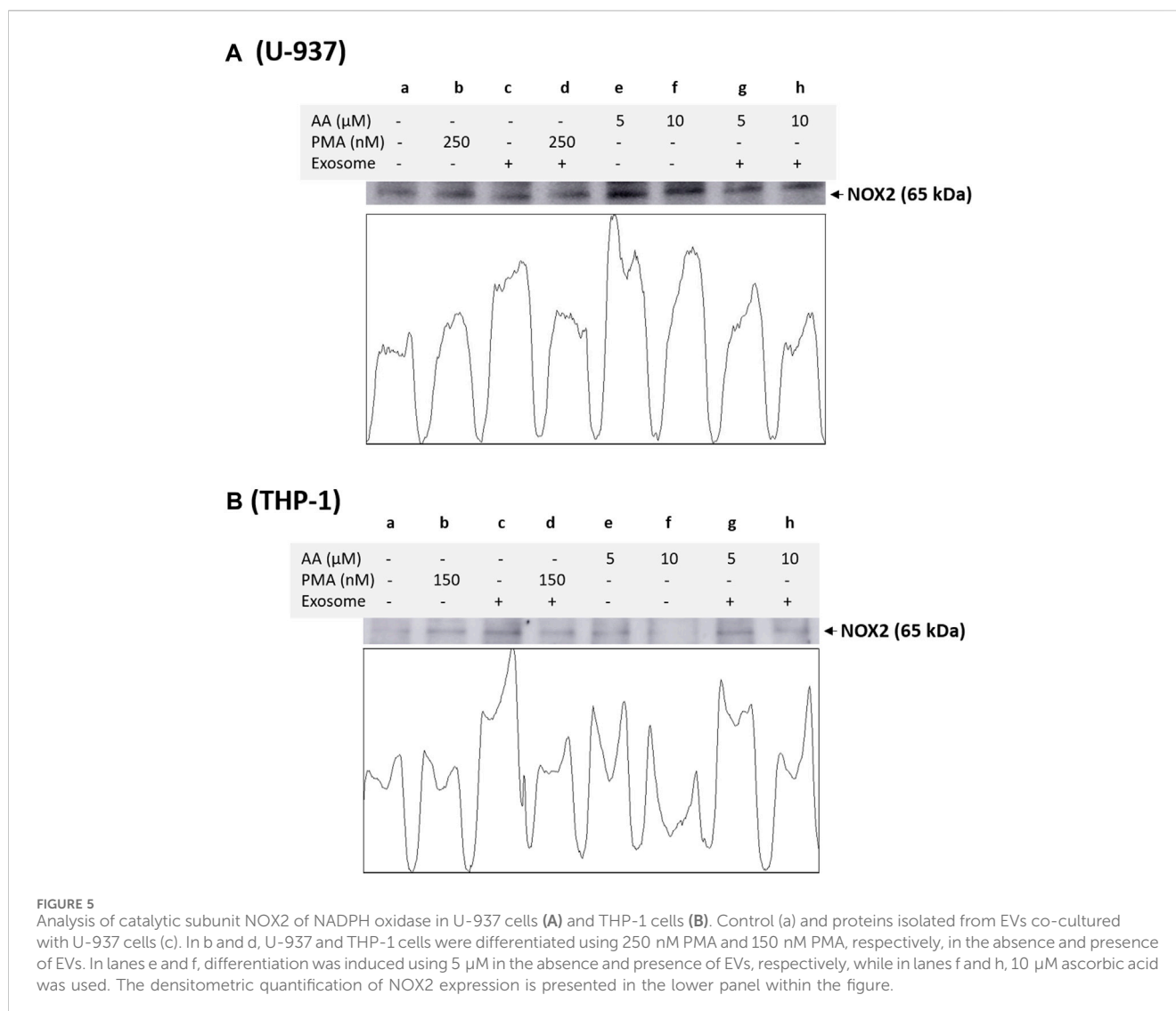
3 Results and discussion

3.1 Characterization of EVs using DLS

Using the dynamic light scattering method, we measured the mean Z-average (mean hydrodynamic size) of the sample obtained by centrifugation from U-937 cells. For the control (filtered and centrifuged FBS), the Z-average was recorded to be 15.7 nm. More than one peak with a polydispersity index of 0.43 was observed (Figure 1A; Table 1). It can be seen that in the sample isolated by centrifugation based on the method described by Shelke and co-workers (with minor modifications) (Shelke et al., 2014), a Z-average of ~154.8 nm was observed with a standard deviation of about 15.2 nm and a polydispersity index of 0.30 (Figure 1B; Table 1). The presence of multiple peaks in the case of PEG samples can be attributed to the centrifugation, aggregation, and orientation of the vesicle (Figure 1C) (Genneback et al., 2013). As the sample acquired by the centrifugation method includes EVs falling within the 30–200 nm range and exhibits the presence of the CD63 marker, it is a likelihood that the isolates may be classified as exosome particles. However, we are uncertain due to a lack of understanding about their origin.

## 3.2 Identification of extracellular markers specific for vesicles

In order to confirm the presence of EVs in the isolated fractions, Western blotting was performed to identify the expression of

FIGURE 5
Analysis of catalytic subunit NOX2 of NADPH oxidase in U-937 cells **(A)** and THP-1 cells **(B)**. Control (a) and proteins isolated from EVs co-cultured with U-937 cells (c). In b and d, U-937 and THP-1 cells were differentiated using 250 nM PMA and 150 nM PMA, respectively, in the absence and presence of EVs. In lanes e and f, differentiation was induced using 5 µM in the absence and presence of EVs, respectively, while in lanes f and h, 10 µM ascorbic acid was used. The densitometric quantification of NOX2 expression is presented in the lower panel within the figure.

exosomal protein markers. CD63 is a 30–60 kDa lysosomal membrane protein that is composed of four alpha-helical transmembrane domains with two extracellular loops (Jung et al., 2006; Gonzalez et al., 2014). Both the N- and the C-terminus point toward the inside of EVs. In EVs, several tetraspanins, especially CD63, CD81, and CD9, have been used as markers of EVs for the last 2 decades. In our study, endogenous CD63 was monitored as a surface marker for EVs (Kim et al., 2019; Mathieu et al., 2021). Proteins were extracted using the procedure outlined in Section 2.6 from EVs obtained through centrifugation. Our immunoblotting analysis revealed a single band with a molecular weight of approximately 60 kDa (Figure 2 and Supplementary Data S2) in U-937 and THP-1 cells. The band at 60 kDa is most likely due to post-translational modifications (glycosylation of CD63 protein) (Engering et al., 2003). Bands at different positions in the range 30 kDa–85 kDa have been reported which can be due to multiple reasons such as but not limited to post-translational modifications and proteolytic cleavage, and other experimental factors (Engering et al., 2003).

3.3 Co-culture of monocytes with EVs during differentiation induction

Cells were treated with differentiation inducers in the absence and presence of EVs (Figure 3). In order to evaluate whether the addition of differentiation inducers led to a change in cell viability of U-937 cells, the trypan blue test was performed in all experimental samples at 24 h and 72 h, including those treated with EVs. In the control (no differentiation agent + no EVs), a viability percentage of 90% and 80% were observed at 24 h and 72 h, respectively. In PMA-differentiated specimens, the recorded viability was 86.5% at 24 h and increased to 95% at 72 h. On the contrary, in samples treated with ascorbic acid, viability remained consistently in the same range, exceeding 80% at various concentrations (5 µM and 10 µM). In EVs treated samples differentiated using PMA, 88% viability was observed at 24 h and 94% at 72 h was recorded. Similarly, in EVs treated samples differentiated using ascorbic acid, it was recorded to be in the same range and maintained above 80% at different concentrations (5 µM and 10 µM); the details have been
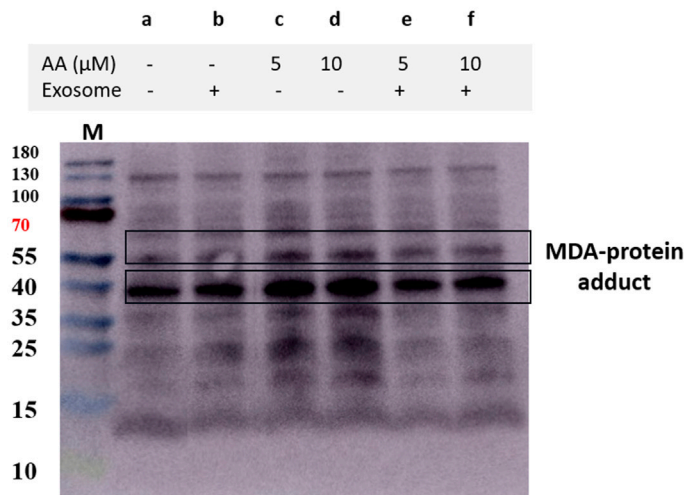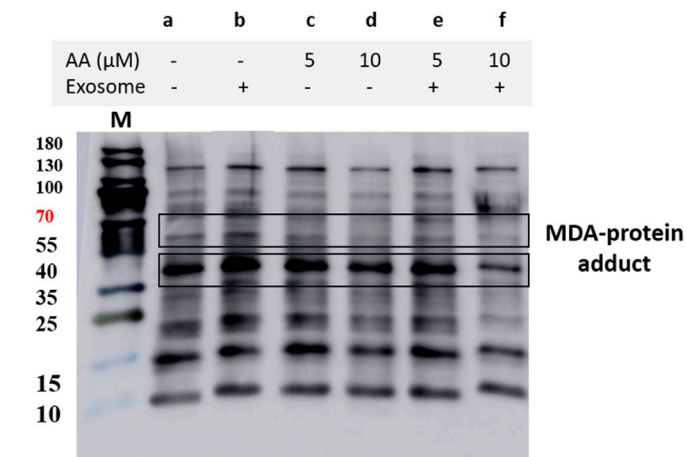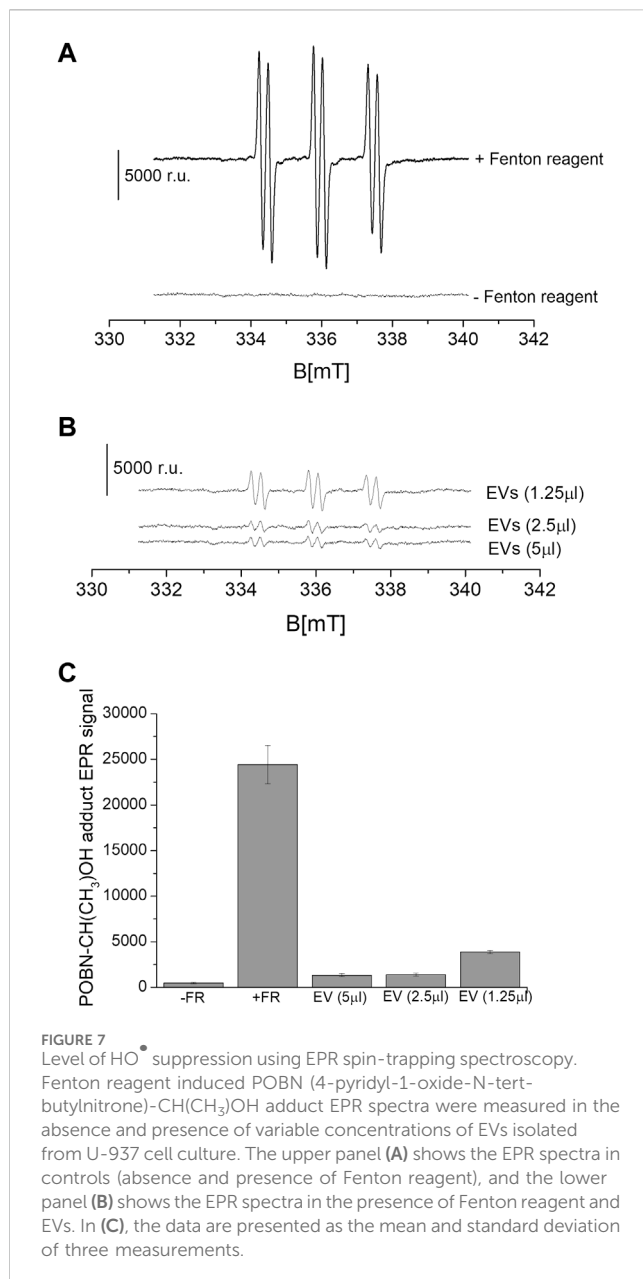
FIGURE 6
Protein MDA adducts formed in U-937 **(A)** and THP-1 cells **(B)** treated with different inducers. The blot illustrates protein modification in cells that were differentiated for 72 h, visualized using anti-MDA antibody. Lane a shows the control and lane b shows the proteins isolated from EVs co-cultured with cells. In lanes c and e, differentiation was induced using 5 μM in the absence and presence of EVs, respectively, while in d and f, 10 μM ascorbic acid was used.

presented in the form of Table (Supplementary Data S3). On the basis of this dataset, it can be concluded that neither exogenous addition of differentiation agents (either PMA or ascorbic acid) nor supplementation of EVs led to any stress leading to alterations in cell proliferation and viability.

3.4 NOX4 and NOX2 expression in monocytes and macrophages

Based on immunoblotting using NOX4 antibody, we monitored its expression at 67 kDa. In a non-differentiated control, a visible expression of NOX4 can be observed, which is typical for monocytes, as monocytes are well known to express this isoform. In differentiated controls [either PMA or ascorbic acid (5 μM and 10 μM)], the expression of NOX4 is slightly suppressed in all cases

except for 10 μM ascorbic acid, which can be hypothesized based on the fact that NOX4 expression is not a characteristic of macrophages. However, under the condition where the EVs are present along with cells, no influence on NOX4 expression is evident compared to the control. Interestingly, in differentiated cells supplemented with EVs for 72 h, a strong suppression of NOX4 expression is evident (especially in ascorbic acid differentiated cells and U-937 cells), which can be hypothesized that when monocytes are transformed to macrophages, NOX4 expression might have been regulated by microRNA (miRNA) (Figure 4). Interestingly, NOX2 expression was found to be only suppressed in macrophages co-cultured with EVs, predominantly in U-937, while in THP-1 cells, no significant suppression was observed (Figure 5). In monocytes co-cultured with EV, an increase in NOX2 expression was observed [Figure 5A (lane c) and Figure 5B (lane c)].

FIGURE 7
Level of HO$^\bullet$ suppression using EPR spin-trapping spectroscopy. Fenton reagent induced POBN (4-pyridyl-1-oxide-N-tert-butylnitrone)-CH(CH$_3$)OH adduct EPR spectra were measured in the absence and presence of variable concentrations of EVs isolated from U-937 cell culture. The upper panel **(A)** shows the EPR spectra in controls (absence and presence of Fenton reagent), and the lower panel **(B)** shows the EPR spectra in the presence of Fenton reagent and EVs. In **(C)**, the data are presented as the mean and standard deviation of three measurements.

In THP-1 cells, we validated our findings using immunoprecipitation of NOX2 using NOX2 antibody and protein A agarose beads. NOX2 expression was found to be significantly suppressed in EVs co-cultured macrophages (Supplementary Data S7). We also observed a decrease in overall MDA formation in EVs treated macrophages (Figure 6), which agrees with previous reports (Song et al., 2015; Song et al., 2021).

3.5 Crosstalk between EVs and oxidative stress

We measured the suppression of ROS under the exogenous addition of EVs on chemically generated HO$^\bullet$. The intensity of the EPR signal was observed in the control samples (Figure 7A).

It can be seen that in the sample that did not contain a Fenton reagent (negative control), a relative signal intensity of about ~800 was observed. Chemically generated HO$^\bullet$ using Fenton reagent (0.1 μM FeSO$_4$ and 2 mM H$_2$O$_2$) led to a high signal intensity reflecting the formation of α-hydroxyethyl radical adduct of POBN [POBN-CH(CH$_3$)OH adduct] (Figure 7A). The intensity of the EPR signal was found to be significantly and linearly suppressed with the exogenous addition of EVs in a dose-dependent manner (Figures 7B, C). The addition of EVs suppressed the signal by up to almost 90%, indicating the antioxidant capacity of the EVs. EVs specifically exosomes mitigate oxidative stress in recipient cells by directly delivering the enzymatic antioxidant [GSH, superoxidedismutase1 (SOD1), thioredoxinreductase1 (TrxR1), methioredoxin reductase (TrxR2) and glutathione peroxidase, among others] or antioxidative enzyme mRNA that later translates aiding to prevention of oxidative stress (Yan et al., 2017; Lin et al., 2022). EVs therapy therefore can be contemplated as an emerging and promising area of regenerative medicine (Muthu et al., 2021; Thakur et al., 2022). EVs through the transfer of cargo to recipient cells can influence cellular functions and therefore, exosomes isolated from different sources can specifically be chosen to target different therapeutic applications. It has been applied in regenerative medicine to promote tissue repairs, in neurological disorders such as Alzheimer's and Parkinson's disease, in cancer therapy, among others (Gao et al., 2021; Zhang et al., 2023).

4 Conclusion

In our study, monocyte-derived EVs suppressed NOX4 and NOX2 expression in differentiated macrophages, indicating a regulation of NADPH oxidase expression in cells supplemented with EVs from monocytes; the regulation is supposedly at the transcription or translation level. The addition of EVs led to suppression of lipid peroxidation and eventually led to a lower protein modification, which is consistent with recent reports that claim EVs as carriers of antioxidants. Based on the study, EVs can be claimed as a good candidate for therapeutic application in diseases associated with oxidative stress. Typically, the administration of antioxidants in cells is mediated through liposomes preparation. In the case of EVs therapy, this challenge can be easily overcome, as the uptake by cells should be much more efficient.

Data availability statement

The raw data supporting the conclusion of this article will be made available by the authors, without undue reservation.

Ethics statement

Ethical approval was not required for the studies on humans in accordance with the local legislation and institutional requirements because only commercially available established cell lines were used.

Author contributions

DR: Conceptualization, Data curation, Formal Analysis, Investigation, Methodology, Writing–original draft. CR: Formal Analysis, Methodology, Writing–review and editing. PP: Formal Analysis, Writing–review and editing. RR: Formal Analysis, Validation, Writing–review and editing. LT: Data curation, Formal Analysis, Methodology, Writing–review and editing. AM: Methodology, Validation, Writing–review and editing. AP: Conceptualization, Data curation, Formal Analysis, Funding acquisition, Investigation, Methodology, Project administration, Supervision, Validation, Visualization, Writing–original draft, Writing–review and editing.

Funding

Conflict of interest

The authors declare that the research was conducted in the absence of any commercial or financial relationships that could be construed as a potential conflict of interest.

Publisher's note

All claims expressed in this article are solely those of the authors and do not necessarily represent those of their affiliated organizations, or those of the publisher, the editors and the reviewers. Any product that may be evaluated in this article, or claim that may be made by its manufacturer, is not guaranteed or endorsed by the publisher.

Supplementary material

The Supplementary Material for this article can be found online at: https://www.frontiersin.org/articles/10.3389/fcell.2024.1342227/full#supplementary-material

References

Ayala, A., Munoz, M. F., and Arguelles, S. (2014). Lipid peroxidation: production, metabolism, and signaling mechanisms of malondialdehyde and 4-hydroxy-2-nonenal. *Oxid. Med. Cell Longev.* 2014, 360438. doi:10.1155/2014/360438

Barile, L., and Vassalli, G. (2017). Exosomes: therapy delivery tools and biomarkers of diseases. *Pharmacol. Ther.* 174, 63–78. doi:10.1016/j.pharmthera.2017.02.020

Bedard, K., and Krause, K.-H. (2007). The NOX family of ROS-generating NADPH oxidases: physiology and pathophysiology. *Physiol. Rev.* 87 (1), 245–313. doi:10.1152/physrev.00044.2005

Bermudez, S., Khayrullina, G., Zhao, Y. J., and Byrnes, K. R. (2016). NADPH oxidase isoform expression is temporally regulated and may contribute to microglial/macrophage polarization after spinal cord injury. *Mol. Cell. Neurosci.* 77, 53–64. doi:10.1016/j.mcn.2016.10.001

Chen, H. W., Chengalvala, V., Hu, H. X., and Sun, D. X. (2021). Tumor-derived exosomes: nanovesicles made by cancer cells to promote cancer metastasis. *Acta Pharm. Sin. B* 11 (8), 2136–2149. doi:10.1016/j.apsb.2021.04.012

Dalrymple, A., McEwan, M., Brandt, M., Bielfeldt, S., Bean, E. J., Moga, A., et al. (2022). A novel clinical method to measure skin staining reveals activation of skin damage pathways by cigarette smoke. *Skin Res. Technol.* 28 (1), 162–170. doi:10.1111/srt.13108

Di Bella, M. A. (2022). Overview and update on extracellular vesicles: considerations on exosomes and their application in modern medicine. *Biology-Basel* 11 (6), 804. doi:10.3390/biology11060804

Doyle, L. M., and Wang, M. Z. (2019). Overview of extracellular vesicles, their origin, composition, purpose, and methods for exosome isolation and analysis. *Cells* 8 (7), 727. doi:10.3390/cells8070727

Engering, A., Kuhn, L., Fluitsma, D., Hoefsmit, E., and Pieters, J. (2003). Differential post-translational modification of CD63 molecules during maturation of human dendritic cells. *Eur. J. Biochem.* 270 (11), 2412–2420. doi:10.1046/j.1432-1033.2003.03609.x

Gao, L., Wang, L., Dai, T., Jin, K., Zhang, Z. K., Wang, S., et al. (2018). Tumor-derived exosomes antagonize innate antiviral immunity. *Nat. Immunol.* 19 (3), 233–245. doi:10.1038/s41590-017-0043-5

Gao, P., Li, X., Du, X., Liu, S., Xu, Y., Qi, D., et al. (2021). Intermediate effects of body mass index and C-reactive protein on the serum cotinine- leukocyte telomere length association. *Front. Aging Neurosci.* 13, 827465. doi:10.3389/fnagi.2021.827465

Genneback, N., Hellman, U., Malm, L., Larsson, G., Ronquist, G., Waldenstrom, A., et al. (2013). Growth factor stimulation of cardiomyocytes induces changes in the transcriptional contents of secreted exosomes. *J. Extracell. Vesicles* 2 (1). doi:10.3402/jev.v2i0.20167

Gonzalez, A., Valeiras, M., Sidransky, E., and Tayebi, N. (2014). Lysosomal integral membrane protein-2: a new player in lysosome-related pathology. *Mol. Genet. Metabolism* 111 (2), 84–91. doi:10.1016/j.ymgme.2013.12.005

Hahner, F., Moll, F., and Schroder, K. (2020). NADPH oxidases in the differentiation of endothelial cells. *Cardiovasc. Res.* 116 (2), 262–268. doi:10.1093/cvr/cvz213

Hervera, A., De Virgiliis, F., Palmisano, I., Zhou, L. M., Tantardini, E., Kong, G. P., et al. (2018). Reactive oxygen species regulate axonal regeneration through the release of exosomal NADPH oxidase 2 complexes into injured axons. *Nat. Cell Biol.* 20 (3), 307–319. doi:10.1038/s41556-018-0039-x

Johnson, S. M., Banyard, A., Smith, C., Mironov, A., and McCabe, M. G. (2020). Large extracellular vesicles can be characterised by multiplex labelling using imaging flow cytometry. *Int. J. Mol. Sci.* 21 (22), 8723. doi:10.3390/ijms21228723

Jung, K. K., Liu, X. W., Chirco, R., Fridman, R., and Kim, H. R. C. (2006). Identification of CD63 as a tissue inhibitor of metalloproteinase-1 interacting cell surface protein. *Embo J.* 25 (17), 3934–3942. doi:10.1038/sj.emboj.7601281

Kalluri, R., and LeBleu, V. S. (2020). The biology, function, and biomedical applications of exosomes. *Science* 367 (6478), eaau6977. doi:10.1126/science.aau6977

Kim, T. H., Hong, S. B., Lim, C. M., Koh, Y., Jang, E. Y., and Huh, J. W. (2019). The role of exosomes in bronchoalvearo lavage from patients with acute respiratory distress syndrome. *J. Clin. Med.* 8 (8), 1148. doi:10.3390/jcm8081148

Krishnamoorthy, L., and Chang, C. J. (2018). Exosomal NADPH oxidase: delivering redox signaling for healing. *Biochemistry* 57 (27), 3993–3994. doi:10.1021/acs.biochem.8b00429

Landry, W. D., and Cotter, T. G. (2014). ROS signalling, NADPH oxidases and cancer. *Biochem. Soc. Trans.* 42, 934–938. doi:10.1042/BST20140060

Lau, N. C. H., and Yam, J. W. P. (2023). From exosome biogenesis to absorption: key takeaways for cancer research. *Cancers* 15 (7), 1992. doi:10.3390/cancers15071992

Lin, T. Y., Chang, T. M., and Huang, H. C. (2022). Extracellular vesicles derived from human umbilical cord mesenchymal stem cells attenuate mast cell activation. *Antioxidants* 11 (11), 2279. doi:10.3390/antiox11112279

Manoharan, R. R., Sedlářová, M., Pospíšil, P., and Prasad, A. (2023). Detection and characterization of free oxygen radicals induced protein adduct formation in differentiating macrophages. *Biochimica biophysica acta. General Subj.* 1867 (5), 130324. doi:10.1016/j.bbagen.2023.130324

Mathieu, M., Nevo, N., Jouve, M., Valenzuela, J. I., Maurin, M., Verweij, F. J., et al. (2021). Specificities of exosome versus small ectosome secretion revealed by live intracellular tracking of CD63 and CD9. *Nat. Commun.* 12 (1), 4389. doi:10.1038/s41467-021-24384-2

Mittler, R., Vanderauwera, S., Suzuki, N., Miller, G., Tognetti, V. B., Vandepoele, K., et al. (2011). ROS signaling: the new wave? *Trends Plant Sci.* 16 (6), 300–309. doi:10.1016/j.tplants.2011.03.007

Muthu, S., Bapat, A., Jain, R., Jeyaraman, N., and Jeyaraman, M. (2021). Exosomal therapy-a new frontier in regenerative medicine. *Stem Cell Investig.* 8, 7. doi:10.21037/sci-2020-037

Nederveen, J. P., Warnier, G., Di Carlo, A., Nilsson, M. I., and Tarnopolsky, M. A. (2021). Extracellular vesicles and exosomes: insights from exercise science. *Front. Physiology* 11, 604274. doi:10.3389/fphys.2020.604274

Pospíšil, P., Prasad, A., and Rác, M. (2019). Mechanism of the formation of electronically excited species by oxidative metabolic processes: role of reactive oxygen species. *Biomolecules* 9 (7), 258. doi:10.3390/biom9070258

Pou, S., Ramos, C. L., Gladwell, T., Renks, E., Centra, M., Young, D., et al. (1994). A kinetic approach to the selection of a sensitive spin-trapping system for the detection of hydroxyl radical. *Anal. Biochem.* 217 (1), 76–83. doi:10.1006/abio.1994.1085

Prasad, A., Duchová, H., Manoharan, R. R., Rathi, D., and Pospíšil, P. (2023). Imaging and characterization of oxidative protein modifications in skin. *Int. J. Mol. Sci.* 24 (4), 3981. doi:10.3390/ijms24043981

Prasad, A., Manoharan, R. R., Sedlářová, M., and Pospíšil, P. (2021). Free radical-mediated protein radical formation in differentiating monocytes. *Int. J. Mol. Sci.* 22 (18), 9963. doi:10.3390/ijms22189963

Shelke, G. V., Lasser, C., Gho, Y. S., and Lotvall, J. (2014). Importance of exosome depletion protocols to eliminate functional and RNA-containing extracellular vesicles from fetal bovine serum. *J. Extracell. Vesicles* 3 (1). doi:10.3402/jev.v3.24783

Shu, S. L., Allen, C. L., Benjamin-Davalos, S., Koroleva, M., MacFarland, D., Minderman, H., et al. (2021). A rapid exosome isolation using ultrafiltration and size exclusion chromatography (REIUS) method for exosome isolation from melanoma cell lines. *MELANOMA Methods Protoc.* 2265, 289–304. doi:10.1007/978-1-0716-1205-7_22

Song, M. G., Ryoo, I. G., Choi, H. Y., Choi, B. H., Kim, S. T., Heo, T. H., et al. (2015). NRF2 signaling negatively regulates phorbol-12-myristate-13-acetate (PMA)-Induced differentiation of human monocytic U937 cells into pro-inflammatory macrophages. *Plos One* 10 (7), e0134235. doi:10.1371/journal.pone.0134235

Song, Y. F., Wang, B. C., Zhu, X. L., Hu, J. L., Sun, J. J., Xuan, J. Z., et al. (2021). Human umbilical cord blood-derived MSCs exosome attenuate myocardial injury by inhibiting ferroptosis in acute myocardial infarction mice. *Cell Biol. Toxicol.* 37 (1), 51–64. doi:10.1007/s10565-020-09530-8

Surman, M., Stepien, E., Hoja-Lukowicz, D., and Przybylo, M. (2017). Deciphering the role of exosomes in cancer development and progression: focus on the proteome. *Clin. Exp. Metastasis* 34 (3-4), 273–289. doi:10.1007/s10585-017-9844-z

Suzuki, Y. J., Carini, M., and Butterfield, D. A. (2010). Protein carbonylation. *Antioxid. Redox Signal* 12 (3), 323–325. doi:10.1089/ars.2009.2887

Takahashi, A., Okada, R., Nagao, K., Kawamata, Y., Hanyu, A., Yoshimoto, S., et al. (2017). Exosomes maintain cellular homeostasis by excreting harmful DNA from cells. *Nat. Commun.* 8, 15287. doi:10.1038/ncomms15287

Thakur, A., Parra, D. C., Motallebnejad, P., Brocchi, M., and Chen, H. J. (2022). Exosomes: small vesicles with big roles in cancer, vaccine development, and therapeutics. *Bioact. Mater.* 10, 281–294. doi:10.1016/j.bioactmat.2021.08.029

Tola, A. J., Jaballi, A., and Missihoun, T. D. (2021). Protein carbonylation: emerging roles in plant redox biology and future prospects. *Plants-Basel* 10 (7), 1451. doi:10.3390/plants10071451

Tsikas, D. (2017). Assessment of lipid peroxidation by measuring malondialdehyde (MDA) and relatives in biological samples: analytical and biological challenges. *Anal. Biochem.* 524, 13–30. doi:10.1016/j.ab.2016.10.021

van Niel, G., D'Angelo, G., and Raposo, G. (2018). Shedding light on the cell biology of extracellular vesicles. *Nat. Rev. Mol. Cell Biol.* 19 (4), 213–228. doi:10.1038/nrm.2017.125

Yan, Y. M., Jiang, W. Q., Tan, Y. W., Zou, S. Q., Zhang, H. G., Mao, F., et al. (2017). hucMSC exosome-derived GPX1 is required for the recovery of hepatic oxidant injury. *Mol. Ther.* 25 (2), 465–479. doi:10.1016/j.ymthe.2016.11.019

Zhang, M., Hu, S., Liu, L., Dang, P., Liu, Y., Sun, Z., et al. (2023). Engineered exosomes from different sources for cancer-targeted therapy. *Signal Transduct. Target. Ther.* 8 (1), 124. doi:10.1038/s41392-023-01382-y

Zhang, W. J., Liu, R., Chen, Y. H., Wang, M. H., and Du, J. (2022). Crosstalk between oxidative stress and exosomes. *Oxidative Med. Cell. Longev.* 2022, 1–11. doi:10.1155/2022/3553617
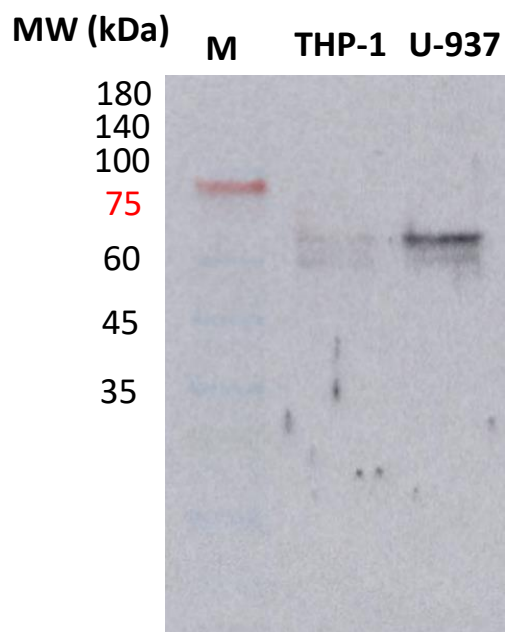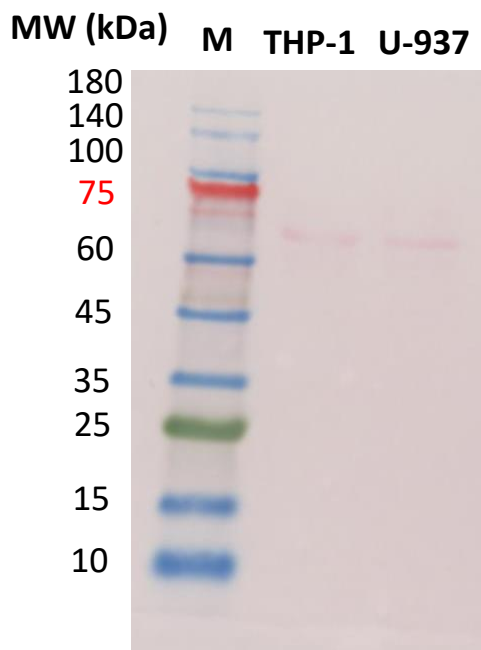
Supplementary data 1

	M	1	2
250			
130			
100			
70			
55			
35			
25			
15			
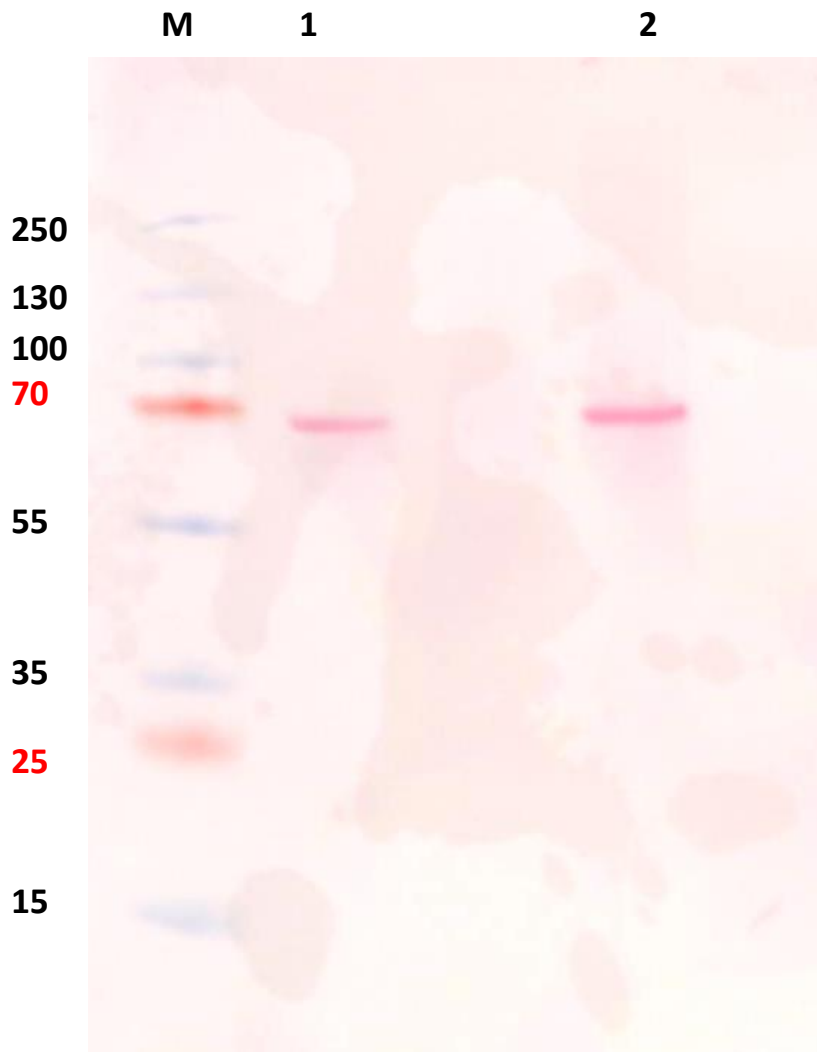
[1] Centrifugation
[2] PEG enrichment

Supplementary data 2 (replicate of Figure 2)

Supplementary data 3

Condition (24h)	total cells/mL	viable cells/mL	viability%		total cells/mL	viable cells/mL	viability%
U937	350000	311000	89		144000	133000	92
U937+PMA	1130000	977000	87		411000	355000	86
U937+Exosome	2140000	1640000	77		422000	389000	92
U937+PMA+Exosome	3400000	2930000	86		511000	461000	90
U937+5μM AA	1270000	1190000	94		417000	383000	92
U937+10μM AA	1730000	1640000	95		1620000	1550000	96
U937+5μM AA+ Exosome	7080000	4450000	91		3770000	3190000	85
U937+10μM AA+ Exosome	7410000	6220000	84		328000	294000	90

Condition (48h)	total cells/mL	viable cells/mL	viability%		total cells/mL	viable cells/mL	viability%
U937	1060000	794000	75		528000	450000	85
U937+PMA	1280000	1190000	96		761000	716000	94
U937+Exosome	816000	744000	91		939000	883000	94
U937+PMA+Exosome	361000	339000	94		372000	350000	94
U937+5μM AA	744000	666000	90		3380000	3210000	95
U937+10μM AA	722000	489000	68		2070000	1990000	96
U937+5μM AA+ Exosome	1790000	1520000	85		1360000	1280000	94
U937+10μM AA+ Exosome	994000	950000	96		1430000	1330000	93

Supplementary data 4- original blot (Figure 4)

A (U-937)

	a	b	c	d	e	f	g	h
AA (µM)	-	-	-	-	5	10	5	10
PMA (nM)	-	250	-	250	-	-	-	-
Exosome	-	-	+	+	-	-	+	+

MW — M

180
130
100
70
55
40
35
25
15
10

NOX4, 67 kDa

B (THP-1)

	a	b	c	d	e	f	g	h
AA (µM)	-	-	-	-	5	10	5	10
PMA (nM)	-	150	-	150	-	-	-	-
Exosome	-	-	+	+	-	-	+	+

MW — M

180
140
100
75
60
45
35
25
15
10

NOX4, 67 kDa
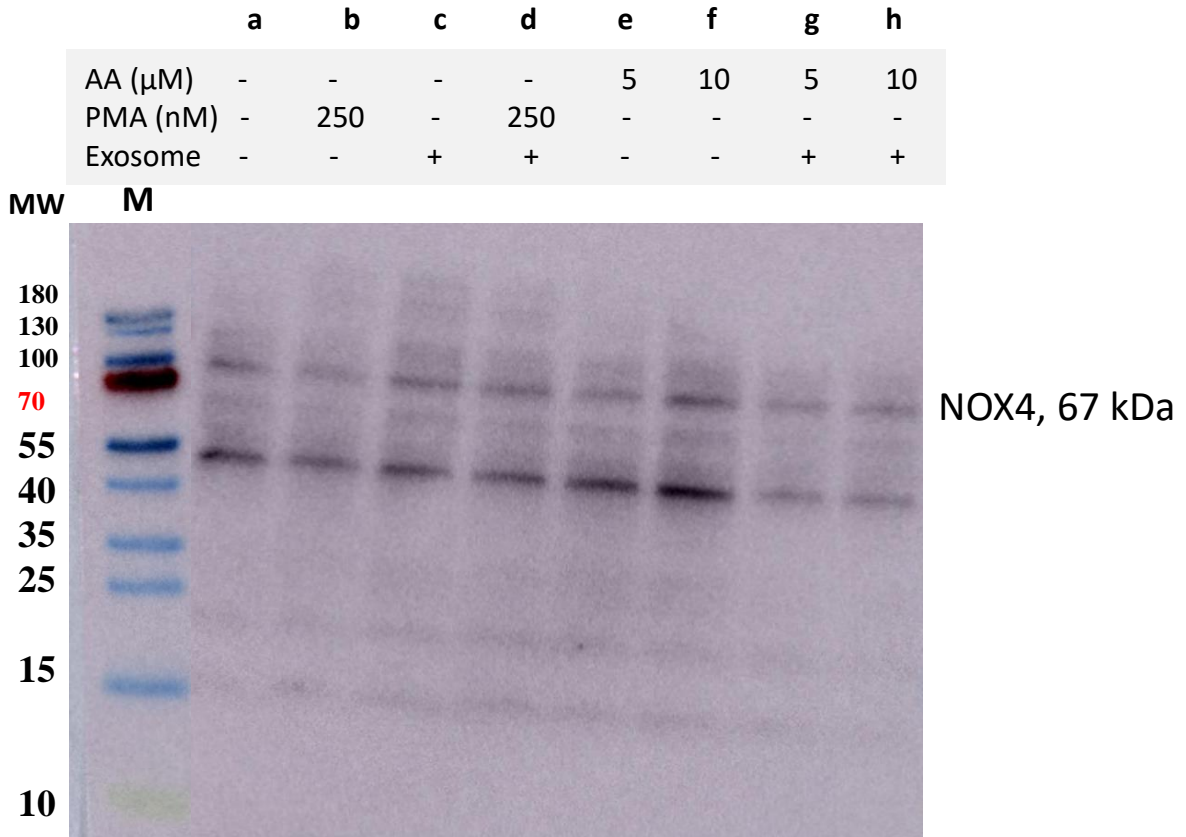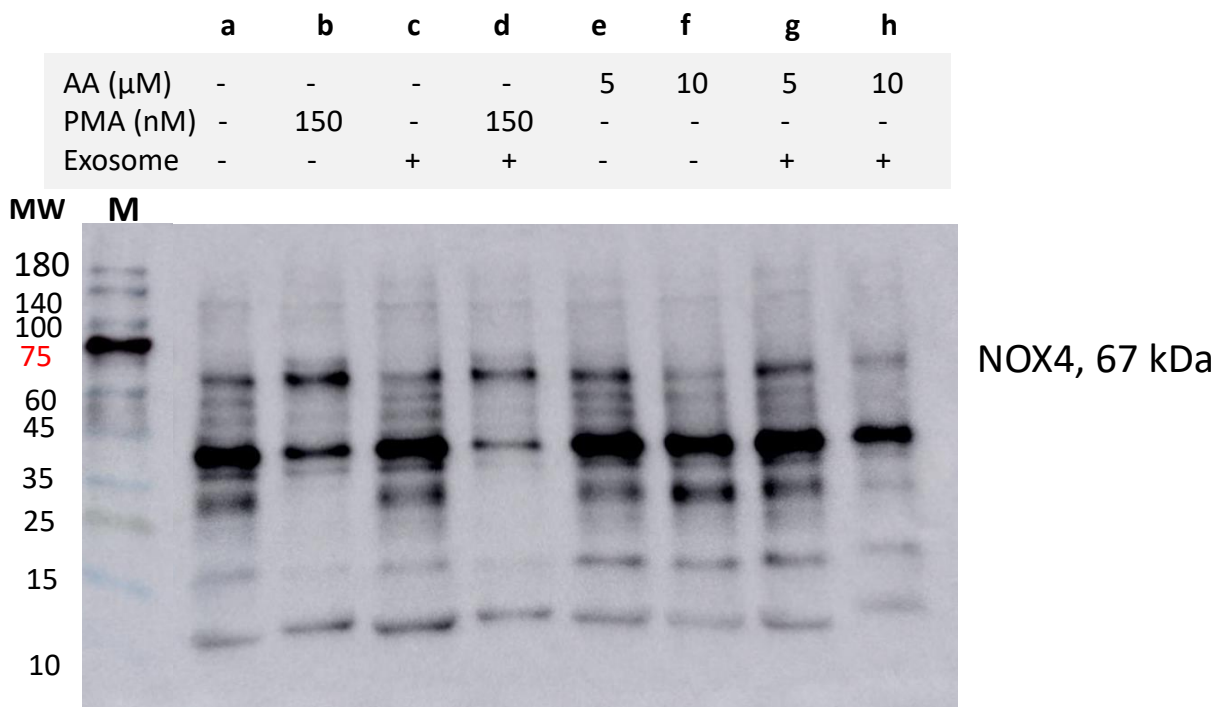
Supplementary data 5- original blot (Figure 5)

A (U-937)

	a	b	c	d	e	f	g	h
AA (µM)	-	-	-	-	5	10	5	10
PMA (nM)	-	250	-	250	-	-	-	-
Exosome	-	-	+	+	-	-	+	+

NOX2, ~65 kDa

M
180
140
100
75
60
45
35
25
15

B (THP-1)

	a	b	c	d	e	f	g	h
AA (µM)	-	-	-	-	5	10	5	10
PMA (nM)	-	150	-	150	-	-	-	-
Exosome	-	-	+	+	-	-	+	+

MW
M
180
140
100
75
60
45
35
25
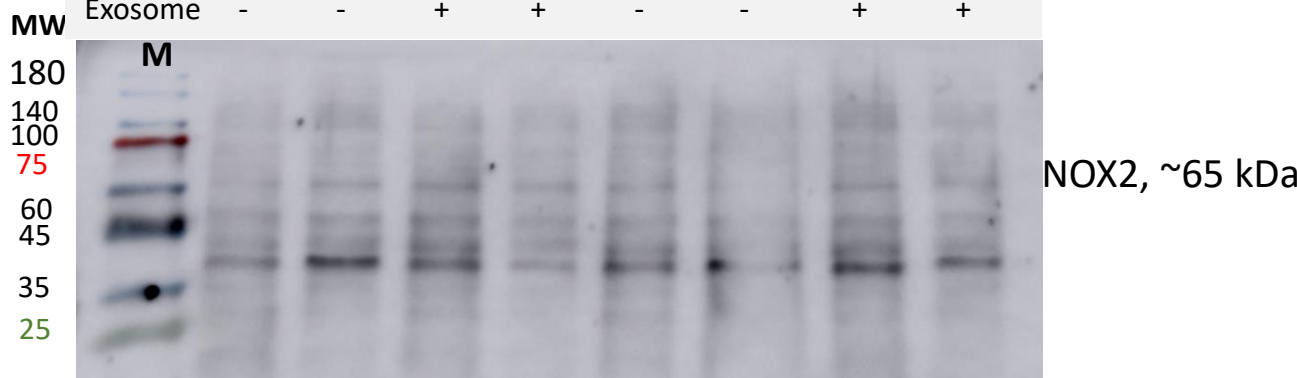
NOX2, ~65 kDa

Supplementary data 6- replicate of Figure 5

U-937

	a	b	c	d	e	f	g	h
AA (µM)	-	-	-	-	5	10	5	10
PMA (nM)	-	250	-	250	-	-	-	-
Exosome	-	-	+	+	-	-	+	+

NOX2, ~65 kDa

Supplementary data 7

	a	b	c	d	e	f	g	h
AA (µM)	-	-	-	-	5	10	5	10
PMA (nM)	-	150	-	150	-	-	-	-
Exosome	-	-	+	+	-	-	+	+

MW (kDa) M
180
140
100
75
60 — NOX2
45
35
25
15
10
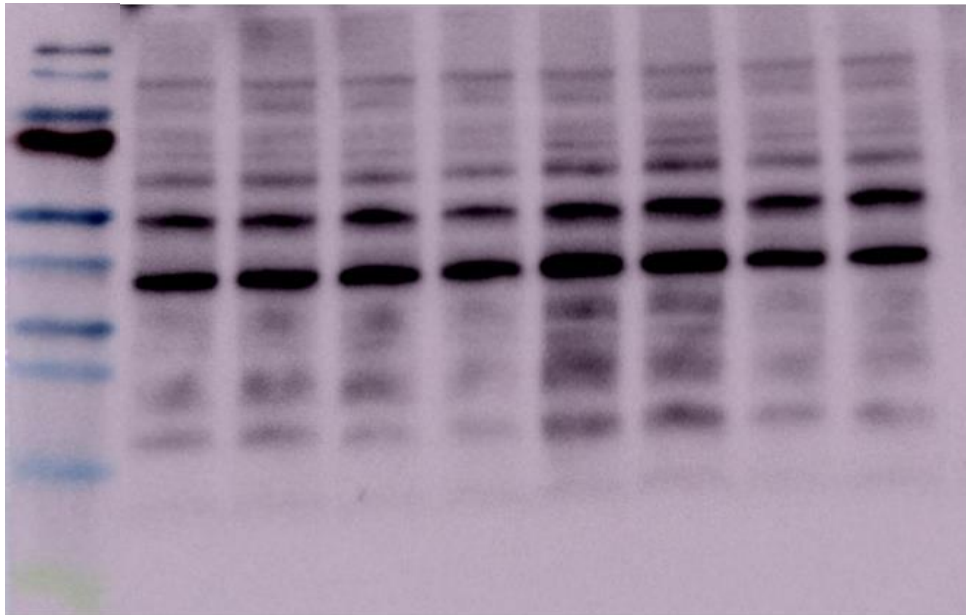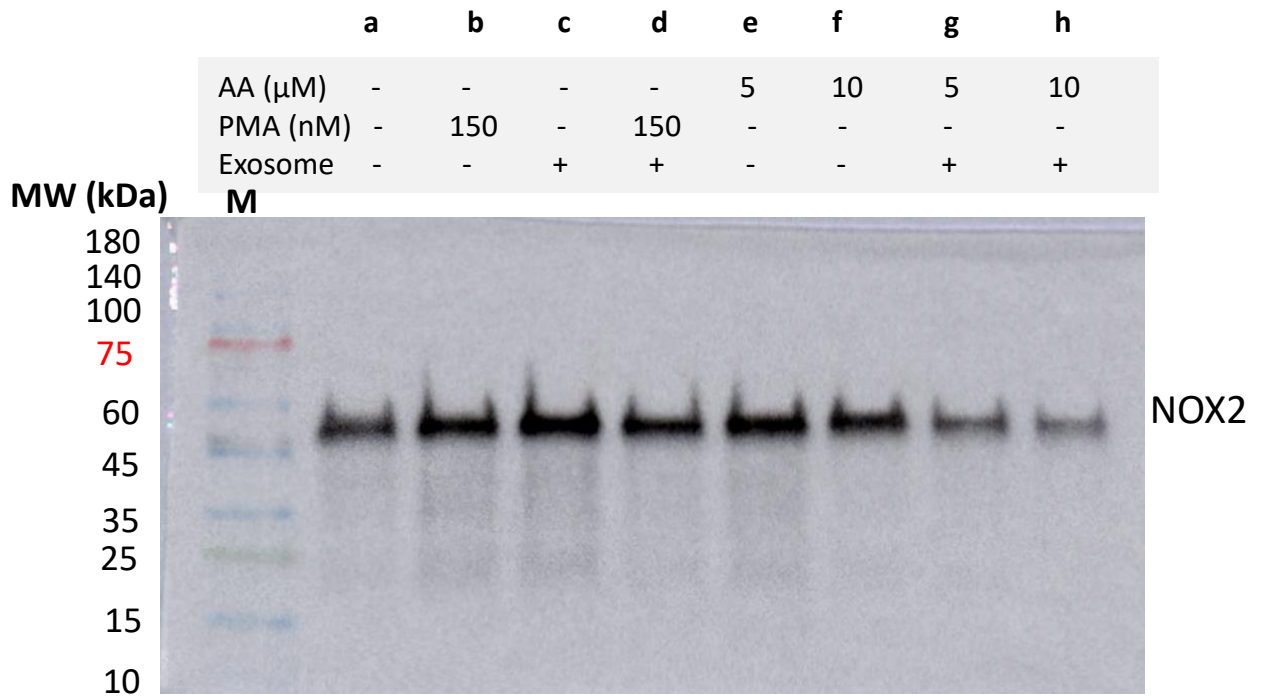
Workflow:

- Protein extraction (as described in manuscript)
- 10 µg protein lysate per variant taken for immunoprecipitation
- Primary antibody (0.25µg, anti-NOX2 antibody)/ sample variant
- Protein lysate and antibody incubated with gentle rocking at 4 ° C overnight.
- Protein A bound to beads (50 µl /mL of cell lysate) added and incubated for 2 hours at 4°C with gentle shaking.
- Washing the beads at 3,000 g for 2 min at 4°C with 1 mL of pre-cooled TBS (collect pellet) (3x).
- Re-suspended in 75µL Tris-buffer saline.
- 25 µL SDS Sample Buffer added; vortex and then centrifuged for 30 s (5000 rpm).
- Sample heated to 100°C for 5 minutes.
- Centrifugation at 10,000 rpm for 2 min.
- Supernatant collected (contains protein of interest) followed by SDS and western blotting.

Supplementary data 8

THP-1

	a	b	c	d	e	f	g	h
AA (μM)	-	-	-	-	5	10	5	10
PMA (nM)	-	150	-	150	-	-	-	-
Exosome	-	-	+	+	-	-	+	+
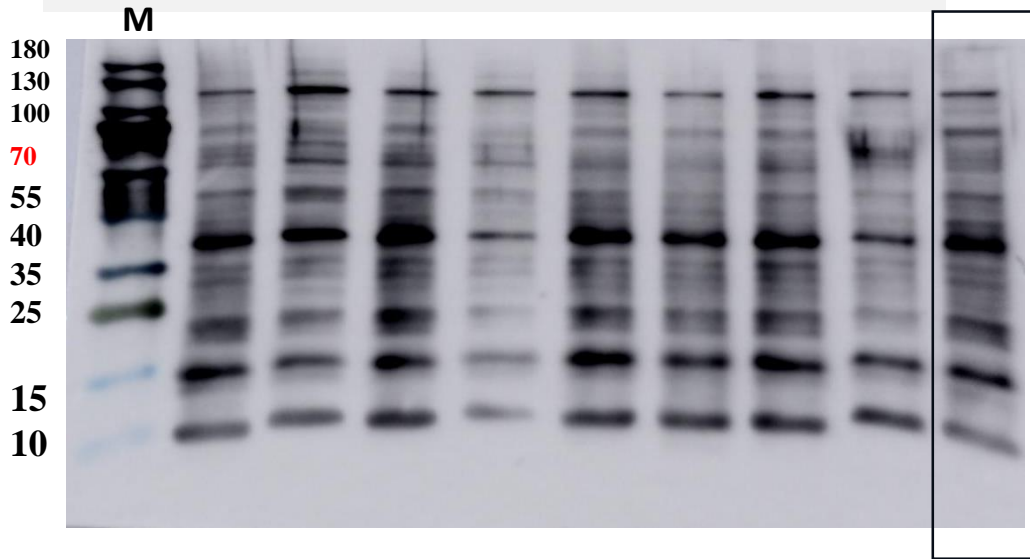
MDA-protein adduct
(positive control with
0.3% H_2O_2)

Supplementary data 9

<u>Chemicals and antibodies:</u>

Ponceau S, Sigma Aldrich (P3504)

Trypan blue, Sigma Aldrich (T6146)

RPMI 1640 w/ stable Glutamine - Biosera (LM-R1639)

Fetal Bovine Serum Qualified – Biosera (FB-1090)

Penicillin-Streptomycin-Glutamine Solution 100X - Serana (RAL-001)

Anti-Malondialdehyde polyclonal antibody, Abcam (ab27642)

Goat Anti-Rabbit IgG (H+L)-HRP Conjugate BioRad (1721019)

NOX4- Monoclonal antibody ab 133303 (Abcam)

NOX2 Polyclonal antibody 19013-1-AP (Proteintech)

CD63 Monoclonal antibody (67605-1-Ig) (Proteintech)

CD9 Monoclonal antibody Proteintech (60232-1-Ig)

HRP-conjugated Affinipure Goat Anti-Mouse IgG(H+L) (SA00001-1)

PageRuler Prestained protein ladder- Thermoscientific (26616)

PageRuler Prestained protein ladder- Thermoscientific (26619)

Prestained protein marker - Proteintech (PL00001)

Protein A-Agarose- Santa Cruz Biotechnology (sc-2001)

Differential effects of ascorbic acid on monocytic cell morphology and protein modification: Shifting from pro-oxidative to antioxidant properties

Ankush Prasad [a,*], Deepak Rathi [a], Michaela Sedlářová [b], Renuka Ramalingam Manoharan [a], Eliška Průdková [a], Pavel Pospíšil [a]

[a] Department of Biophysics, Faculty of Science, Palacký University, Šlechtitelů 27, 783 71, Olomouc, Czech Republic
[b] Department of Botany, Faculty of Science, Palacký University, Šlechtitelů 27, 783 71, Olomouc, Czech Republic

ARTICLE INFO

ABSTRACT

In this study, we investigated the properties of ascorbic acid (vitamin C), which is a naturally occurring water-soluble vitamin. Our goal is to evaluate its pro-oxidative and/or antioxidant capabilities. To do this, we initially used a confocal laser scanning microscope (CLSM) to visualize the differentiation pattern in U-937 cells under the treatment of variable concentrations of ascorbic acid. Prior to induction, U-937 cells showed a spherical morphology. After treatment, significant morphological changes were observed in the form of prominent pseudopodia and amoeboid structures. Interestingly, pseudopodia incidences increased with an increase in ascorbic acid concentrations. In addition, our analysis of protein modification using anti-malondialdehyde antibodies showed changes in more than one protein. The findings reveal the link between the differentiation of U-937 cells into macrophages and the protein modifications triggered by the production of reactive oxygen species when U-937 cells are exposed to ascorbic acid. Furthermore, the transformation of ascorbic acid from a pro-oxidative to an antioxidant property is also demonstrated.

1. Introduction

Ascorbic acid (vitamin C) is a natural water-soluble vitamin and a potent reducing and antioxidant agent [1–3]. It functions in fighting bacterial infections, in detoxification, and, in the formation of collagen in fibrous tissue, teeth, bones, connective tissue, skin, and capillaries, besides absorption of iron [4,5]. Since it is obtained from food and available through a wide range of supplements, severe deficiency caused by ascorbic acid is rather rare. In unusual cases, it can lead to conditions such as weakness, fatigue, joint and muscle aches, and bleeding gums, which are also symptoms associated with scurvy [6].

Ascorbic acid is a powerful antioxidant and helps to protect the body from the harmful effects of free radicals [7] Besides this, ascorbic acid is essential for the synthesis of collagen, helps in stimulating the production of white blood cells, iron absorption, synthesis of neurotransmitters. It also acts as natural antihistamines and promotes the formation of connective tissues [8–12]. Free radicals or reactive oxygen species (ROS) are unstable molecules that can damage cells and are associated with the

development of chronic diseases such as cancer, heart diseases, and Alzheimer's disease [13–17]. Ascorbic acid, as an antioxidant, neutralizes free radicals by providing electrons to stabilize them, thus reducing their ability to cause cell damage [1,2]. It also helps regenerate other antioxidants, such as vitamin E, and further improves antioxidant properties [18,19]. It is also known for its anti-inflammatory effect; it is important to note that the body can absorb only limited amount of ascorbic acid at a time and that excessive amounts are excreted in the urine. Ascorbic acid supplements are usually safe, but excessive intake can cause side effects such as diarrhea, nausea, and stomach cramps.

Ascorbate (/ascorbate anion) can induce the transformation of Fe^{3+} into Fe^{2+}, which can lead to the formation of the hydroxyl radical ($HO^{\bullet}$) in the cytoplasmic pool. Due to this property, ascorbate (/ascorbate anion) can also act as a pro-oxidant. Additionally, the oxidation of ascorbate results in the generation of the ascorbyl radical ($AH^{\bullet}$) via monodehydroascorbate radical ($A^{\bullet-}$) [20,21]. Hence, it is essential to approach hypothesis formulation with utmost care to ascertain whether the experimentally obtained results stem directly from ascorbate or ROS

---

during cell supplementation.

In the current study, we aimed to evaluate the pro-oxidant and antioxidant capabilities of ascorbic acid. We have used the U-937 cell line, which is a pro-monocytic myeloid leukemia cell line of human origin [22]. Under *in vitro* conditions, an unlimited number of uniform cells can be prepared from U-937 cells [23]. These leukemia cells bear the t(10; 11)(p13; q14) translocation, which results in a fusion between the MLLT10 (myeloid/lymphoid or mixed-lineage leukemia) gene and the Ap-3-like clathrin assembly protein PICALM (clathrin assembly lymphoid myeloid leukemia), which is likely important for the tumorous nature of the cell line [24]. We investigated the relationship of ROS production under the effects of variable concentrations/the length of incubation of ascorbic acid. When the immune reactions are activated, monocytes migrate to different tissues and organs within the body. After reaching the target, depending on the specific signals from local micro-environments, they can be differentiated into diverse types of cells. One of the principal cell types which can be differentiated from monocytes are the macrophages. The monocyte-to-macrophage differentiation process involves several phases: Upon accessing the target tissue, monocytes are exposed to cytokines/chemokines which are secreted by the neighbouring cells. Following this, signalling pathways within the monocytes are initiated leading to changes in gene expression/cellular morphology, which is also a typical characteristic of macrophages. Macrophages acquire enlarged morphology with increased capacity for phagocytosis. Additionally, it has been known that the gene expression profile shifts to support macrophage-specific functions such as the generation of inflammatory mediators and the potential for antigen presentation.

Visualization of differentiation under induction was accomplished utilizing confocal laser scanning microscopy (CLSM). Interestingly, it has been shown that ascorbic acid has the potential as a differentiation agent, i.e., unspecialized cells become specialized in different types of cells with specific functions. Research shows that ascorbic acid can induce differentiation in various types of cells, including stem cells, cancerous cells, and immune cells [25,26]. In immune cells, ascorbic acid has been shown to improve the differentiation and function of certain types of immune cells, including T cells and dendritic cells. Overall, the ability of ascorbic acid to induce differentiation in different types of cells is an interesting field of research for potential therapeutic applications. Thus, instead of inducing differentiation using another chemical stimulant, we evaluated the dependence and relation of three parameters: differentiation induction of monocytes to macrophages in U-937, pro-oxidant concentration, and antioxidant concentration of ascorbic acid. Furthermore, protein immunoblotting was used to understand protein modification. Our results show a correlation between the differentiation of U-937 cells into macrophages and protein modification under the effect of generated ROS.

2. Materials and methods

2.1. Chemicals and antibodies

For blotting, a polyclonal anti-malondialdehyde (anti-MDA) antibody suitable for the measurement of MDA was used. The primary antibody was purchased from Abcam (Cambridge, CB2 0AX, UK) [Anti-Malondialdehyde antibody (ab27642)]; CD11b Monoclonal Antibody-FITC from eBioscience™ (ThermoFischer Scientific, USA) and secondary antibody was purchased from Bio-Rad (Hercules, CA, USA) [Goat Anti-Rabbit IgG-HRP Conjugate (1706515)]. Cell culture medium, antibiotics, and inhibitors used were from Biosera (Nuaillé, France) and Roche (Mannheim, Germany).

2.2. Cell line and growing condition

The U-937 cell line is a human pro-monocytic myeloid leukemia cell line [22] obtained from the American Type Culture Collection (ATCC;

Rockville, MD, USA). The TC20 automated cell counter (Bio-Rad Laboratories, Hercules, CA, United States) was used to determine cell density and was monitored using 0.25 % trypan blue dye. Experiments were performed when viability was close to or above 70 %. To growth medium (RPMI-1640) pre-supplemented with 0.05 mM L-glutamine were added 10 % fetal bovine serum (FBS) and 1 % of the antibiotics (penicillin and streptomycin) in v/v ratio.

2.3. Induction of differentiation

The differentiation of U-937 cells was studied under ascorbic acid concentrations ranging from 0.1 to 10 μM. Culture medium with 1×10^5 cell suspension/mL was supplemented with ascorbic acid at the final concentration of either 0.1 μM, 1 μM, 5 μM or 10 μM for 72h, and followed by a resting phase of 24 h to achieve cell adhesion and express macrophage characteristic cytokine expression. For validation, we also employed a widely recognized differentiation inducer, phorbol 12-myristate 13-acetate (PMA) (Sigma Aldrich, St. Louis, Missouri, United States) at final concentrations of 150 and 250 nM. The timing of the induction protocol was deduced from our pilot experiments focusing on U-937 cell differentiation stages in relation to ascorbic acid treatment.

2.4. Cell viability assay

The TC20 automated cell counter was used to determine the cell viability (expressed as total cell counts mL^{-1}) after incubation of U-937 cells with 0.25 % trypan blue in a ratio of 4:1 for approximately 2 min. Trypan blue is used to determine the ratio of living and dead cells in a cell suspension, and it is because the dye enters only dead cells and stains them blue, while live cells have intact cell membranes and remain bright and unstained [27]. In our experimental condition, cell density and viability were measured after treatment of U-937 cells with ascorbic acid for 72 h and following the 24 h resting period. The data obtained are presented in Fig. 1.

2.5. Confocal laser scanning microscopy

A Fluorview 1000 confocal unit attached to the IX80 microscope was used to image U-937 cells on glass slides (Olympus Czech Group, Prague, Czech Republic). Staining with FM4-64 (15 μM, RT), which is a lipophilic dye was used to monitor cell membrane integrity, and Hoechst 33342 (2 μM, RT) was used to visualize the nucleus under the experimental conditions mentioned. FM4-64 excitation was done using a 543 nm He–Ne laser and its emission was recorded in the range of 655–755 nm. The cells were co-stained with FM4-64 and Hoechst 33342 [Sigma Aldrich GmbH (Germany)]. Following an incubation of 5 min, the cells were transferred to a glass slide for visualization. For immunohistochemistry, after treatments with 5 μM and 10 μM ascorbic acid for 48 h, the culture medium was removed from the culture plates, and 3.5 % paraformaldehyde was added for cell fixation for 30 min. The cells were then washed three times with phosphate buffered saline containing 0.1 % Tween-20 (PBST) for 5 min each.

Afterward, the fixed cells were blocked with 0.5 % BSA in phosphate buffered saline (PBS) for 30 min at room temperature (RT). Subsequently, the blocked samples were probed with CD11b Monoclonal Antibody-FITC (dilution 1:2500) for 60 min at RT, followed by three washes with PBS (5 min each) and Immunofluorescence was measured using excitation achieved by a 488 nm line of an argon laser, and the signal was detected by a 505–550 nm emission filter.

2.6. Protein immunoblotting

Ascorbic acid (72 h, 0.1–10 μM) or PMA (72 h, 150 and 250 nM) pretreated U-937 cells were incubated in serum-free medium for 24 h (resting time), cells were then collected by centrifugation and washed with phosphate buffer saline (PBS) (pH 7.4) twice. Following this step,

A

72 h ascorbic acid treated
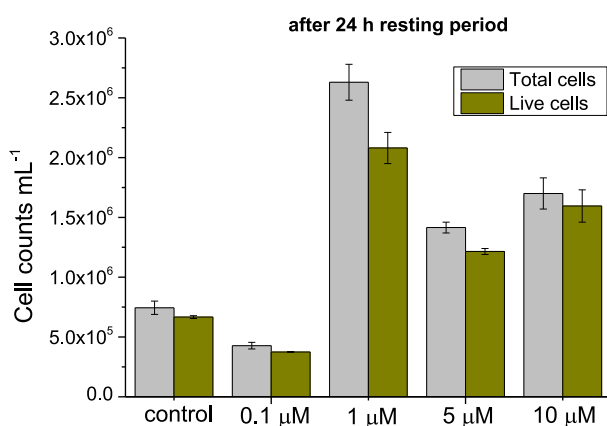

B

after 24 h resting period
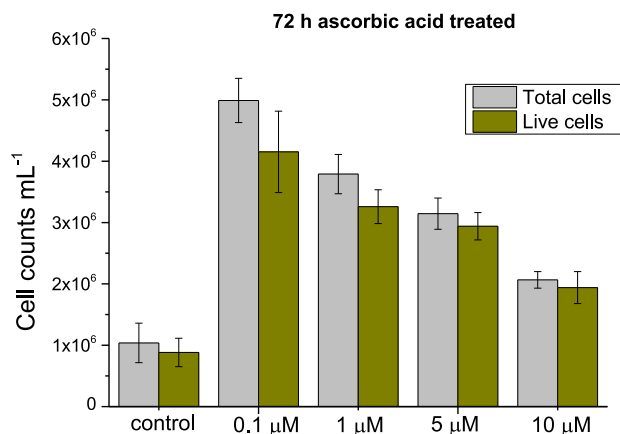
Fig. 1. Cell viability of U-937 cells. U-937 cells at different concentrations of ascorbic acid (0.1 μM, 1 μM, 5 μM and 10 μM). The data are presented as the mean value (±SE) of biological replicates (n = 2).

cells were sonicated in RIPA lysis buffer [150 mM NaCl, 50 mM Tris (pH 8.0), 0.5 % sodium deoxycholate, 0.1 % SDS, 1 % NP-40] containing 1 % (v/v) protease and phosphatase inhibitor. The processed homogenate was centrifuged at 14,000 rpm (30 min, 4 °C) and the collected supernatant fraction was quantified using a Pierce BCA protein estimation kit (Thermo Fisher Scientific, Paisley, UK).

For anti-MDA blotting, samples were prepared with 5× Laemmli sample buffer along with 100 mM Dithiothreitol (DTT); and a protein concentration of 10 μg/lane was used for electrophoresis. The protein samples were then boiled for 10 min at 70 °C. The proteins were seperated on 10% SDS gels and then transferred to nitrocellulose membranes using the Trans-Blot Turbo transfer system (Bio-Rad, California, USA). The nitrocellulose membranes were then blocked for 90 min at room temperature (RT) with 5 % BSA in tris-buffered saline (TBS) (pH 7.4) and 0.1 % Tween 20 (referred to as TBST). The blocked membranes were probed for 90 min at RT with anti-MDA antibody (dilution 1: 5000) followed by 3X washing (10 min each) with TBST; incubated for another 90 min at RT with HRP-conjugated goat anti-rabbit secondary antibody (dilution 1:10000). Following 3 steps of TBST (10 min each), immunocomplexes were imaged using the Amersham imager 600 and Immobilon Western Chemiluminescent HRP Substrate (Sigma Aldrich, GmbH, Germany) (GE Healthcare, UK).

3. Results

3.1. Cell viability using the trypan blue exclusion test

Quantitative estimation of viable cells exposed to varying concentrations of ascorbic acid in U-937 cells was carried out using trypan blue. U-937 cells were treated for 72 h followed by a 24 h of resting period. In Fig. 1A, the gray bar indicates the total cell count, while the green bar indicates the number of live cells within the population (SE, n = 2), while Fig. 1B indicates the cell viability after the resting period. From Fig. 1, it is evident that cell viability under different concentrations used in the experiments is more than 80 % with ascorbic acid treatment. There was a minor/negligible effect noticed in comparison to the control at different concentrations. Therefore, it is considered that the cells are metabolically active in response to the treatments.

3.2. Cell differentiation induced by ascorbic acid and various inducers

Visual changes were monitored 72 h after the addition of ascorbic acid using a confocal laser scanning microscope. Cell morphology was altered after 72 h of incubation with doses of ascorbic acid. When exposed to various differentiation inducers such as PMA, dimethyl sulfoxide (DMSO), retinoic acid, Zn^{2+}, 12-O-tetradecanoylphorbol-13-acetate (TPA), and low concentrations of glutamine, pro-monocytic cells tend to undergo maturation into monocytes or macrophages. To confirm whether the cellular integrity of the U-937 cells under the experimental conditions does not lead to damage of cells, FM4-64 which is a lipophilic styryl compound, and Hoechst 33342 were used. It can be observed that in U-937 cells treated with variable concentration of ascorbic acid (Fig. 2), no obvious cell damage occurred, and cellular integrity (red fluorescence) and nuclear integrity (blue fluorescence) were maintained under all conditions. Differentiated U-937 cells have distinct extensions bearing amoeboid morphology. Before the treatment, the cell morphology exhibited a clear, spherical structure, whereas, after treatment, significant morphological alterations can be observed in the form of prominent pseudopodia, the incidence of which can be seen to be higher with increasing concentration of ascorbic acid from 0.1 μM until 5 μM. A reduction in these morphological structures was observed at higher concentrations of ascorbic acid (10 μM) (Fig. 2).

3.3. Expression of cell surface marker CD11b

To confirm the differentiation of pro-monocytic cells into macrophages, we tracked the expression of the CD11b surface marker. As shown in the results (Fig. 3), it is evident that in untreated U-937 cells, the surface marker expression is minimal. However, in cells treated with ascorbic acid (at 5 and 10 μM concentrations), FITC fluorescence is visibly present under both treatment conditions.

3.4. Effect of ascorbic acid in U-937 cells and associated protein modification

Protein modification occurs when MDA, a reactive aldehyde compound, reacts with amino acid residues of proteins, resulting in the formation of MDA-protein adducts. This is often used as a marker of oxidative stress and lipid peroxidation in cells and tissues. Whole-cell homogenate from U-937 cells treated with PMA and ascorbic acid separated using SDS-PAGE followed by immunoblotting using anti-malondialdehyde (anti-MDA) antibody showed modification of more than one protein. In PMA-treated U-937 cells, the formation of MDA is most pronounced as displayed by protein bands at approximately 40 kDa (Fig. 4A) which is also evident from the densitogram presented in Fig. 4B. In ascorbic acid treated U-937 cells, the formation of MDA is most pronounced in the protein bands at approximately 20 kDa and 40 kDa, and this effect becomes more prominent with increasing concentrations of ascorbic acid (Fig. 5A and Supplementary data 1). A
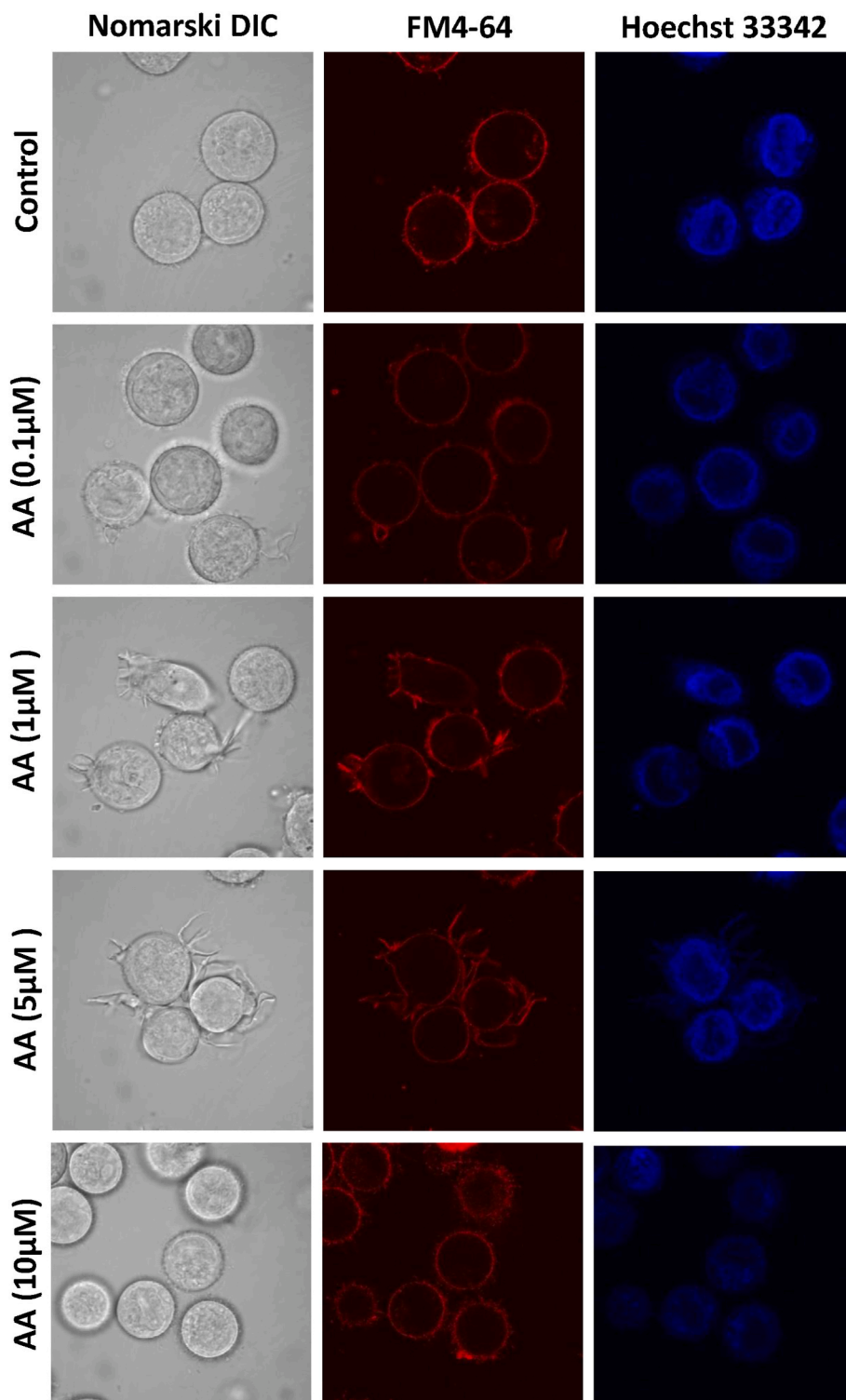
Fig. 2. Double staining using Hoechst 33342 and FM4-64 in 72 h differentiated U-937 cells. Differentiation was induced using variable concentrations of ascorbic acid (0.1–10 μM). Images were captured in various channels at a magnification of 1000 × after staining for 5 min (from left to right are Nomarski DIC, FM4-64 and Hoechst 33342). For each variant, the presented images represent several scans conducted on both biological and technical replicates.

consistent and linear increase in band intensity at this molecular weight range is observed in treated cells, especially with 1 μM and 5 μM ascorbic acid, as indicated in the densitogram shown in Fig. 5B. Notably, in cells differentiated with 10 μM ascorbic acid, a sudden decline in band intensity is evident. We confirmed our findings by employing reverse-phase HPLC to measure the concentration of MDA in cells treated with 1 and 5 μM ascorbic acid, comparing them to the control (indicated as -).

A significant increase was observed in case of ascorbic acid differentiated cell (supplementary data 2). These findings can be associated with the differentiation pattern illustrated in Fig. 2. Unexpectedly, the band intensity at 40 kDa exhibits a slight reduction in the 0.1 μM ascorbic acid-treated sample when compared to the control. We attribute this phenomenon to potential non-specific interactions.
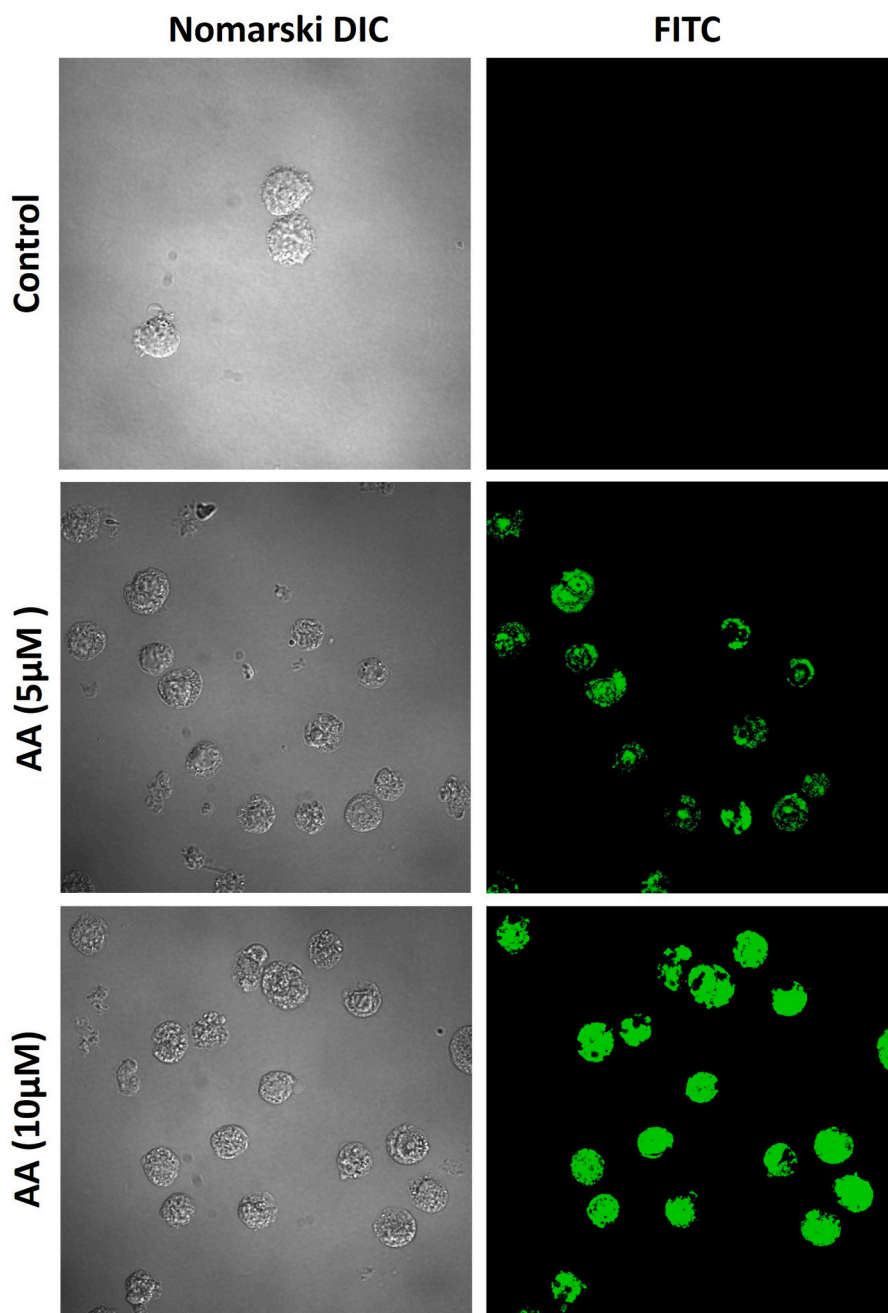
Fig. 3. Expression of CD11b surface marker in cell treated without (upper panel) and in the presence of 5 μM (middle panel) and 10 μM (lower panel) of ascorbic acid for 48 h. The images from left to right represent Nomarski DIC and FITC fluorescence.

4. Discussion

Monocytes are circulatory precursors that originate from a myeloid lineage which can further differentiate into macrophages or dendritic cells after recruitment in tissues and blood stream [28]. Our immune system gains the advantage of phagocytosis, antigen presentation, and cytokine production from these cells. U-937, a pro-monocytic cell lines differentiate into macrophages or into dendritic cells *in vitro* in presence of different inducers [29]. The basic feature of this cell line is the synthesis and secretion of lysozyme with the absence of immunoglobulin production.

When cells such as U-937 and THP-1 cells are exposed to differentiation inducers such as PMA, retinoic acid etc., their proliferation is slowed while the differentiation process is triggered. The monocytes under these treatments are known as "macrophage-like" because of their structure. However, the properties of the transformed cell line are not yet well known. It depends on the dose and time of treatment with inducers. Cells treated with different inducers have been shown to express elevated levels of CD11b and CD14. It also starts to induce adherence accompanied by cell cycle arrest [30]. Cell differentiation is also known to activate the calcium and phospholipid-dependent isoforms of protein kinase C (PKC) thereby inducing AMP metabolism, which leads to its maturation into a macrophage [31,32]. It is now well accepted that the treatment with differentiation inducers exogenously activates the NADPH oxidase complex, which can lead to the formation of $O_2^{\bullet-}$ [33]. In the presence of superoxide dismutase (SOD), it can form H_2O_2 and subsequently $HO^{\bullet}$ in the presence of transition metal ions [34]. During the last decades, differentiation studies were done utilizing PMA and
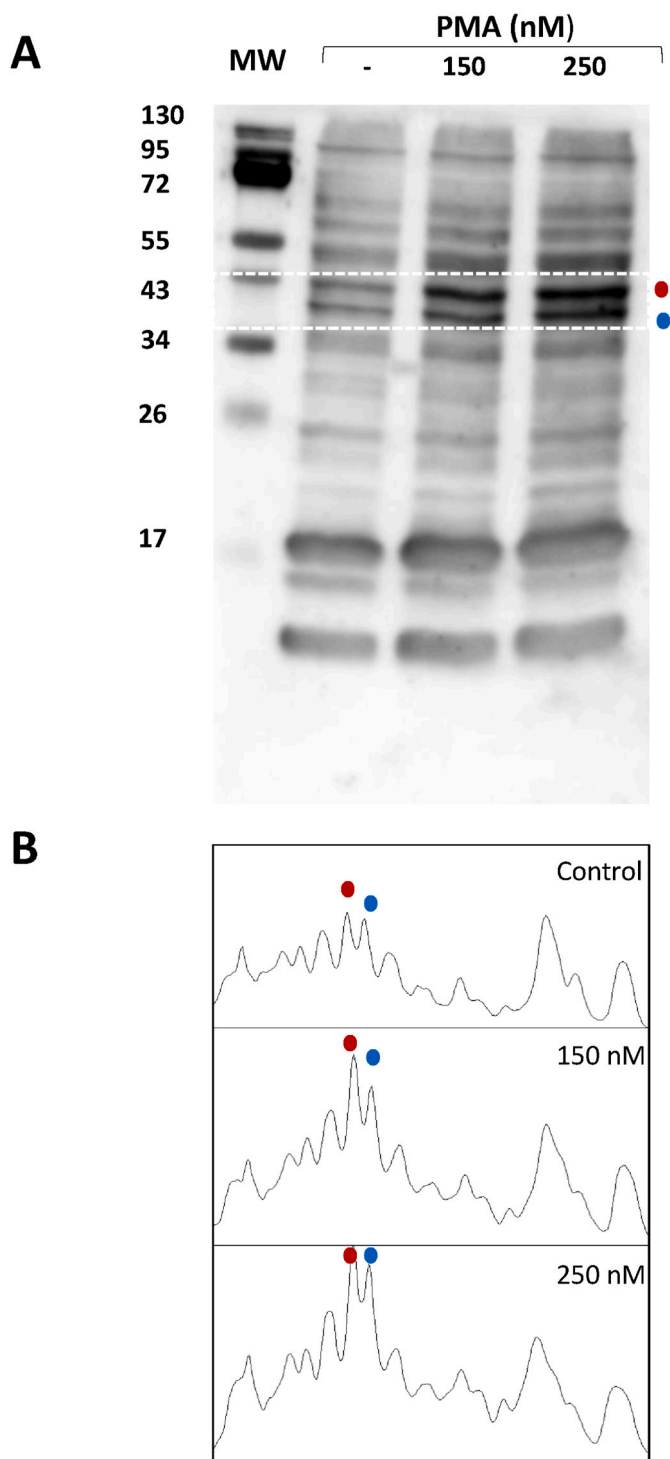
Fig. 4. A. Protein MDA adducts formed in U-937 cells treated with 250 nM PMA. This illustrates protein modification in U-937 cells that were differentiated for 72 h, visualized on blot with anti-MDA antibody. **B.** Quantification of protein bands from an anti-MDA blot by densitogram analysis.

retinoic acid as inducers whereas, more recently, ascorbic acid has been known to relate to cell differentiation [35], the molecular mechanism of which is still unclear. Differentiation studies on dental stem cells have been performed using ascorbic acid in the time range of 24–72 h; however, the stability of ascorbic acid over the period of several days in solution should be taken in account considering the instability of the compound [36].

With the production of ROS in cells, biomolecules such as lipids,

proteins, and nucleic acids can be damaged. Reactive oxygen species can directly oxidize proteins, leading to structural and functional impairments, as well as the formation of protein aggregates and cross-linking. Altogether, it can lead to change in normal protein folding and conformation resulting which the protein-protein interaction and enzymatic activity can be hampered. Amino acids, including but not limited to cysteine, methionine, and histidine are known to be most affected by ROS generation. Lipid particularly due to the presence of polyunsaturated fatty acids (PUFA's) are prone to peroxidation leading to the formation of lipid hydroperoxide and subsequently other reactive lipid species. In our study, MDA which is formed as a by-product of lipid peroxidation known to be generated through a series of reaction involving cleavage of the peroxide bonds and rearrangement of the resulting radicals. In addition to most damage to lipids and proteins, ROS is known to react with DNA/RNA, oxidizing its bases, leading to the formation of DNA adducts, chains, and DNA-cross links. If not repaired, this can eventually lead to mutations and genomic instability that can be responsible for disease development.

Our study shows the differentiation behavior of U-937 cells under exogenous supplementation of ascorbic acid. During the process of cell differentiation, it has been observed that there is a higher expression of NADPH oxidase complex, which eventually can be hypothesized with the increase in the production of ROS. Based on our previous study, we observed a higher expression of NOX-4 in differentiated U-937 cells [16]. There might be a direct/indirect role of ROS in the activation of NADPH expression and eventually self-oxidation.

5. Conclusions

Prooxidative *vs.* antioxidative action of ascorbic acid (vitamin C) was evaluated in relation to differentiation of U-937 cell line into macrophages. Analysis of protein modification using anti-malondialdehyde antibodies showed changes in more than one protein. The findings demonstrate the relationship between the differentiation of U-937 cells into macrophages and the protein modification caused by the production of ROS under the influence of ascorbic acid together with a switch from pro-oxidative to the antioxidant property of the compound under investigation. Findings from this study indicate ascorbic acid promotes differentiation of monocytes into macrophages underlying its role in immune response besides its antioxidant activity. Studies focusing on ascorbic acid role in differentiation and development have to be considered.

CRediT authorship contribution statement

Ankush Prasad: Conceptualization, Data curation, Formal analysis, Investigation, Methodology, Project administration, Validation, Visualization, Writing – original draft, Writing – review & editing. **Deepak Rathi:** Data curation, Formal analysis, Methodology, Writing – original draft, Writing – review & editing. **Michaela Sedlářová:** Data curation, Investigation, Methodology, Writing – review & editing. **Renuka Ramalingam Manoharan:** Investigation, Methodology, Writing – review & editing. **Eliška Průdková:** Data curation, Investigation, Writing – review & editing. **Pavel Pospíšil:** Data curation, Formal analysis, Investigation, Writing – review & editing.
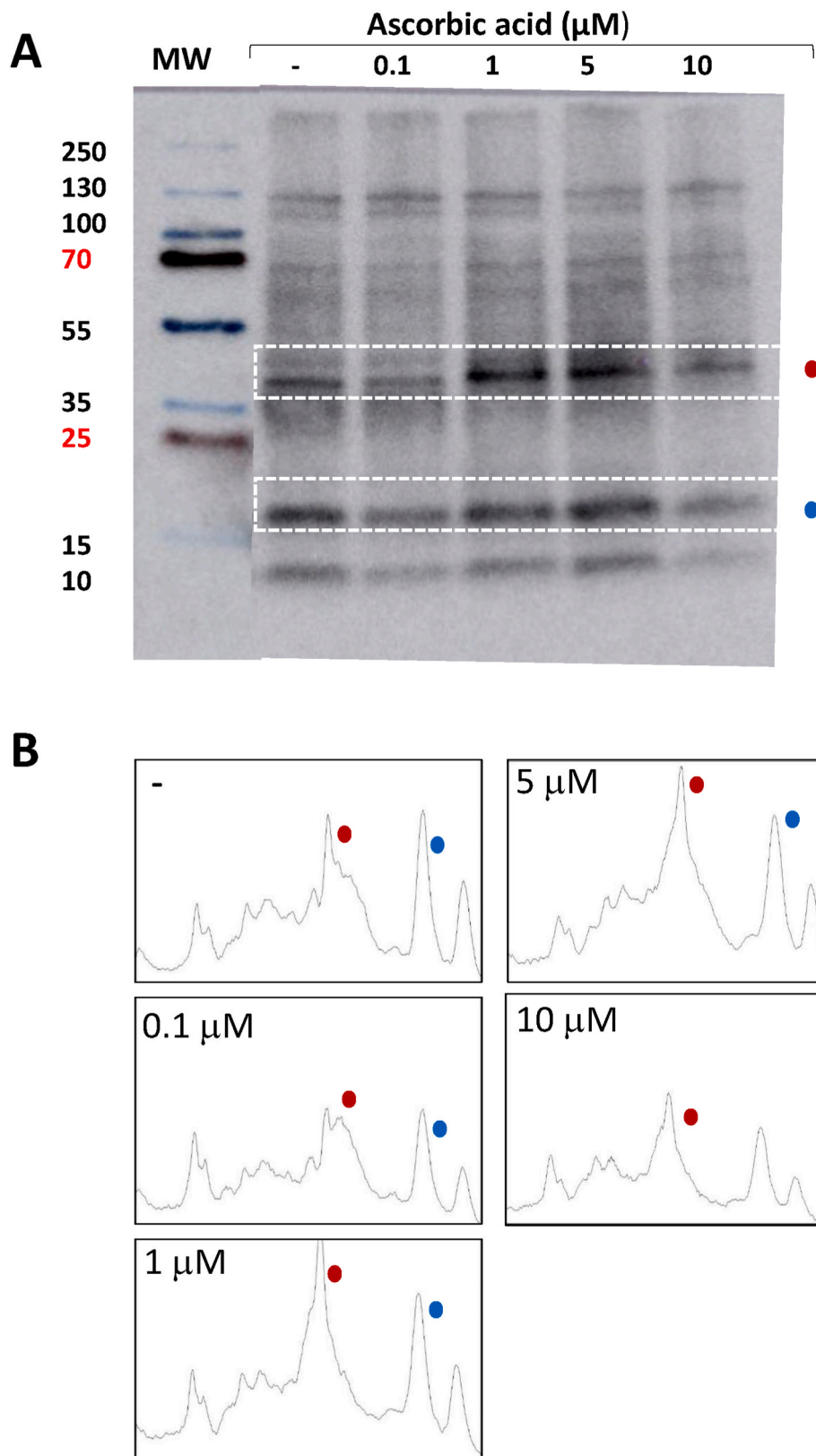
Fig. 5. A. Protein MDA adducts formed in U-937 cells treated with 0.1–10 μM ascorbic acid. This illustrates protein modification in U-937 cells that were differentiated for 72 h, visualized on blot with anti-MDA antibody. **B.** Quantification of protein bands from an anti-MDA blot by densitogram analysis.

Declaration of competing interest

The authors declare that they have no known competing financial interests or personal relationships that could have appeared to influence the work reported in this paper.

Data availability

Data will be made available on request.

Appendix A. Supplementary data

Supplementary data to this article can be found online at https://doi.org/10.1016/j.bbrep.2023.101622.

References

[1] J. Du, J.J. Cullen, G.R. Buettner, Ascorbic acid: chemistry, biology and the treatment of cancer, Biochim. Biophys. Acta Rev. Canc 1826 (2) (2012) 443–457.

[2] S.B. Nimse, D. Pal, Free radicals, natural antioxidants, and their reaction mechanisms, RSC Adv. 5 (35) (2015) 27986–28006.

[3] A.M. Macan, T.G. Kraljevic, S. Raic-Malic, Therapeutic perspective of vitamin C and its derivatives, Antioxidants 8 (8) (2019) 36.

[4] D.J.R. Lane, D.R. Richardson, The active role of vitamin C in mammalian iron metabolism: much more than just enhanced iron absorption, Free Radic. Biol. Med. 75 (2014) 69–83.

[5] A.C. Carr, S. Maggini, Vitamin C and immune function, Nutrients 9 (11) (2017).

[6] F.R. Ricaurte, T. Kewan, H. Daw, Scurvy: a rare cause of anemia, Cureus 11 (9) (2019).

[7] D. Njus, P.M. Kelley, Y.J. Tu, H.B. Schlegel, Ascorbic acid: the chemistry underlying its antioxidant properties, Free Radic. Biol. Med. 159 (2020) 37–43.

[8] N.N. DePhillipo, Z.S. Aman, M.I. Kennedy, J.P. Begley, G. Moatshe, R.F. LaPrade, Efficacy of vitamin C supplementation on collagen synthesis and oxidative stress after musculoskeletal injuries A systematic review, Orthopaedic J. Sports Med. 6 (10) (2018).

[9] G.N.Y. van Gorkom, R. Wolterink, C. Van Elssen, L. Wieten, W.T.V. Germeraad, G. M.J. Bos, Influence of vitamin C on lymphocytes: an overview, Antioxidants 7 (3) (2018).

[10] N.Y. Li, G.J. Zhao, W.L. Wu, M.X. Zhang, W.Y. Liu, Q.F. Chen, X.Q. Wang, The efficacy and safety of vitamin C for iron supplementation in adult patients with iron deficiency anemia A randomized clinical trial, JAMA Netw. Open 3 (11) (2020).

[11] J.M. Pullar, A.C. Carr, S.M. Bozonet, M.C.M. Vissers, High vitamin C status is associated with elevated mood in male tertiary students, Antioxidants 7 (7) (2018).

[12] R. Jarisch, D. Weyer, E. Ehlert, C. Koch, E. Pinkowski, P. Jung, W. Kähler, R. Girgensohn, W. Hemmer, A. Koch, Influence of orally taken vitamin C on histamine levels and motion sickness, J. Allergy Clin. Immunol. 127 (2) (2011) AB261. AB261.

[13] A. Phaniendra, D.B. Jestadi, L. Periyasamy, Free radicals: properties, sources, targets, and their implication in various diseases, Indian J. Clin. Biochem. 30 (1) (2015) 11–26.

[14] S. Di Meo, T.T. Reed, P. Venditti, V.M. Victor, Role of ROS and RNS Sources in Physiological and Pathological Conditions, Oxidative Medicine and Cellular Longevity 2016, 2016.

[15] R. Radi, Oxygen radicals, nitric oxide, and peroxynitrite: redox pathways in molecular medicine, Proc. Natl. Acad. Sci. U.S.A. 115 (23) (2018) 5839–5848.

[16] A. Prasad, R.R. Manoharan, M. Sedlářová, P. Pospíšil, Free radical-mediated protein radical formation in differentiating monocytes, Int. J. Mol. Sci. 22 (18) (2021) 17.

[17] P. Pospíšil, A. Prasad, M. Rac, Mechanism of the formation of electronically excited species by oxidative metabolic processes: role of reactive oxygen species, Biomolecules 9 (7) (2019).

[18] A.C. Chan, K. Tran, T. Raynor, P.R. Ganz, C.K. Chow, Regeneration of vitamin E in human platelets, J. Biol. Chem. 266 (26) (1991) 17290–17295.

[19] A.C. Chan, Partners in defense, vitamin-E and vitamin-C, Can. J. Physiol. Pharmacol. 71 (9) (1993) 725–731.

[20] B. Poljsak, Z. Gazdag, S. Jenko-Brinovec, S. Fujs, M. Pesti, J. Belagyi, S. Plesnicar, P. Raspor, Pro-oxidative vs antioxidative properties of ascorbic acid in chromium (VI)-induced damage: an in vivo and in vitro approach, J. Appl. Toxicol. 25 (6) (2005) 535–548.

[21] A. Gegotek, E. Skrzydlewska, Antioxidative and anti-inflammatory activity of ascorbic acid, Antioxidants 11 (10) (2022).

[22] C. Sundstrom, K. Nilsson, Establishment and characterization of A human histiocytic lymphoma cell line (U-937), Int. J. Cancer 17 (5) (1976) 565–577.

[23] C.R. Nascimento, N.A.R. Fernandes, L.A.G. Maldonado, C. Rossa, Comparison of monocytic cell lines U937 and THP-1 as macrophage models for in vitro studies, Biochem. Biophy. Rep. 32 (2022).

[24] M.H. Dreyling, J.A. MartinezCliment, M. Zheng, J. Mao, J.D. Rowley, S. K. Bohlander, The t(10;11)(p13;q14) in the U937 cell line results in the fusion of the AF10 gene and CALM, encoding a new member of the AP-3 clathrin assembly protein family, Proc. Natl. Acad. Sci. U.S.A. 93 (10) (1996) 4804–4809.

[25] J.W. Fu, Z.Y. Wu, J.F. Liu, T.F. Wu, Vitamin C: a stem cell promoter in cancer metastasis and immunotherapy, Biomed. Pharmacother. 131 (2020).

[26] A. Ang, J.M. Pullar, M.J. Currie, M.C.M. Vissers, Vitamin C and immune cell function in inflammation and cancer, Biochem. Soc. Trans. 46 (2018) 1147–1159.

[27] W. Strober, Trypan blue exclusion test of cell viability, Curr. Protoc. Im. 111 (2015). A3.B.1-A3.B.3.

[28] W. Chanput, J.J. Mes, H.J. Wichers, THP-1 cell line: an in vitro cell model for immune modulation approach, Int. Immunopharm. 23 (1) (2014) 37–45.

[29] A. Prasad, M. Sedlářová, A. Balukova, A. Ovsii, M. Rac, M. Krupka, S. Kasai, P. Pospíšil, Reactive oxygen species imaging in U937 cells, Front. Physiol. 11 (2020).

[30] T. Starr, T.J. Bauler, P. Malik-Kale, O. Steele-Mortimer, The phorbol 12-myristate-13-acetate differentiation protocol is critical to the interaction of THP-1 macrophages with Salmonella Typhimurium, PLoS One 13 (3) (2018).

[31] P.S. Lim, C.R. Sutton, S. Rao, Protein kinase C in the immune system: from signalling to chromatin regulation, Immunology 146 (4) (2015) 508–522.

[32] M. Musashi, S. Ota, N. Shiroshita, The role of protein kinase C isoforms in cell proliferation and apoptosis, Int. J. Hematol. 72 (1) (2000) 12–19.

[33] A. Karlsson, J.B. Nixon, L.C. McPhail, Phorbol myristate acetate induces neutrophil NADPH-oxidase activity by two separate signal transduction pathways: dependent or independent of phosphatidylinositol 3-kinase, J. Leukoc. Biol. 67 (3) (2000) 396–404.

[34] J. Prousek, Fenton chemistry in biology and medicine, Pure Appl. Chem. 79 (12) (2007) 2325–2338.

[35] H. Qiao, J.M. May, Macrophage differentiation increases expression of the ascorbate transporter (SVCT2), Free Radic. Biol. Med. 46 (8) (2009) 1221–1232.

[36] A. Diederich, H.J. Fründ, B. Trojanowicz, A. Navarrete Santos, A.D. Nguyen, C. Hoang-Vu, C.R. Gernhardt, Influence of ascorbic acid as a growth and differentiation factor on dental stem cells used in regenerative endodontic therapies, J. Clin. Med. 12 (2023) 1196.
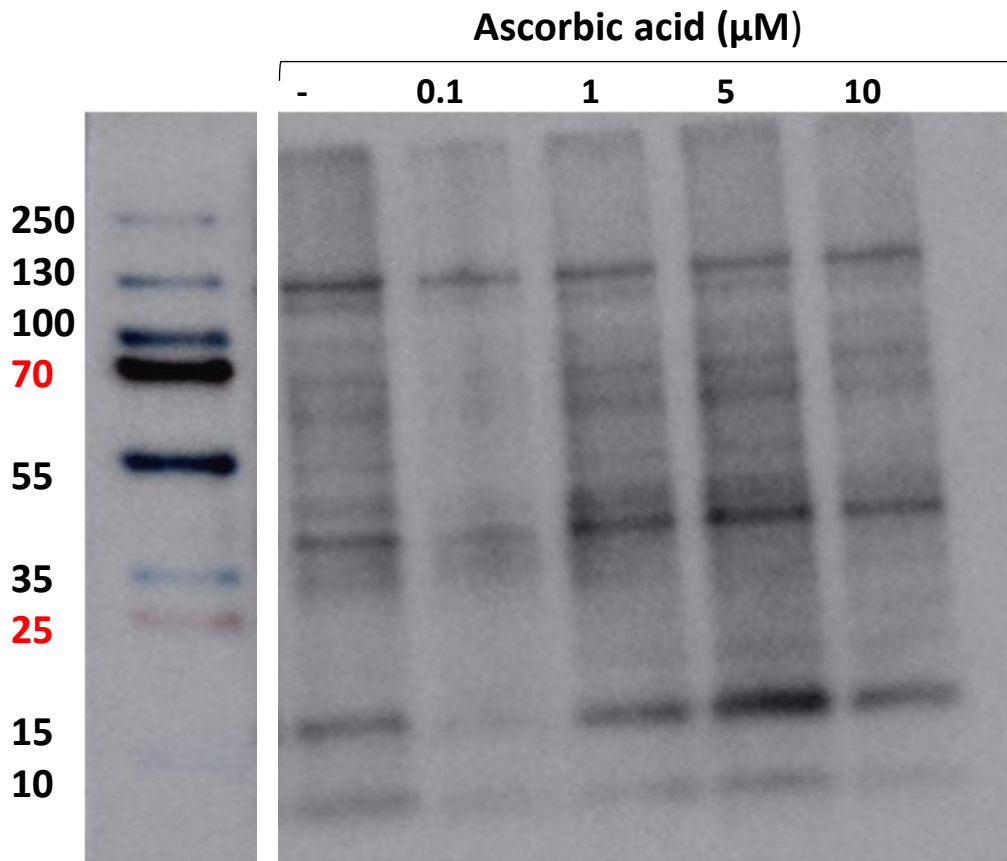
Supplementary dataset 1

Figure S1: Protein MDA adducts formed in U-937 cells treated with 0.1-10 μM ascorbic acid. This illustrates protein modification in U-937 cells that were differentiated for 72 h, visualized on blot with anti-MDA antibody.
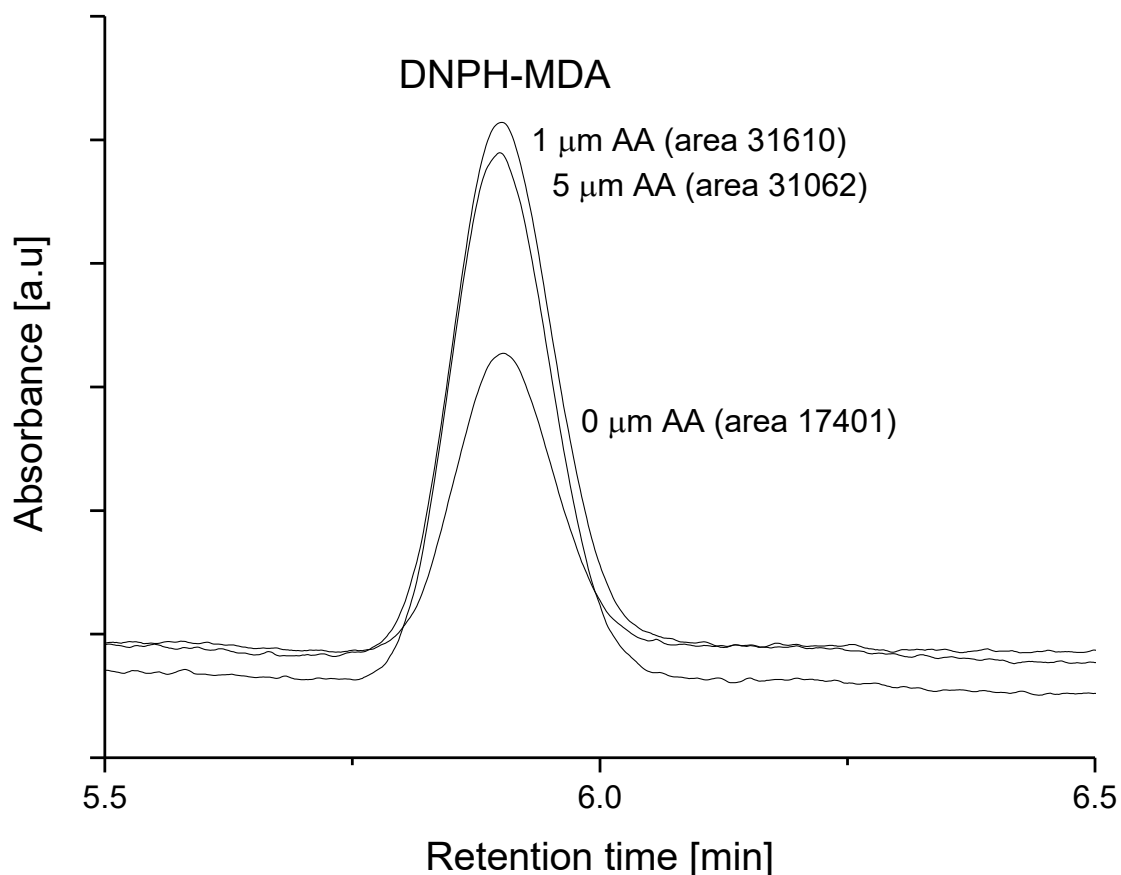
Supplementary dataset 2

Figure S2: Quantification of MDA in non-differentiated (control) and differentiated U-937 cells (72 h, 1 and 5 μM AA) monitored by the reverse-phase HPLC. The retention time of MDA-DNPH derivative was at 5.8 min.

Experimental protocol used is briefly mentioned below:

The total amount of MDA was assessed through reverse-phase HPLC analysis, following the procedure outlined by Pilz et al. (2000). In summary, HPLC-grade water (LC-MS grade) was added to the fraction samples to reach a total volume of 200 μl. To release MDA from proteins via alkaline hydrolysis, 40 μl of 6 M aqueous sodium hydroxide was added and incubated at 60 °C for 30 minutes. Proteins were precipitated by acidifying the sample using 100 μl of 35% (v/v) perchloric acid, followed by centrifugation at 16,000 g for 10 minutes. The supernatant (125 μl) was transferred to a new Eppendorf tube, and MDA was derivatized by adding 1 μl of 50 mM 2,4-dinitrophenyl hydrazine (DNPH) prepared in 2 M sulphuric acid and incubated at RT for 30 minutes. A 50 μl volume of the derivatized MDA was injected into the HPLC (Alliance e 2695 HPLC System, Waters, Milford, MA, U.S.A.) equipped with a 2998 Photodiode Array (PDA) detector. The isocratic separation was carried out using an Arion ASTRA® C18-HE HPLC column (3.0 μm 150 mm × 4.6 mm) (Chromes s. r.o., Prague, Czech Republic) with acetonitrile: water (50:50 v/v) as the solvent system and a flow rate of 1 ml min^{-1}. The MDA-DNPH derivative was detected in the samples at 310 nm with the PDA detector. Operation and data processing were performed using Empower software.

Article

Bioactive Compounds and Their Impact on Protein Modification in Human Cells

Ankush Prasad [1,*], Claudio Rossi [2,*], Renuka Ramalingam Manoharan [1], Michaela Sedlářová [3], Lorenzo Cangeloni [2], Deepak Rathi [1], Gabriella Tamasi [2], Pavel Pospíšil [1] and Marco Consumi [2]

[1] Department of Biophysics, Faculty of Science, Palacký University, Šlechtitelů 27, 783 71 Olomouc, Czech Republic; renuka.rmanoharan@gmail.com (R.R.M.); deepak1234rathi@gmail.com (D.R.); pavel.pospisil@upol.cz (P.P.)
[2] Department of Biotechnology, Chemistry and Pharmacy, University of Siena, Via Aldo Moro 2, 53100 Siena, Italy; cangeloni@student.unisi.it (L.C.); gabriella.tamasi@unisi.it (G.T.); marco.consumi@unisi.it (M.C.)
[3] Department of Botany, Faculty of Science, Palacký University, Šlechtitelů 27, 783 71 Olomouc, Czech Republic; michaela.sedlarova@upol.cz
* Correspondence: ankush.prasad@upol.cz (A.P.); claudio.rossi@unisi.it (C.R.)

Abstract: Reactive oxygen species (ROS) represent a group of molecules with a signaling role that are involved in regulating human cell proliferation and differentiation. Increased ROS concentrations are often associated with the local nonspecific oxidation of biological macromolecules, especially proteins and lipids. Free radicals, in general, may randomly damage protein molecules through the formation of protein-centered radicals as intermediates that, in turn, decay into several end oxidation products. Malondialdehyde (MDA), a marker of free-radical-mediated lipid oxidation and cell membrane damage, forms adducts with proteins in a nonspecific manner, leading to the loss of their function. In our study, we utilized U-937 cells as a model system to unveil the effect of four selected bioactive compounds (chlorogenic acid, oleuropein, tomatine, and tyrosol) to reduce oxidative stress associated with adduct formation in differentiating cells. The purity of the compounds under study was confirmed by an HPLC analysis. The cellular integrity and changes in the morphology of differentiated U-937 cells were confirmed with confocal microscopy, and no significant toxicity was found in the presence of bioactive compounds. From the Western blot analysis, a reduction in the MDA adduct formation was observed in cells treated with compounds that underlaid the beneficial effects of the compounds tested.

Keywords: bioactive compounds; antioxidants; nutraceuticals; monocyte; macrophage; reactive oxygen species; phorbol 12-myristate 13-acetate; protein modification; malondialdehyde; redox reactions

1. Introduction

Nutrients that are not synthesized inside the human body but supplied with the diet have potential health benefits by affecting our microbiome; they are important for the metabolism, immunity, and protection of cells/organs from metabolic or systematic byproducts, for instance, free radicals and inflammatory molecules that can otherwise be harmful if exceeded beyond the scavenging limit of the non-enzymatic or enzymatic defense system [1–3]. The wide range of such molecules includes both plant and animal origins, e.g., polyphenols, carotenoids, vitamins, omega-3 fatty acids, organic acids, amino acid derivatives, etc. [4–6]. These natural compounds are being studied for their role in the alteration in biological reactions and their activity as antioxidant, anti-inflammatory, stress-protective, anticancer, cardioprotective, and neuroprotective agents. In the present study, we selected four bioactive compounds, i.e., chlorogenic acid, oleuropein, tomatine, and tyrosol, of which oleuropein and tomatine were extracted from their natural sources (olive and tomato leaves, respectively). Chlorogenic acid and tyrosol were commercial products. Their role as anti-inflammatory and antioxidant agents in vitro systems was evaluated.

Among antioxidants, chlorogenic acid is one of the polyphenols present in plants, abundantly consumed with fruits, vegetables, coffee, and tea. It is formed from the esterification of quinic acid and certain trans-cinnamic acids, most commonly caffeic, *p*-coumaric, and ferulic acids [7]. Chlorogenic acids are characterized by different subgroups consisting of caffeoylquinic, *p*-coumaroylquinic, and feruloyquinic acids. These acids are abundant at different concentrations and in isomeric mixtures in drinking beverages such as coffee, tea, and wine [7]. In published studies, beverages such as coffee and various fruits that contained these acids lowered the risk of some chronic diseases with their antioxidant, anti-inflammatory, and antibacterial properties [8,9]. A study on a rat model in a gastric epithelial model showed that chlorogenic acids are not hydrolyzed in the gastrointestinal tract and are actively absorbed [10]. Chlorogenic acid and its microbial metabolites were proposed to decrease the proliferation of colon cancer cells [11].

Tomatine, a glycoalkaloid with antibiotic and insecticide effects, can be extracted from the stems, leaves, and green unripe tomatoes (*Solanum lycopersicum* L.); it represents one of the main parts of the Mediterranean diet, which is known to contain other antioxidants, phenolic compounds, etc. [12]. In recent studies, the extracts obtained from green unripe tomatoes have been shown to have antihypertensive [13], anticancer, and antimicrobial properties that induce the cell death rate of cancer cells, which have been studied in different cancer cell lines [14,15]. On the contrary, the direct effects of tomatine or tomato extract on protein modification in any in vivo experiments have not been studied.

α-tomatine was found to be the most effective agent against cancer cell growth. In tomato extract upon in vitro digestion (condition as in vivo gastrointestinal environment), around 45–50% antioxidant activity was still retained [16]. The compound is also known to balance the level of free radicals in cells and control oxidative damage [17–19]. The cell toxicity, antioxidants, and other physiological effects of tomatine depend on the ripening stage [20,21].

Oleuropein can be extracted from olive leaves (*Olea europaea* L.). It consists of a molecule of elenolic acid linked to orthodiphenol hydroxytyrosol by an ester bond, and to a molecule of glucose by a glycosidic bond extracted from olive leaves, and is one of the main phenolic secoiridoids [22]. This compound has well-known anti-inflammatory and antioxidant effects, as evidenced in different studies [23–26]. The effect of oleuropein was studied in rats, and the oxidative stress and antioxidant activity were observed by the evaluation of the levels of malondialdehyde (MDA), superoxide dismutase (SOD), catalase (CAT), glutathione peroxidase (GPX), myeloperoxidase (MPO), and nitric oxide (NO). Different anti-inflammatory genes and cytokines such as IL-1β, TNF-α, IL-10, COX-2, iNOS, TGF-β1, MCP-1, and NF-κB, the pro-apoptotic gene Bax, and the antiapoptotic gene Bcl2 were also evaluated in rat tissue and found altered [22]. After oleuropein treatment, the MDA, MPO, and NO levels were significantly lower, and the levels of SOD, CAT, and GPX were elevated [22].

Tyrosol, a derivative of phenethyl alcohol, is a phenylethanoid. The main sources of tyrosol are olive leaves, and olive oil can form esters with fatty acids [27]. In clinical studies, tyrosol exerted protective effects against oxidative damage caused by oxidized LDL in the adenocarcinoma cell line [28]. It was also suggested that tyrosol may neutralize cellular damage induced by reactive oxygen metabolites. Studies on the effect of tyrosol on levels of superoxide anion radicals ($O_2^{\bullet-}$), hydrogen peroxide (H_2O_2), and nitric oxide ($^{\bullet}NO$) were studied in stimulated macrophages with ascorbic acid and phorbol esters, where tyrosol showed a negative effect on $O_2^{\bullet-}$ and H_2O_2 production [29]. Tyrosol is also known to modulate NF-κB activation, which plays a very important role in inflammatory reactions. Chemically synthesized tyrosol sulfate (Tyr-SUL) and tyrosol glucuronate (Tyr-GLU) and their metabolites were also studied for their anti-inflammatory and antioxidant activities; tyrosol inhibits ROS level rise and downregulates the expressions of glutathione peroxidase 1, glutamate-cysteine ligase catalytic subunit, and heme oxygenase-1 genes [30]. This investigation was carried out to evaluate the potential of these compounds for the prevention of protein modification, and tests were performed on a cell line.

The U-937 cell line we used in our study is a human pro-monocytic myeloid leukemia cell line [31]. A recent study revealed their differentiation behavior and their relationship to ROS production under the effect of inducers [32]. The advantage of using U-937 cells is that they do not succumb to the Hayflick limit [33,34]. In the current study, phorbol 12 myristate 13-acetate (PMA) was used as a differentiation inducer. The differentiation depends on the inducer, its concentration, and the length of incubation [35]. Induction of the differentiation by PMA occurs through the activation of protein kinase C (PKC) isozymes, and the subsequent generations of ROS are known to be closely interlinked. More specifically, $O_2^{\bullet-}$ is generated by nicotinamide adenine dinucleotide phosphate hydrogen (NADPH) oxidase, which can later be converted to H_2O_2 by SOD or subsequently to hydroxyl radical (HO$^{\bullet}$) in the presence of transition metal ions. In human cells, NADPH oxidase is primarily responsible for producing the ROS needed for redox signaling; various growth factors and cytokines stimulate ROS production by activating this enzyme [36]. Although it is unclear whether the ROS produced by the mitochondria contributes to redox signaling, it is becoming increasingly clear that the H_2O_2 released into the cytosol plays a role in various signaling networks, including cell cycle transition and redox balance [37]. Highly reactive species generated under normal physiological and oxidative stress conditions are able to directly oxidize proteins or through lipid derivatives that react with protein functional groups. These protein carbonyl derivatives serve as markers in elucidating ROS-mediated protein oxidation events. Malondialdehyde, an aldehyde derivative, forms adducts with proteins, thereby leading to a loss in protein function. In the present study, we focused on evaluating bioactive compounds in their ability to reduce the impact of ROS-mediated protein modification using U-937 as a cell line model. The differentiation of U-937 cells under the PMA induction was visualized by confocal laser scanning microscopy (CLSM), with a focus on the plasma membrane and nuclei integrity. Subsequently, the effect of four bioactive compounds (chlorogenic acid, oleuropein, tomatine, and tyrosol) on U-937 cells was evaluated using the immunoblotting technique to understand protein modifications.

2. Results and Discussion

2.1. Characterization of Bioactive Compounds

To characterize the oleuropein and α-tomatine originating in the extracts from olive and tomato leaves, HPLC-UV and HPLC-MS analyses were performed, respectively. In Figure 1, the UV chromatograms of the oleuropein standard and the olive leaves extract are reported. Figure 2 shows the stacked mass chromatograms of the α-tomatine standard and tomato leaf extract. The percent purity of the extracted compounds was evaluated on a calibration curve and is presented in Table 1. Other peaks observed in the chromatograms of the tomato leaves extracts were related to minor glycoalkaloids, dehydrotomatine, and β-tomatine. In the olive leaves extracts, the other compounds were hydroxytyrosol, some flavonoids (luteolin and apigenin glycosides), and the phenylpropanoid verbascose.

Table 1. The concentration of main components in the tomato and olive leaf extracts ($n = 9$).

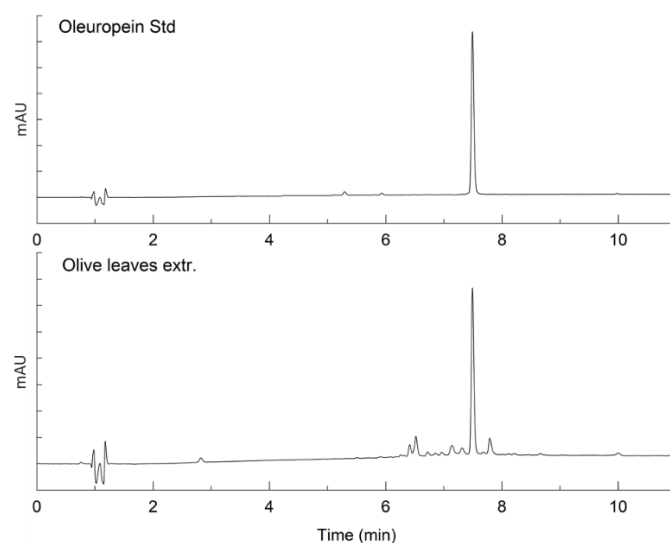| Compound	Average Concentration (mg/g)	Standard Deviation	% RSD	% Purity (*w/w*)
Oleuropein	0.602	0.010	0.01	60.8 $\pm$ 0.27
α-Tomatine	0.953	0.052	5.42	94.2 $\pm$ 0.49

Figure 1. Stacked UV chromatogram of the oleuropein standard and the olive leaf extract.
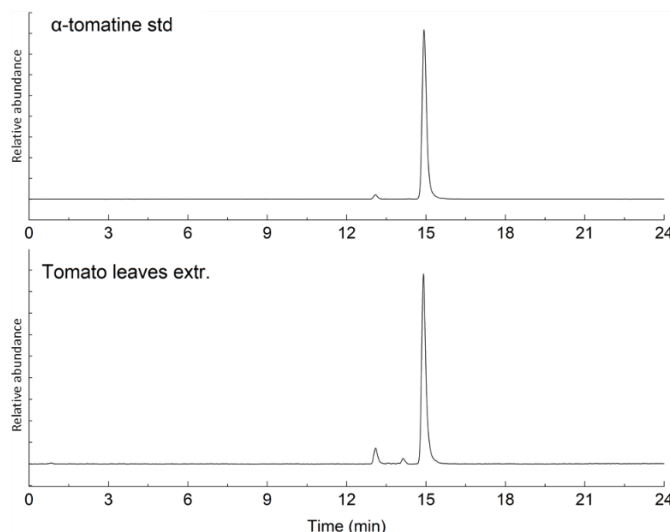

Figure 2. Stacked mass chromatograms of α-tomatine standard and the tomato leaf extract.

2.2. Cell Viability Using MTT Assay

Quantitative estimation of viable cells exposed to bioactive compounds in U-937 cells was carried out using an MTT assay. U-937 cells were treated with PMA along with bioactive compounds for 72 h. From Figure 3, the cell viability under different concentrations of bioactive compounds used in the experiments exceeded 70%. Prior to the assay, differentiation of cells was induced with 250 nM PMA, a concentration optimized in our previous study [38]. The effect of bioactive compounds applied at several concentrations was dose-dependent; in Figure 3, it is expressed using PMA as 100% control. With increasing concentrations (1.5, 3.1, 6.2, 12.5, 25, and 50 μM), the percentage of viable cells decreased linearly, but was found to be always higher than 70% in the concentration used in our study. Chlorogenic acid (Figure 3A) had the strongest effect on cell viability compared with oleuropein (Figure 3B), tomatine (Figure 3C), and tyrosol (Figure 3D). The percentage viability in the case of chlorogenic acid was ~70%, while in the case of the others, it was well above 80%. As mentioned above, cell viability corresponds to metabolically active cells in response to treatments. The decrease in cell viability was evident for concentrations above 12.5 μM; therefore, we utilized 10 μM or lower as the standard concentration

for treatment. The results were further validated using the trypan blue exclusion test (Supplementary Data S1).

2.3. U-937 Cell Morphology

Cell morphology was monitored using CLSM following incubation with 250 nm PMA (Figure 4) for 72 h, and a high percentage of induction was observed. Differentiated U-937 cells have a distinct extension bearing amoeboid morphology, which confirms the maturation of promonocytic cells into monocytes or macrophages. Control cells (−PMA, upper panel) showed a mainly spherical, translucent structure, while most treated cells (+PMA, lower panel) formed pseudopodia. In U-937 cells treated with PMA in the absence or presence of bioactive compounds (Figure 5 and Supplementary Data S2), cellular integrity was maintained both for the plasma (middle panel) and nuclear (right panel) membranes. Figures 4 and 5 and Supplementary Data S2 present multiple observation and scans performed on biological and technical replicates.
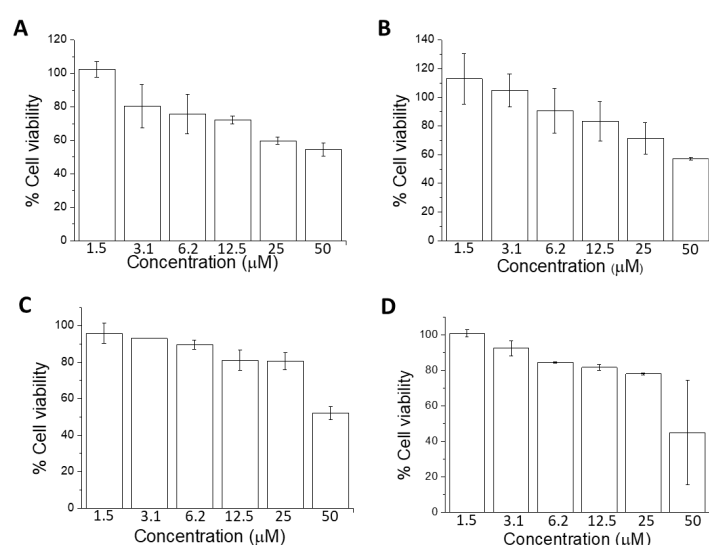
Figure 3. Cell viability of U-937 cells. PMA-treated U-937 cells with chlorogenic acid (**A**), oleuropein (**B**), α-tomatine (**C**), and tyrosol (**D**) at different concentrations. Data are presented as mean ± SE.
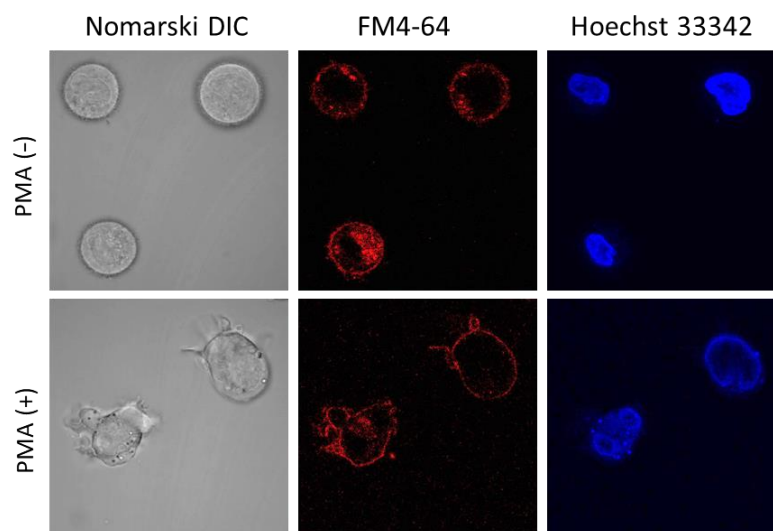
Figure 4. Double staining using FM4-64 and Hoechst 33342 in nondifferentiated (upper panel) and 72 h differentiated (lower panel) U-937 cells incubated for 5 min. Images (magnification 1000×) were taken in different channels (from left to right are Nomarski DIC, FM4-64, and Hoechst 33342).

When cells such as U-937 cells are exposed to inducers such as PMA, their proliferation slows while the differentiation process is triggered. The monocytes under the PMA treatment are known as "macrophage-like" because of their structure [39–41]. However, the properties of the transformed cell line are not yet well-known. Phorbol 12-myristate 13-acetate works as a tumor promoter, and it is known to be involved in gene transcription, cell growth, differentiation, immune pathway, programmed cell death, and receptor desensitization through PKC signaling pathways [42]. It also starts to induce adherence accompanied by cell cycle arrest [43]. PMA is also known to activate the calcium- and phospholipid-dependent isoforms of PKC, thus inducing AMP metabolism, leading to its maturation into a macrophage. It is now well-accepted that adding PMA exogenously activates the NADPH oxidase complex, which can lead to the formation of $O_2^{\bullet-}$. In the presence of SOD, it can create H_2O_2 and subsequently $HO^{\bullet}$ [3,43–46].
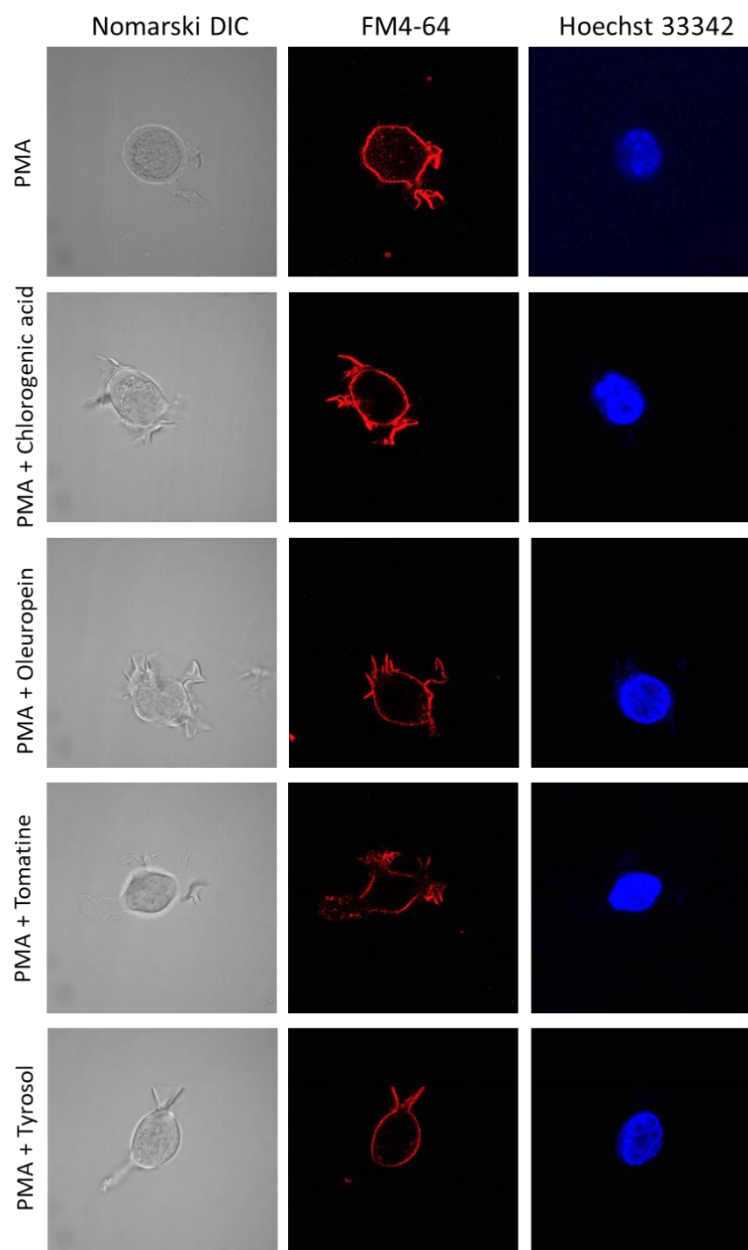
Figure 5. Double staining using Hoechst 33342 and FM4-64 in 72 h differentiated U-937 cells and in the presence of either of the bioactive compounds (chlorogenic acid, oleuropein, α-tomatine, and tyrosol, 10 μM). The staining was performed for 5 min, and images (magnification 1000×) were taken in different channels (from left to right are Nomarski DIC, FM4-64 and Hoechst 33342).

2.4. Protein Modification in Differentiating Cells and Impact of Bioactive Compounds

The whole-cell homogenate of U-937 cells treated with PMA alone (48 and 72 h) or together with bioactive compounds (24 h) was separated using SDS-PAGE. Immunoblotting using anti-MDA antibodies showed a modification of more than one protein. In 48 h differentiated cells (with last 24 h in the presence of bioactive compounds), the MDA was most evident in the protein band, corresponding approximately to 13 and 20 kDa (Figures 6A and 7). On the densitogram presented as a part of Figure 7, it can be clearly seen that there was a significant suppression in the bands mentioned above. In the 72 h differentiated cells (with last 24 h in the presence of bioactive compounds), significant suppression in the bands at 13, 15, 45, and 100 kDa was seen. α-tomatine showed the maximum antioxidant capacity compared with chlorogenic acid in the 72 h differentiated cells (Figures 6B and 7).
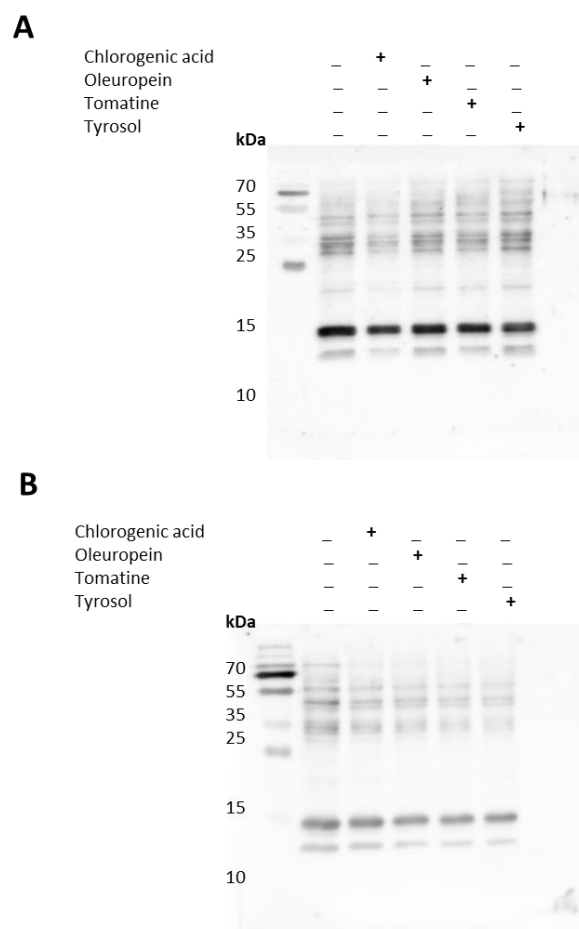
Figure 6. Identification of protein MDA adducts in whole-cell homogenates of U-937 cells treated with bioactive compounds PMA or PMA + bioactive compounds. Anti-MDA blot represents protein modification in U-937 cells differentiated for 48 h (**A**) and 72 h (**B**).

Under oxidative stress, the plasma membrane lipids of cells can undergo oxidation that indirectly results in HO•-mediated protein carboxylation [47]. Polyunsaturated acyl chains of phospholipids, arachidonic acid and linoleic acid (polyunsaturated fatty acids), are extremely prone to peroxidation and breakdown through nonenzymatic hock cleavage, which forms a different kind of lipid-derived aldehydes and ketones [48]. These lipid-derived aldehydes and ketones can diffuse into the cell and modify proteins in the cells. In previous studies, it was suggested that lipid-derived aldehydes are more reactive than direct oxidation of the amino acid side chain formed from protein carbonylation [49]. The scheme presented in Figure 8 shows the different steps involved in the protein modification as a result of ROS generation and successive oxidative radical reactions. Reactive oxygen

species are important metabolic products of cells, and play a beneficial role in cell defense, but their reaction with other proteins can be harmful [37]. The main protein modification is sulfoxide, which is the result of oxidation of methionine, cysteine to sulfenic, sulfinic, and sulfonic acids due to different redox reactions. Hydrogen peroxide, for instance, can cause the oxidation of the side chain of protein amino acids, which results in the formation of semialdehyde amino acids; most reactions occur with lysine, arginine, and proline [50].
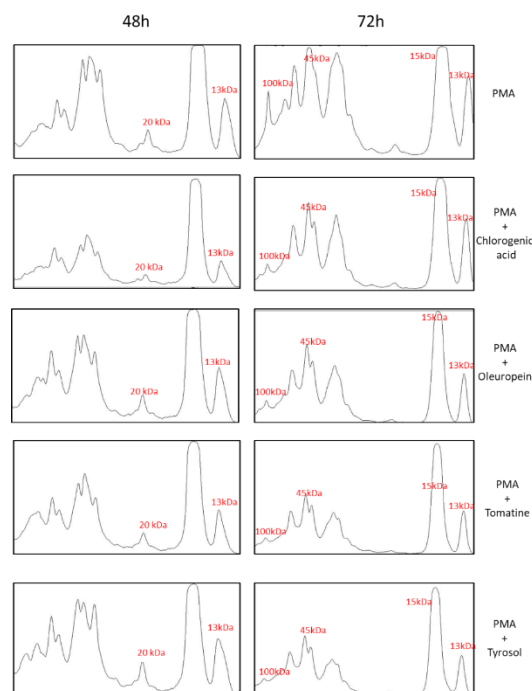
Figure 7. Quantification of protein bands from an anti-MDA blot (Figure 6) by densitogram analysis is shown and selected proteins are indicated with respective molecular weight (red).
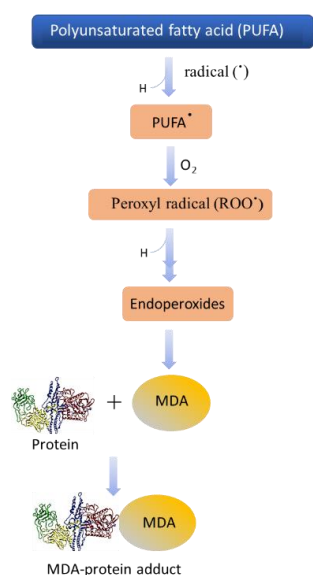
Figure 8. Schematic representation showing the steps involved in protein modification as the results of ROS generation and successive oxidative radical reactions.

3. Methods and Materials

3.1. Extracts

Oleuropein extract was prepared from the leaves of olives (*Olea europaea* L.) by following the protocol of Tamasi et al., and the tomatine was obtained from the leaves of tomatoes (*Solanum lycopersicum* L.). The extraction protocols were previously reported for tomatine [21,51,52]. In brief, lyophilized leaves were treated with a hydroalcoholic mixture (EtOH/H_2O; 80:20 *v/v*). For tomatine extraction, the mixture was acidified with acetic acid (1%, *v/v*). The suspension was extracted through an ultrasonic-assisted procedure to enhance the extraction process, then it was centrifuged, and the liquid fraction was collected. The extraction procedure was repeated twice on the remaining solid residue. Finally, the extracts were dried under a nitrogen stream, freeze-dried, and stored at $-20 \pm 1\,°C$, in dim-light conditions, before further analysis. All samples were extracted in triplicate. Chlorogenic acid (purity > 97%) and tyrosol (purity > 98%) were commercial products and were used without extra purification.

3.2. Reagents and Antibodies

All the solvents were purchased from Sigma-Aldrich (Milan, Italy): ethanol (EtOH, gradient grade for HPLC, ≥99.9%), methanol (MeOH, gradient grade for HPLC, ≥99.9%), acetonitrile (ACN, LC-MS grade, ≥99.9%), water (H_2O, LC-MS grade, ≥99.9%), acetic acid (CH_3COOH, ≥98%), and formic acid (HCOOH, LC-MS grade, ≥98.5%). The oleuropein standard was purchased from Sigma-Aldrich (Milan, Italy) (98%), and the tomatine standard was purchased from Extrasynthese (Lyon, France) (≥98.5%). Cell culture media and antibiotics were purchased from Biosera (Nuaille, France). Phorbol 12-myristate 13-acetate (PMA) was obtained from Sigma-Aldrich (St. Louis, MO, USA). The rabbit polyclonal anti-malondialdehyde (MDA) antibody and MTT cell proliferation assay kit were purchased from Abcam [anti-malondialdehyde (MDA) antibody (ab27642)] (Cambridge, UK). Polyclonal goat anti-rabbit IgG conjugated with horseradish peroxidase (HRP) was obtained from Bio-Rad (Hercules, CA, USA). Protease and phosphatase inhibitors were obtained from Roche (Mannheim, Germany).

3.3. HPLC-MS Analysis for α-Tomatine Determination in Tomato Leaf Extracts

The extracts of tomato leaves were analyzed to determine the content of α-tomatine by HPLC-MS analysis. The extracts were resuspended in methanol (MeOH), and the analysis was performed on an UltiMate 3000 HPLC coupled with an LTQ XL mass spectrometer equipped with a HESI II electrospray ion source. Xcalibur software was used to acquire and process the data. The determination of the α-tomatine content was performed following a method previously optimized and published, with some slight modifications [21,51]. A Phenomenex Kinetex Polar C18 (150 × 2.1 mm, 2.6 μm, 100 Å) with a SecurityGuard C18 guard column (2 × 2.1 mm), thermostated at $35 \pm 1\,°C$, was used for the chromatographic separation. The eluents were H_2O containing 0.1% formic acid (A) and acetonitrile containing 0.1% formic acid (B). The gradients were: isocratic 20% B (0–1 min), curve gradient 20–50% B curve parameter: 8 (1–23 min), and linear gradient 50–95% B (23–25 min). The injection volume was 3 μL, and the flow rate was kept at 0.4 mL/min. The electrospray parameters were optimized by direct injection of a tomatine standard diluted in the elution solvent composition in positive mode: spray voltage, 5 kV; sheath and auxiliary gas, 35 and 10 arbitrary units, respectively; the capillary temperature was maintained at 200 °C. The quantitative determination of α-tomatine was carried out in SIM mode via external calibration, using peimine as the internal standard. The same amount of internal standard (IS, 1.0 mg/L in MeOH) was added to all standards and on the samples (analyzed on the same day). The calibration curve was acquired by injecting standard solutions in the linearity range of concentrations, 0.025–10 mg/L, obtaining the equation y = 0.36693x, R^2 = 0.9965. The limit of detection (LOD) and limit of quantification (LOQ) values were also determined as 0.007 and 0.020 mg/L, respectively. All samples were extracted and

analyzed in triplicate (n = 9), and results are expressed in milligrams per gram as mean concentration ± standard deviation.

3.4. HPLC-UV Analysis for Oleuropein Determination in Olive Leaf Extracts

Olive leaf extracts were analyzed to determine the content of oleuropein by HPLC-UV analysis using a previous method with slight modifications [52]. The extracts were reconstituted in MeOH, and HPLC-UV analyses were performed on an UltiMate 3000 instrument equipped with an RS-3000 Diode Array Detector operating at 280 nm. Xcalibur software was used to acquire and process the data. A Kinetex Polar C18 column (150 × 2.1 mm, 2.6 μm, 100 Å; Phenomenex, Bologna, Italy) with a SecurityGuard C18 guard column (2 × 2.1 mm), thermostated at 35 ± 1 °C, was used for the chromatographic separation. The solvents used for the elution gradient were A (H_2O containing 0.1% formic acid) and B (acetonitrile containing 0.1% formic acid); the linear gradient was eluted from 5% to 50% of B (0–10 min), and from 50% to 95% of B (10–15 min). The injection volume was 3 μL, and the flow rate of 0.4 mL/min. The quantitative determination of oleuropein was carried out via external calibration. The calibration curve was acquired by injecting standard solutions in the linearity range of concentrations, 5–100 mg/L, obtaining the equation y = 1930.8x, R^2 = 0.9998. The LOD and LOQ were also determined as 1.00 and 3.00 mg/L, respectively. All samples were extracted and analyzed in triplicate (n = 9), and the results are expressed in milligrams per gram as mean concentration ± standard deviation.

3.5. Cell Line Origin and Cultivation

The U-937 cell line was obtained from the American Type Culture Collection (ATCC; Rockville, MD, USA). Cells were grown in RPMI-1640 supplemented with 0.05 mM L-glutamine, 10% fetal bovine serum (FBS), and 1% antibiotics (penicillin and streptomycin) in the *v/v* ratio. Experiments were carried out when viability was close to or above 70%. An automated cell counter (Bio-Rad Laboratories, Hercules, CA, USA) was used to determine cell density, and viability was monitored using 0.05% trypan blue dye.

3.6. Cell Line and Differentiation Condition

For experiments, cells were differentiated with 250 nM PMA at two different time points of 48 and 72 h. Following differentiation, cells were incubated with the bioactive compounds mentioned above for 24 h. All experiments were carried out in complete medium. A cell density of 1 × 10^6 CFU/mL was used for treatment.

3.7. MTT Cell Proliferation Assay

Cell viability was determined using a Cell Proliferation Assay Kit (ab211091) (Sigma Aldrich GmbH, Mannheim, Germany). For the test, U-937 cells were seeded in replicates (*n* = 2) on a 96-well microplate and treated with PMA in the presence or absence of bioactive compounds (10 μM) at 37 °C. Followed by incubation, the media were discarded, and serum-free medium was added along with MTT reagent and incubated for 3 h at 37 °C. To avoid interference by the MTT reagent, MTT solvent was added, and the 96-well microplate was kept on the shaker for 15 min. The absorbance was recorded at 590 nm, and the results are presented as percentage of the control in Section 2.2. Data are expressed as ±SEM of at least two measurements.

3.8. Confocal Laser Scanning Microscopy

A Fluorview 1000 confocal unit attached to the IX80 microscope was utilized to visualize U-937 cells on slides (Olympus Czech Group, Prague, Czech Republic). Staining with FM4-64 (15 μM) and Hoechst 33342 (2 μM) for 5 min at RT was used to monitor the integrity of cell membranes and nuclei under experimental conditions. A lipophilic dye FM4-64 (Sigma Aldrich GmbH, Mannheim, Germany) bound to the plasma membrane was excited using a 543 nm He-Ne laser, and its emission was recorded within the range of 655–755 nm. Hoechst 33342 is a membrane-permeant stain specific for AT-rich regions of

double-stranded DNA for which excitation was achieved by a 405 nm diode laser, and the signal was recorded with 430–470 nm bandpass filter.

3.9. Protein Immunoblotting

After differentiation and incubation with the bioactive compounds, U-937 cells were collected by centrifugation and washed with PBS (pH 7.4) to remove residual media. Cell pellets thus obtained were resuspended in lysis buffer(150 mM NaCl, 50 mM Tris (pH 8.0), 0.5% sodium deoxycholate, 0.1% SDS, and 1% NP-40) containing 1% (*v/v*) protease and phosphatase inhibitor (*v/v*) and subjected to sonication. The processed homogenate was centrifuged at $14,000\times g$, and the collected supernatant fraction was quantified using a Pierce BCA protein estimation kit (Thermo Fisher Scientific, Paisley, UK). Protein samples were prepared with $5\times$ Laemmli sample buffer along with 100 mM 2-Mercaptoethanol, and a concentration of 10 µg/lane was used for electrophoresis.

Whole-cell homogenates separated on 10% SDS gel were then transferred to nitrocellulose membranes using a Trans-Blot Turbo transfer system (Bio-Rad, Hercules, CA, USA). Nitrocellulose membranes were then blocked for 2 h at RT with 5% BSA in phosphate-buffered saline (PBS) (pH 7.4) containing 0.1% Tween 20. The blocked membranes were probed overnight with an anti-MDA antibody at 4 °C and incubated for 1 h at room temperature with HRP-conjugated anti-rabbit secondary antibody (dilution 1:10,000). Immunocomplexes thus formed were visualized using Immobilon Western Chemiluminescent HRP Substrate (Sigma Aldrich, GmbH, Mannheim, Germany) and captured with an Amersham 600 imager (GE Healthcare, Amersham, UK).

4. Conclusions

Activation or differentiation of monocytes into macrophages is mediated by the expression of various proinflammatory mediators and the generation of $O_2^{\bullet-}$. Lipids, more specifically polyunsaturated fatty acids, are highly vulnerable to oxidative stress. The compounds evaluated in the present study exhibited less cytotoxicity. Additionally, they do not interfere with the process of U-937 differentiation toward monocytic lineages, as confirmed by confocal analysis. Malondialdehyde, a byproduct of lipid peroxidation, is toxic, and its enhanced expression is known to be involved in various pathogenesis, including carcinogenesis, diabetics, and neurological disorders. It is a highly reactive molecule, with three carbon dialdehyde molecules that interact with functional groups on proteins, forming adducts. Immunoblotting analysis with anti-MDA antibody revealed that among the tested compounds, tomatine and tyrosol exhibited enhanced antioxidant activity compared with chlorogenic acid and oleuropein. A further transcriptomic analysis of U-937 after differentiation and incubation with antioxidants is required, which will help in the identification of the genes involved and their upregulation before and after antioxidant treatment.

Supplementary Materials: The following supporting information can be downloaded at: https://www.mdpi.com/article/10.3390/ijms23137424/s1.

Author Contributions: Conceptualization, A.P., C.R.; methodology, A.P., C.R., R.R.M., L.C., M.S. and G.T.; validation, A.P., C.R. and G.T.; formal analysis, A.P., C.R., R.R.M., M.S. and G.T.; data curation, A.P., R.R.M., M.S., L.C.; writing—original draft preparation, A.P. and D.R.; writing—review and editing, C.R., R.R.M., M.S., G.T., P.P. and M.C.; project administration, A.P. and C.R.; funding acquisition, A.P. and C.R. All authors have read and agreed to the published version of the manuscript.

Institutional Review Board Statement: Not applicable.

Informed Consent Statement: Not applicable.

**Data Availability Statement:** Not applicable.

Conflicts of Interest: The authors A.P., C.R., R.R.M., M.S., L.C., D.R., G.T., P.P. and M.C. declare no conflict of interest.

References

1. Gutteridge, J.M.C.; Halliwell, B. Free radicals and antioxidants in the year 2000—A historical look to the future. *Ann. N. Y. Acad. Sci.* **2000**, *899*, 136–147. [CrossRef] [PubMed]
2. Halliwell, B. Reactive species and antioxidants. Redox biology is a fundamental theme of aerobic life. *Plant Physiol.* **2006**, *141*, 312–322. [CrossRef] [PubMed]
3. Halliwell, B.; Gutteridge, J. *Free Radicals in Biology and Medicine*, 4th ed.; Oxford University Press: Oxford, UK, 2007.
4. Wang, X.; Quinn, P.J. Vitamin E and its function in membranes. *Prog. Lipid Res.* **1999**, *38*, 309–336. [CrossRef]
5. Young, A.J.; Lowe, G.M. Antioxidant and prooxidant properties of carotenoids. *Arch. Biochem. Biophys.* **2001**, *385*, 20–27. [CrossRef] [PubMed]
6. Munne-Bosch, S.; Alegre, L. The function of tocopherols and tocotrienols in plants. *Crit. Rev. Plant Sci.* **2002**, *21*, 31–57. [CrossRef]
7. Liang, N.; Kitts, D.D. Role of chlorogenic acids in controlling oxidative and inflammatory stress conditions. *Nutrients* **2016**, *8*, 16. [CrossRef]
8. Nabavi, S.F.; Tejada, S.; Setzer, W.N.; Gortzi, O.; Sureda, A.; Braidy, N.; Daglia, M.; Manayi, A. Chlorogenic acid and mental diseases: From chemistry to medicine. *Curr. Neuropharmacol.* **2017**, *15*, 471–479. [CrossRef]
9. Lu, H.J.; Tian, Z.M.; Cui, Y.Y.; Liu, Z.C.; Ma, X.Y. Chlorogenic acid: A comprehensive review of the dietary sources, processing effects, bioavailability, beneficial properties, mechanisms of action, and future directions. *Compr. Rev. Food Sci. Food Saf.* **2020**, *19*, 3130–3158. [CrossRef]
10. Lafay, S.; Gil-Izquierdo, A.; Manach, C.; Morand, C.; Besson, C.; Scalbert, A. Chlorogenic acid is absorbed in its intact form in the stomach of rats. *J. Nutr.* **2006**, *136*, 1192–1197. [CrossRef]
11. Ekbatan, S.S.; Li, X.Q.; Ghorbani, M.; Azadi, B.; Kubow, S. Chlorogenic acid and its microbial metabolites exert anti-proliferative effects, s-phase cell-cycle arrest and apoptosis in human colon cancer caco-2 cells. *Int. J. Mol. Sci.* **2018**, *19*, 723. [CrossRef]
12. Silva-Beltrán, N.P.; Ruiz-Cruz, S.; Cira-Chávez, L.A.; Estrada-Alvarado, M.I.; Ornelas-Paz, J.D.J.; López-Mata, M.A.; Del-Toro-Sánchez, C.L.; Zavala, J.F.A.; Márquez-Ríos, E. Total phenolic, flavonoid, tomatine, and tomatidine contents and antioxidant and antimicrobial activities of extracts of tomato plant. *Int. J. Anal. Chem.* **2015**, *2015*, 284071. [CrossRef] [PubMed]
13. Marcolongo, P.; Gamberucci, A.; Tamasi, G.; Pardini, A.; Bonechi, C.; Rossi, C.; Giunti, R.; Barone, V.; Borghini, A.; Fiorenzani, P.; et al. Chemical characterisation and antihypertensive effects of locular gel and serum of *Lycopersicum esculentum* L. var. "Camone" tomato in spontaneously hypertensive rats. *Molecules* **2020**, *25*, 3758. [CrossRef] [PubMed]
14. Friedman, M.; Levin, C.E.; Lee, S.-U.; Kim, H.-J.; Lee, I.-S.; Byun, J.-O.; Kozukue, N. Tomatine-containing green tomato extracts inhibit growth of human breast, colon, liver, and stomach cancer cells. *J. Agric. Food Chem.* **2009**, *57*, 5727–5733. [CrossRef] [PubMed]
15. Serratì, S.; Porcelli, L.; Guida, S.; Ferretta, A.; Iacobazzi, R.M.; Cocco, T.; Maida, I.; Tamasi, G.; Rossi, C.; Manganelli, M.; et al. Tomatine displays antitumor potential in in vitro models of metastatic melanoma. *Int. J. Mol. Sci.* **2020**, *21*, 5243. [CrossRef]
16. Toor, R.K.; Savage, G.P.; Lister, C.E. Release of antioxidant components from tomatoes determined by an in vitro digestion method. *Int. J. Food Sci. Nutr.* **2009**, *60*, 119–129. [CrossRef]
17. Huang, S.-L.; He, H.-B.; Zou, K.; Bai, C.-H.; Xue, Y.-H.; Wang, J.-Z.; Chen, J.-F. Protective effect of tomatine against hydrogen peroxide-induced neurotoxicity in neuroblastoma (SH-SY5Y) cells. *J. Pharm. Pharmacol.* **2014**, *66*, 844–854. [CrossRef]
18. Friedman, M. Anticarcinogenic, cardioprotective, and other health benefits of tomato compounds lycopene, alpha-tomatine, and tomatidine in pure form and in fresh and processed tomatoes. *J. Agric. Food Chem.* **2013**, *61*, 9534–9550. [CrossRef]
19. Kúdelová, J.; Seifrtova, M.; Suchá, L.; Tomšík, P.; Havelek, R.; Řezáčová, M. Alpha-tomatine activates cell cycle checkpoints in the absence of DNA damage in human leukemic MOLT-4 cells. *J. Appl. Biomed.* **2013**, *11*, 93–103. [CrossRef]
20. Chandra, H.M.; Ramalingam, S. Antioxidant potentials of skin, pulp, and seed fractions of commercially important tomato cultivars. *Food Sci. Biotechnol.* **2011**, *20*, 15–21. [CrossRef]
21. Pardini, A.; Consumi, M.; Leone, G.; Bonechi, C.; Tamasi, G.; Sangiorgio, P.; Verardi, A.; Rossi, C.; Magnani, A. Effect of different post-harvest storage conditions and heat treatment on tomatine content in commercial varieties of green tomatoes. *J. Food Compos. Anal.* **2021**, *96*, 103735. [CrossRef]
22. Motawea, M.H.; Ali, H.A.E.; Elharrif, M.G.; Desoky, A.A.E.; Ibrahimi, A. Evaluation of anti-inflammatory and antioxidant profile of oleuropein in experimentally induced ulcerative colitis. *Int. J. Mol. Cell. Med.* **2020**, *9*, 224–233. [PubMed]
23. Burja, B.; Kuret, T.; Janko, T.; Topalović, D.; Živković, L.; Mrak-Poljšak, K.; Spremo-Potparević, B.; Žigon, P.; Distler, O.; Čučnik, S.; et al. Olive leaf extract attenuates inflammatory activation and DNA damage in human arterial endothelial cells. *Front. Cardiovasc. Med.* **2019**, *6*, 56. [CrossRef] [PubMed]
24. Castejon, M.L.; Rosillo, M.A.; Montoya, T.; Gonzalez-Benjumea, A.; Fernandez-Bolanos, J.M.; Alarcon-de-la-Lastra, C. Oleuropein down-regulated IL-1 beta-induced inflammation and oxidative stress in human synovial fibroblast cell line SW982. *Food Funct.* **2017**, *8*, 1890–1898. [CrossRef]

25. Ryu, S.-J.; Choi, H.-S.; Yoon, K.-Y.; Lee, O.-H.; Kim, K.-J.; Lee, B.-Y. Oleuropein suppresses LPS-induced inflammatory responses in RAW 264.7 cell and zebrafish. *J. Agric. Food Chem.* **2015**, *63*, 2098–2105. [CrossRef] [PubMed]

26. Ahamad, J.; Toufeeq, I.; Khan, M.A.; Ameen, M.S.M.; Anwer, E.T.; Uthirapathy, S.; Mir, S.R.; Ahmad, J. Oleuropein: A natural antioxidant molecule in the treatment of metabolic syndrome. *Phytother. Res.* **2019**, *33*, 3112–3128. [CrossRef] [PubMed]

27. Lucas, R.; Comelles, F.; Alcántara, D.; Maldonado, O.S.; Curcuroze, M.; Parra, J.L.; Morales, J.C. Surface-active properties of lipophilic antioxidants tyrosol and hydroxytyrosol fatty acid esters: A potential explanation for the nonlinear hypothesis of the antioxidant activity in oil-in-water emulsions. *J. Agric. Food Chem.* **2010**, *58*, 8021–8026. [CrossRef]

28. Giovannini, C.; Straface, E.; Modesti, D.; Coni, E.; Cantafora, A.; De Vincenzi, M.; Malorni, W.; Masella, R. Tyrosol, the major olive oil biophenol, protects against oxidized-LDL-induced injury in Caco-2 cells. *J. Nutr.* **1999**, *129*, 1269–1277. [CrossRef]

29. Moreno, J.J. Effect of olive oil minor components on oxidative stress and arachidonic acid mobilization and metabolism by macrophages RAW 264.7. *Free Radic. Biol. Med.* **2003**, *35*, 1073–1081. [CrossRef]

30. Muriana, F.J.G.; la Paz, S.M.-D.; Lucas, R.; Bermudez, B.; Jaramillo, S.; Morales, J.C.; Abia, R.; Lopez, S. Tyrosol and its metabolites as antioxidative and anti-inflammatory molecules in human endothelial cells. *Food Funct.* **2017**, *8*, 2905–2914. [CrossRef]

31. Sundström, C.; Nilsson, K. Establishment and characterization of a human histiocytic lymphoma cell line (U-937). *Int. J. Cancer* **1976**, *17*, 565–577. [CrossRef]

32. Prasad, A.; Sedlářová, M.; Balukova, A.; Rác, M.; Pospíšil, P. Reactive oxygen species as a response to wounding: In vivo imaging in *Arabidopsis thaliana*. *Front. Plant Sci.* **2020**, *10*, 1660. [CrossRef] [PubMed]

33. Golubev, A.; Khrustalev, S.; Butov, A. An in silico investigation into the causes of telomere length heterogeneity and its implications for the Hayflick limit. *J. Theor. Biol.* **2003**, *225*, 153–170. [CrossRef]

34. Gomez, D.E.; Armando, R.G.; Farina, H.G.; Lorenzano Menna, P.; Cerrudo, C.S.; Daniel Ghiringhelli, P.; Alonso, D.F. Telomere structure and telomerase in health and disease (Review). *Int. J. Oncol.* **2012**, *41*, 1561–1569. [CrossRef]

35. Chanput, W.; Mes, J.J.; Wichers, H.J. THP-1 cell line: An in vitro cell model for immune modulation approach. *Int. Immunopharmacol.* **2014**, *23*, 37–45. [CrossRef] [PubMed]

36. Droge, W. Free radicals in the physiological control of cell function. *Physiol. Rev.* **2002**, *82*, 47–95. [CrossRef]

37. Zorov, D.B.; Juhaszova, M.; Sollott, S.J. Mitochondrial reactive oxygen species (ROS) and ROS-induced ROS release. *Physiol. Rev.* **2014**, *94*, 909–950. [CrossRef]

38. Prasad, A.; Manoharan, R.R.; Sedlářová, M.; Pospíšil, P. Free radical-mediated protein radical formation in differentiating monocytes. *Int. J. Mol. Sci.* **2021**, *22*, 9963. [CrossRef]

39. Maeß, M.B.; Wittig, B.; Cignarella, A.; Lorkowski, S. Reduced PMA enhances the responsiveness of transfected THP-1 macrophages to polarizing stimuli. *J. Immunol. Methods* **2014**, *402*, 76–81. [CrossRef]

40. Lund, M.E.; To, J.; O'Brien, B.A.; Donnelly, S. The choice of phorbol 12-myristate 13-acetate differentiation protocol influences the response of THP-1 macrophages to a pro-inflammatory stimulus. *J. Immunol. Methods* **2016**, *430*, 64–70. [CrossRef]

41. STedesco, S.; De Majo, F.; Kim, J.; Trenti, A.; Trevisi, L.; Fadini, G.P.; Bolego, C.; Zandstra, P.W.; Cignarella, A.; Vitiello, L. Convenience versus biological significance: Are PMA-differentiated THP-1 cells a reliable substitute for blood-derived macrophages when studying in vitro polarization? *Front. Pharmacol.* **2018**, *9*, 71. [CrossRef]

42. Chen, J.; Giridhary, K.V.; Zhang, L.; Xu, S.; Wang, Q.J. A protein kinase C/protein kinase D pathway protects LNCaP prostate cancer cells from phorbol ester-induced apoptosis by promoting ERK1/2 and NF-kappa B activities. *Carcinogenesis* **2011**, *32*, 1198–1206. [CrossRef] [PubMed]

43. Garg, R.; Caino, M.C.; Kazanietz, M.G. Regulation of transcriptional networks by PKC isozymes: Identification of c-rel as a key transcription factor for PKC-regulated genes. *PLoS ONE* **2013**, *8*, e67319. [CrossRef] [PubMed]

44. Prasad, A.; Kumar, A.; Suzuki, M.; Kikuchi, H.; Sugai, T.; Kobayashi, M.; Pospíšil, P.; Tada, M.; Kasai, S. Detection of hydrogen peroxide in Photosystem II (PSII) using catalytic amperometric biosensor. *Front. Plant Sci.* **2015**, *6*, 862. [CrossRef] [PubMed]

45. Kikuchi, H.; Prasad, A.; Matsuoka, R.; Aoyagi, S.; Matsue, T.; Kasai, S. Scanning electrochemical microscopy imaging during respiratory burst in human cell. *Front. Physiol.* **2016**, *7*, 25. [CrossRef] [PubMed]

46. Pospíšil, P.; Prasad, A.; Rác, M. Mechanism of the formation of electronically excited species by oxidative metabolic processes: Role of reactive oxygen species. *Biomolecules* **2019**, *9*, 258. [CrossRef]

47. Ayala, A.; Muñoz, M.F.; Argüelles, S. Lipid peroxidation: Production, metabolism, and signaling mechanisms of malondialdehyde and 4-hydroxy-2-nonenal. *Oxidative Med. Cell. Longev.* **2014**, *2014*, 360438. [CrossRef]

48. Hauck, A.K.; Bernlohr, D.A. Oxidative stress and lipotoxicity. *J. Lipid Res.* **2016**, *57*, 1976–1986. [CrossRef]

49. McDonagh, B. Detection of ROS induced proteomic signatures by mass spectrometry. *Front. Physiol.* **2017**, *8*, 470. [CrossRef]

50. Grimsrud, P.A.; Xie, H.; Griffin, T.J.; Bernlohr, D.A. oxidative stress and covalent modification of protein with bioactive aldehydes. *J. Biol. Chem.* **2008**, *283*, 21837–21841. [CrossRef]

51. Tamasi, G.; Pardini, A.; Bonechi, C.; Donati, A.; Pessina, F.; Marcolongo, P.; Gamberucci, A.; Leone, G.; Consumi, M.; Magnani, A.; et al. Characterization of nutraceutical components in tomato pulp, skin and locular gel. *Eur. Food Res. Technol.* **2019**, *245*, 907–918. [CrossRef]

52. Tamasi, G.; Baratto, M.C.; Bonechi, C.; Byelyakova, A.; Pardini, A.; Donati, A.; Leone, G.; Consumi, M.; Lamponi, S.; Magnani, A.; et al. Chemical characterization and antioxidant properties of products and by-products from *Olea europaea* L. *Food Sci. Nutr.* **2019**, *7*, 2907–2920. [CrossRef] [PubMed]

Supplementary data S1

A- PMA
B- PMA + chlorogenic acid
C- PMA + oleuropein
D-PMA + α-tomatine
E-PMA + tyrosol
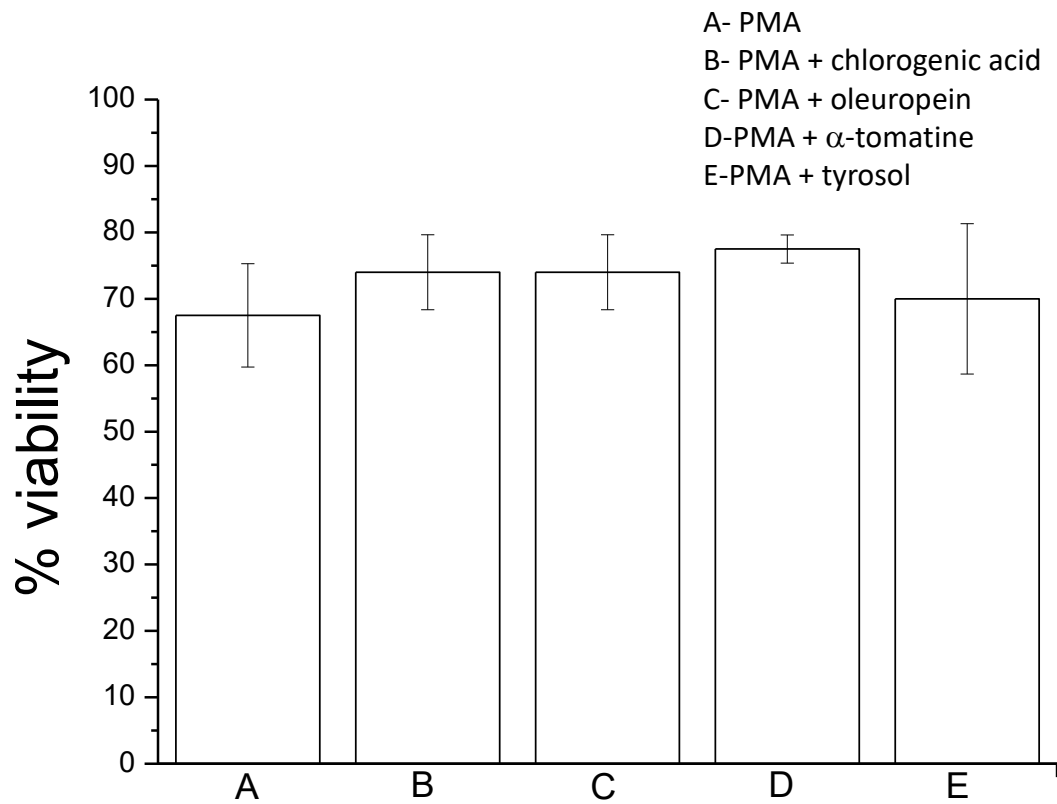
Supplementary data S1: Effect of PMA (250 nM) (A) and in presence of chlorogenic acid (B), oleuropein (C), α-tomatine (D) and tyrosol (E) on viability of U937 cells. The viability was measured in 72h differentiated U-937 celsl with last 24 h of incubation with bioactive compounds. Trypan blue (0.1%) was mixed in the ratio 1:1. The ratio of alive:dead cell was measured using a counting slide (dual chamber for cell counter, Bio-Rad) on an automated cell counter and %viability is plotted.

Supplementary data S2
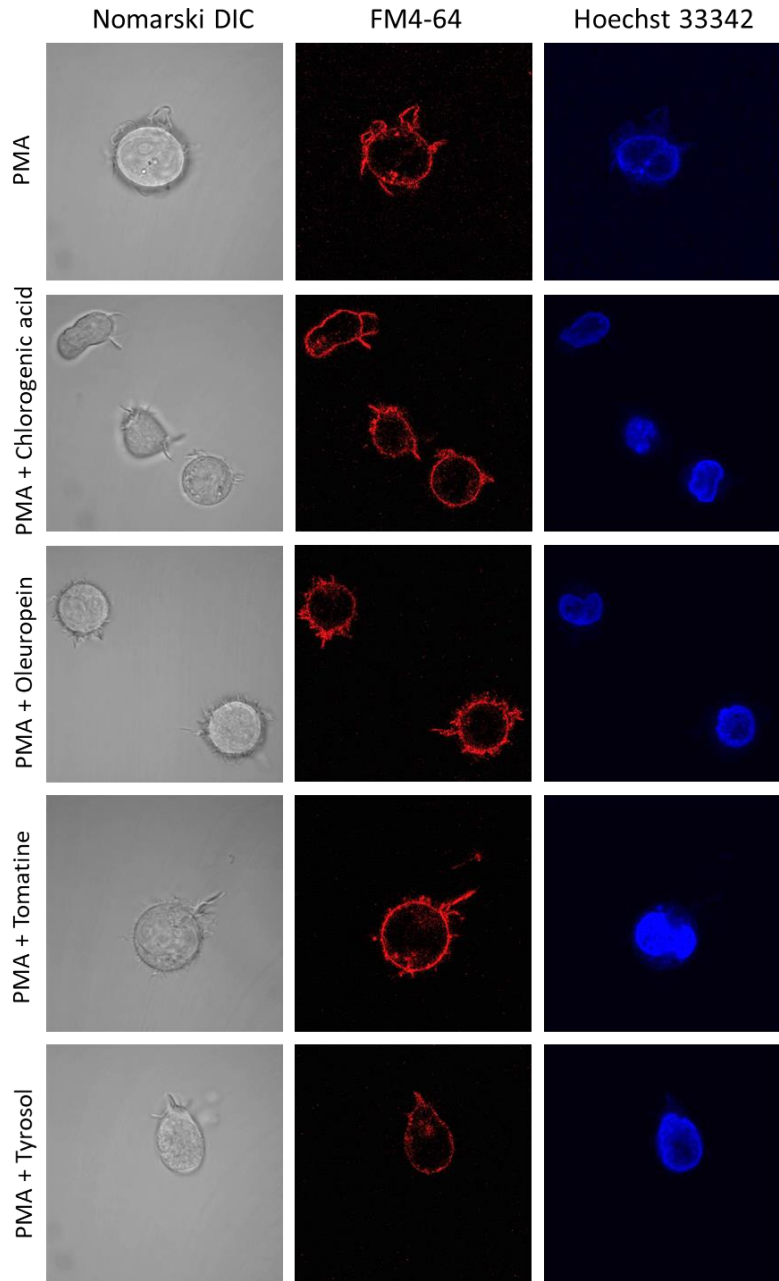
Supplementary data S2: Double staining with Hoechst 33342 and FM4-64 in 48 h differentiated U937 cells and in the presence of either of the bioactive compounds (chlorogenic acid, oleuropein, α-tomatine and tyrosol, 10µM). The staining was done for 5 min and images were taken in different channels (from left to right are Nomarski DIC, FM4-64 and Hoechst 33342).

Article

Imaging and Characterization of Oxidative Protein Modifications in Skin

Ankush Prasad *[ID], Hana Duchová [ID], Renuka Ramalingam Manoharan [ID], Deepak Rathi [ID] and Pavel Pospíšil [ID]

Department of Biophysics, Faculty of Science, Palacký University, Šlechtitelů 27, 783 71 Olomouc, Czech Republic
* Correspondence: ankush.prasad@upol.cz

Abstract: Skin plays an important role in protection, metabolism, thermoregulation, sensation, and excretion whilst being consistently exposed to environmental aggression, including biotic and abiotic stresses. During the generation of oxidative stress in the skin, the epidermal and dermal cells are generally regarded as the most affected regions. The participation of reactive oxygen species (ROS) as a result of environmental fluctuations has been experimentally proven by several researchers and is well known to contribute to ultra-weak photon emission via the oxidation of biomolecules (lipids, proteins, and nucleic acids). More recently, ultra-weak photon emission detection techniques have been introduced to investigate the conditions of oxidative stress in various living systems in in vivo, ex vivo and in vitro studies. Research into two-dimensional photon imaging is drawing growing attention because of its application as a non-invasive tool. We monitored spontaneous and stress-induced ultra-weak photon emission under the exogenous application of a Fenton reagent. The results showed a marked difference in the ultra-weak photon emission. Overall, these results suggest that triplet carbonyl ($^3C=O^*$) and singlet oxygen ($^1O_2$) are the final emitters. Furthermore, the formation of oxidatively modified protein adducts and protein carbonyl formation upon treatment with hydrogen peroxide (H_2O_2) were observed using an immunoblotting assay. The results from this study broaden our understanding of the mechanism of the generation of ROS in skin layers and the formation/contribution of various excited species can be used as tools to determine the physiological state of the organism.

Keywords: porcine skin; protein modification; oxidative radical reaction; protein carbonyls; two-dimensional imaging; ultra-weak photon emission; malondialdehyde; reactive oxygen species

1. Introduction

Numerous crucial bodily processes and functions, such as thermoregulation, metabolism, sensory perception, excretion, hormones, and vitamin synthesis, can be attributed to the largest organ, the skin, either partially or to their full extent [1]. Additionally, the skin represents the primary mechanical obstruction that secures the body against invading pathogens, solar irradiation, fluctuating temperature, dehydration, and various chemical and mechanical aggressions [2–4]. Therefore, it is imperative to study the mechanisms of its multitudinous role to discover novel effective treatments/procedures to maintain/restore its healthy condition. To achieve this, researchers often turn to animal models as a representation of human skin [5,6]. In addition to alleviating ethical and financial burdens, the variety of model systems and tools available makes them an attractive alternative [7–9]. These systems must possess high levels of similarity with human skin in terms of the attribute(s) that are integral to a given research purpose. Pig/porcine skin ranks at the top (particularly in dermatology) due to the myriad anatomical, biochemical, and physiological similarities found in pigs and humans [10]. Its advantage also lies in its widespread accessibility and cost-effectiveness, which can be traced to pigs being the most produced/consumed meat worldwide [11]. Similarities are found starting from the multilayered skin composition,

which can be grouped into three main layers: the epidermis, the dermis, and the hypodermis (also called subcutis) [10,12]. However, no animal model system shares all the features of human skin in its entirety. For our study, porcine skin was selected as an ex vivo model, owning to its comparably higher similarity with human skin in the features essential for our research (such as its morphology and biochemical composition) than the other available models.

Skin is rich in reactive oxygen species (ROS), such as, but not limited to, hydrogen peroxide (H_2O_2) and hydroxyl radical ($HO^\bullet$) [7,13,14]. This is due to their endogenous and exogenous production/stimulation. Constant contact with molecular oxygen (O_2), xenobiotics, solar radiation, oxidative metabolism, pathogens destroying immune cells, physiological and psychological stress are examples that affect the delicate balance of natural oxidants/antioxidants in the cell and, subsequently, the tissue/organ/organism [15,16]. Under regulated conditions, ROS are generally neutralized by a network of non-enzymatic antioxidants, such as glutathione and ascorbic acid or enzymatic antioxidants such as superoxide dismutase (SOD), catalase (CAT), glutathione peroxidase (GPX), glutathione reductase, and thioredoxin reductase (TRX). A key enzyme that detoxifies H_2O_2 is the peroxisomal localized catalase. Enzymatic antioxidants act in a coordinated way to maintain normal redox homeostasis [13,17]. If this condition is not restored through innate enzymatic and non-enzymatic mechanisms/exogenous antioxidants, it leads to a condition called oxidative stress [18,19]. The eustress is attributed to ROS involved in cellular signaling, but the risk comes when oxidative stress prevails, reaches toxic levels, and important biomolecules are negatively affected [18]. Biomolecule oxidation was found to be the cause/factor in the formation/aggravation of several diseases, such as diabetes, psoriasis, Alzheimer's disease, and other diseases related to age [20,21]. Oxidative stress-induced protein modifications are a common feature in several pathologies and are routinely employed as a marker of oxidative processes, along with malondialdehyde (MDA), which is a by-product of lipid peroxidation [22].

This study aims to increase our understanding of ROS-induced oxidative stress in skin. Exogenous oxidant (H_2O_2), with or without transition metal ions, was used to mimic chemical/environmental pollutants. The exogenous use of transition metals enhances the oxidative process drastically; thus, its use in our two-dimensional studies was intended to enhance the subsequent photon emission, described later in the section. Using a non-invasive ultrasensitive charge-coupled device (CCD) camera, a $^1O_2$ scavenger (sodium ascorbate), and the interference filter, we attempted to understand the degree of damage to biomolecules reflected by ultra-weak photon emission. As skin is rich in iron and other transition metals, we believe that the cascade of reactions (mediated by the formation of the $HO^\bullet$) might have played a role in the eventual oxidative damage to lipids and proteins. To further understand the mechanism and possible oxidative consequences, we used protein immunoblotting, where anti-MDA and anti-DNP antibodies were used to observe the protein modification.

2. Results and Discussion

2.1. Spontaneous and Fenton Reagent-Induced Ultra-Weak Photon Emission from Skin

The two-dimensional image of the ultra-weak photon emission was measured spontaneously from the porcine ears and after the topical application of the Fenton reagent in the setup shown and described in detail in Section 3. Variable concentrations of H_2O_2 (0, 2.5 mM, 5 mM, and 10 mM) and $FeSO_4$ were topically applied to the skin biopsies and the corresponding ultra-weak photon emission images were captured (Figure 1). The upper panel (Figure 1A) shows the photographs of the prepared skin biopsies; Figure 1B shows the spontaneous ultra-weak photon emission images to demonstrate any variability in the spontaneous ultra-weak photon emission; Figure 1C shows the dependence of the ultra-weak photon emission with the increasing concentration of Fenton reagent. It is obvious that with the increasing concentration of oxidants, there is a corresponding increase in the intensity of the ultra-weak photon emission. Following the optimization, we further

carried out our study on ex vivo porcine ear, where the treatment condition was limited to 10 mM H_2O_2/250 µM $FeSO_4$ (Figure 2). Figure 2A (left panel) shows an image of the ultra-weak photon emission from an ex vivo porcine ear without any stimulation/induction of oxidative stress. In Figure 2B, the ultra-weak photon emission image was measured following the treatment with the Fenton reagent. Figure 2C shows the photon intensity at the pixels marked on the images by white dotted lines. As apparent from the intensity of the ultra-weak photon emission, the skin not treated with Fenton reagent (control) shows no enhancement, whereas the skin treated with Fenton reagent shows a maximum intensity of ~25 counts/pixel.
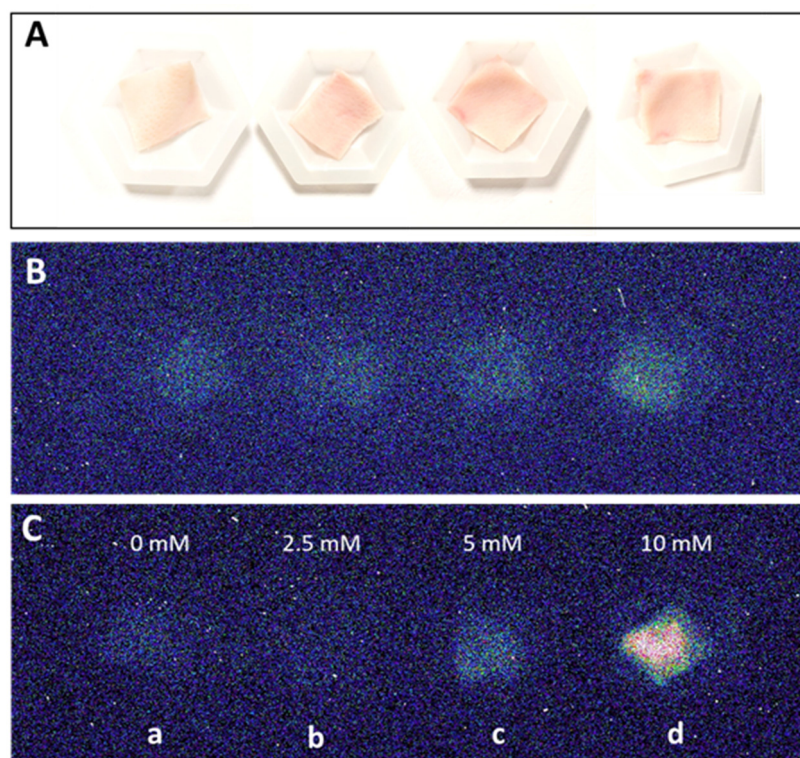
Figure 1. Two-dimensional photon emission imaging using a CCD camera from skin biopsies. Photographs (**A**) and spontaneous two-dimensional ultra-weak photon emission images (**B**). In (**C**), induced photon emission images were captured after topical treatment of skin biopsies with 2.5 mM, 5 mM and 10 mM (**b–d**) H_2O_2/250 µM $FeSO_4$ versus control (**a**). Dark adaptation of 30 min was conducted prior to the exogenous application of $FeSO_4$ and H_2O_2.

Sodium ascorbate (10mM), which is a scavenger of $^1O_2$ [23], was topically applied to the porcine skin 10 min before the application of the Fenton reagent. It is evident that the presence of sodium ascorbate before the application of Fenton reagent noticeably lowered the ultra-weak photon emission (Figure 3). As evident from the intensity of the photon emission, the Fenton reagent-treated porcine skin shows a higher intensity, which was found to be suppressed almost completely in the case of the skin pretreated with sodium ascorbate. It is thus obvious that the involvement of $^1O_2$ dimol photon emission in the overall ultra-weak photon emission can be substantial (Figure 3). The conclusion is based on the fact that in an oxygen-rich environment, the excitation energy from $^3C=O^*$ can be transferred to O_2 via triplet-singlet energy transfer, which can lead to the formation of $^1O_2$. The collision of two $^1O_2$ results in photon emission in the red band of the spectrum (634 and 703 nm), referred to as dimol emission [24].

To confirm the claimed primary sources ($^3C=O^*$) of the photon emission under the induced oxidative stress, we mounted a blue-green interference filter type 644 with a transparency between 340–540 nm in front of the objective lens with the experimental condition, as in Figure 3. It can be seen that if the transparency was limited in the range

of the blue-green region, typically destined for $^3C=O^*$ emission, partial photon emission can still be captured (Figure 4). This indicates that $^3C=O^*$ can be one of the significant contributors of ultra-weak photon emission during oxidative radical reaction in the skin.

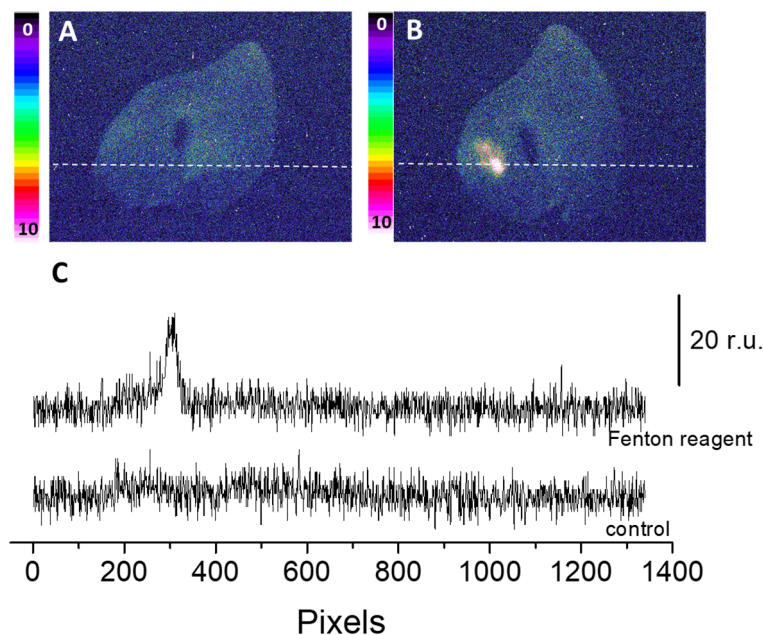**Figure 2.** Spontaneous (**A**) and Fenton reagent-induced two-dimensional image of the ultraweak photon emission (**B**) from a porcine ear. In B, 10 mM H_2O_2/250 μM $FeSO_4$ was topically applied. All other experimental conditions are as described in Figure 1. In (**C**), the Y-axis shows the number of photon counts after 30 min accumulation, whereas the X-axis denotes the pixel of the image.
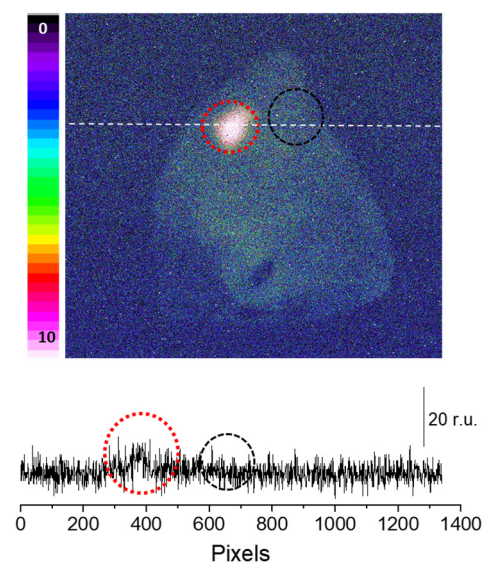
Figure 3. Fenton reagent-induced two-dimensional photon emission imaging from the porcine ear. The ultra-weak photon emission imaging was performed in a porcine ear treated with 10 mM H_2O_2/250 μM $FeSO_4$ in the absence (red circle) and presence (black circle) of sodium ascorbate (10 mM). Samples were treated with sodium ascorbate 10 min before to the topical application of Fenton reagent. The Y-axis in the lower panel indicates the number of photon counts after 30 min of accumulation, whereas the X-axis shows the pixel of the image.

2.2. Protein Modification under Generated ROS

Reactive oxygen species create oxidative radical reactions in cells due to several cellular components, for example, DNA, protein, lipids, and carbohydrates undergo mod-

ifications [25]. In the present study, the proteins undergoing modification by ROS were characterized using an immunoblotting technique. We limited the stress induction to H_2O_2 treatment alone as such high oxidative damage is not necessarily required to study protein modification using western blotting; the level of endogenous transition metal ions is believed to be sufficient to mediate the process. On the contrary, to image photon emission as a result of oxidative damage, we need a moderate to high level of oxidative damage and, thus, metal ions were additionally supplemented.
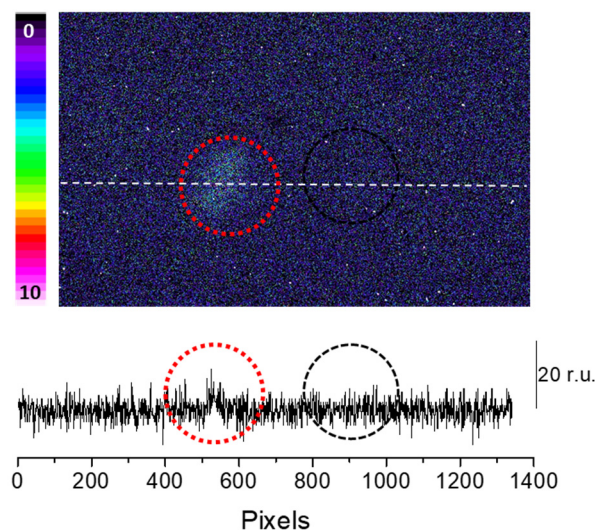
Figure 4. Fenton reagent-induced two-dimensional ultra-weak photon emission imaging from porcine ear measured after the topical application of Fenton reagent (10 mM H_2O_2 / 250 μM $FeSO_4$) in the presence of interference filter type 644 (340–540 nm). The circle indicates the untreated (red) and treated (black) areas of the porcine skin with sodium ascorbate. Other experimental conditions as described in Figure 3. The Y-axis in the lower panel reflects the number of photon counts accumulated after 30 min, whereas the X-axis denotes the pixel of the image.

To study the protein modification (protein carboxylation and protein carbonyl formation), we used anti-MDA and anti-DNP, respectively. For characterization, skin biopsies treated with H_2O_2 (10 mM) and control non-treated samples were separated using SDS PAGE and the samples were loaded in duplicate. Anti-MDA antibodies bind to MDA-modified proteins, thereby enabling the detection of MDA-protein adducts. Malondialdehyde reacts specifically with amino acid residues such as Lys, Arg, His and Cys. With reference to the anti-MDA blot (Figure 5A), MDA-protein adduct formations were observed around 15 kDa, 45 kDa, 50 kDa, 65 kDa, 130 kDa and 250 kDa. However, the band density of 65 kDa, 130 kDa and 250 kDa proteins were found to be enhanced in comparison to the control untreated groups. Differences in the levels were represented as densitogram in separate panels for each protein (Figure 5B) and the mechanism involved is presented in Figure 6.

To monitor the protein carbonyl formation, derivatization was conducted, as mentioned in Section 3.4. The western blot analysis of the control and H_2O_2-treated skin biopsies displayed protein carbonyl levels, as measured by the anti-DNP antibodies (Figure 6A). A distinct band at 130 kDa was observed in both groups with varied patterns. It is clear that the carbonylated proteins isolated from the control groups are significantly less formed than the treatment groups. Figures 7 and 8 (created with elements from BioRender.com) show the steps involved in the formation of the MDA-protein adduct and protein carbonyl formation, respectively. Differences between the control and treatment groups are presented as a separate densitogram (Figure 6B). Additional studies targeting the identification and characterization of selected proteins from both anti-MDA and anti-DNP blots are under study.
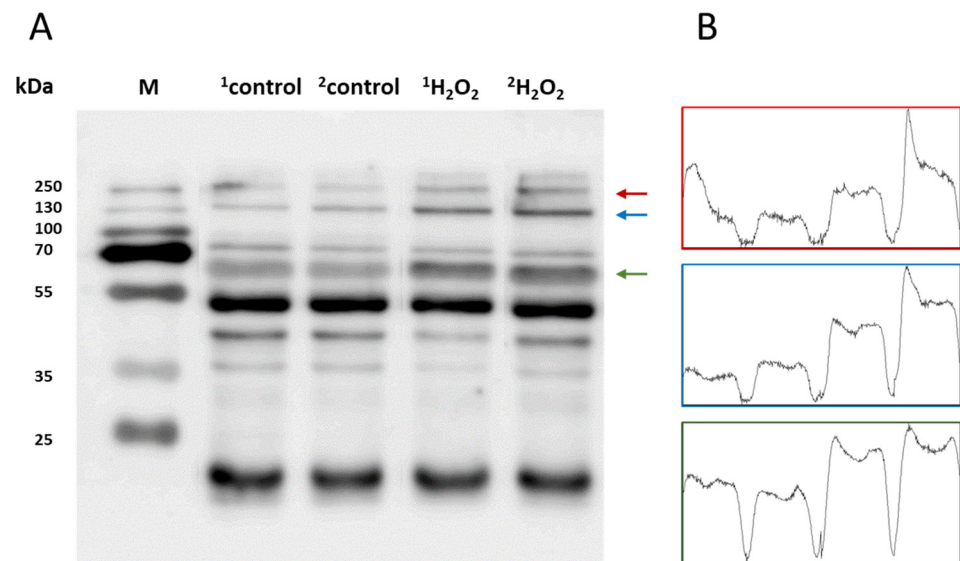
Figure 5. (**A**) Identification of MDA-protein adducts in homogenates of porcine skin cells. Lanes 1–2 show control samples, while lanes 3–4 are skin samples treated with H_2O_2 (10 mM) (**B**). Quantification of protein bands (by densitogram analysis) from an anti-MDA blot is presented, and proteins of interest are indicated by arrows.
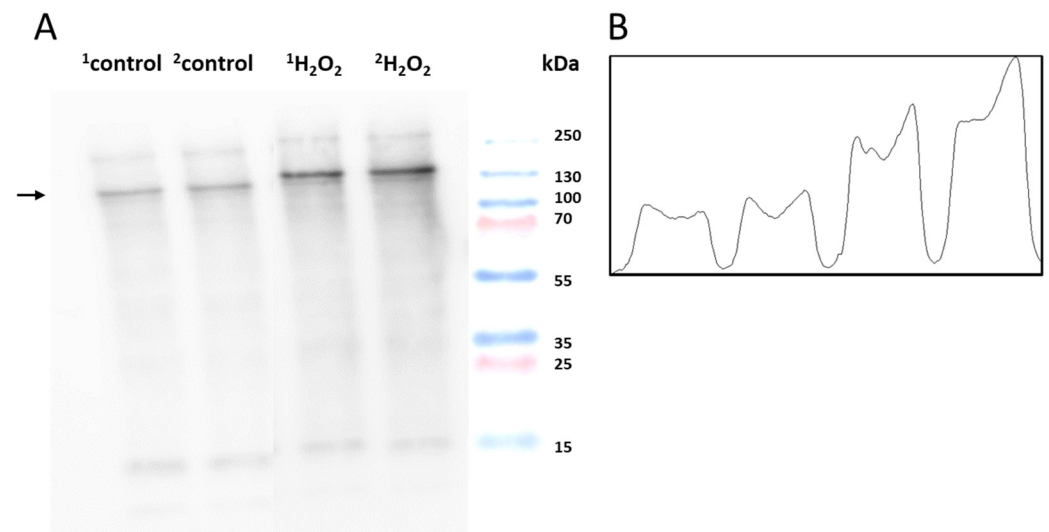

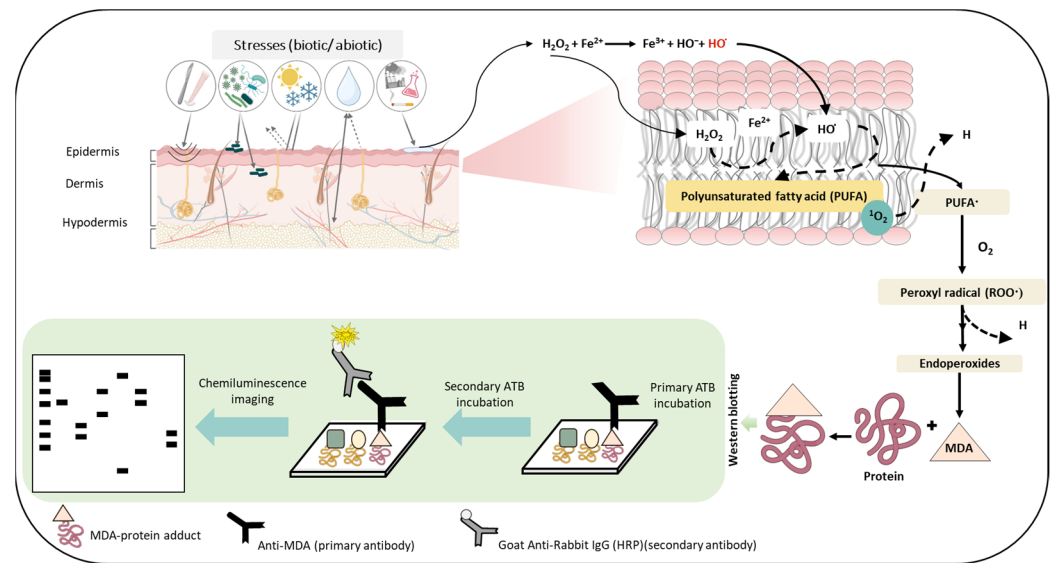**Figure 6.** (**A**) Identification of DNP-carbonyl derivatives in homogenates of porcine skin cells. Lane 1–2 shows control sample, while lanes 3–4 are skin samples treated with H_2O_2 (10 mM) (**B**) Quantification of protein bands (by densitogram analysis) from an anti-DNP blot is presented, and the selected proteins of interest are indicated by arrows.

Figure 7. Schematic representation depicting the steps involved in the formation of the MDA-protein adduct as the consequence of ROS generation and successive oxidative radical reactions. The figures show stress factors (biotic and abiotic) that can lead to the formation of ROS which eventually can lead to lipid peroxidation and subsequently to the generation of the MDA-protein adduct. The lower panel depicts the use of immunoblotting techniques to detect MDA-protein formation.
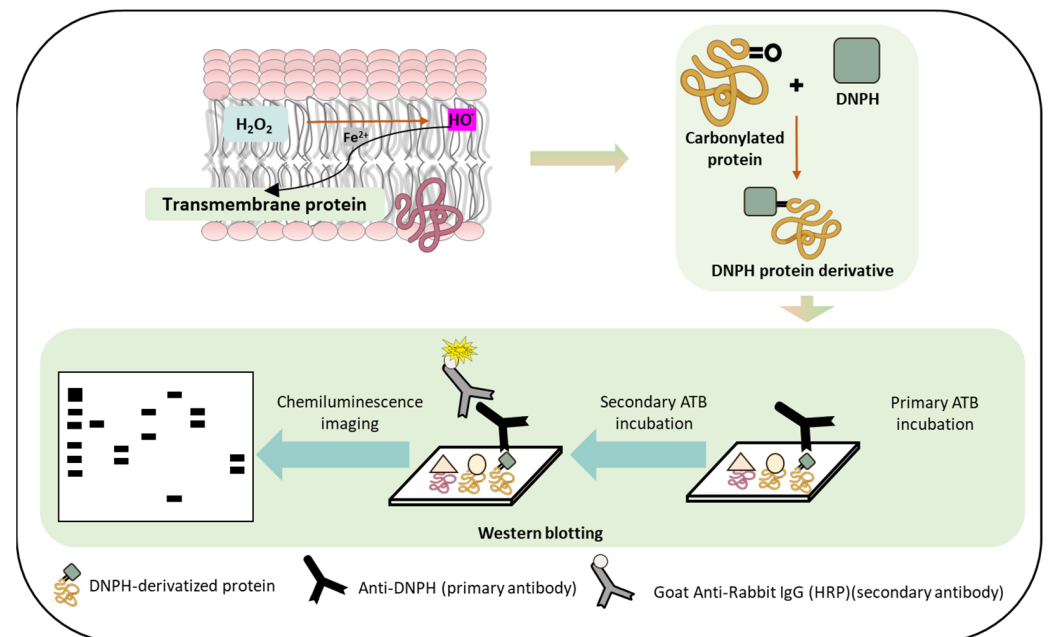
Figure 8. Schematic representation depicting the pathways of protein carbonyl formation which can occur as a result of protein oxidation. The lower panel depicts the use of immunoblotting techniques to detect protein carbonyl formation.

3. Materials and Methods

3.1. Porcine Skin

Porcine ears were obtained from a local slaughterhouse. They were transported at a low temperature (on ice) within the first 30 min. Whole ear/skin biopsies for two-dimensional imaging and immunoblotting were prepared according to the procedure described by Chiu and Burd (2005) [26], with minor modifications. Skin samples, collected each day, were used for each set of measurements.

3.2. Reagents and Antibodies

Fenton reagent preparation was conducted using H_2O_2 (Sigma-Aldrich Chemie GmbH, Mannheim, Germany) and ferrous sulfate ($FeSO_4.7H_2O$) (BDH Laboratory Supplies, Poole, UK). A variable concentration of H_2O_2 (2.5 mM, 5 mM, 10 mM) was used with a fixed concentration of iron sulphate ($FeSO_4$) (250 µM) to chemically generate $HO^\bullet$. The procedure for topical application and its duration are specified in the figure legends, as applicable. Phosphatase and protease inhibitors were purchased from Roche (Mannheim, Germany). Rabbit polyclonal anti-MDA antibody was purchased from Abcam [anti-MDA antibody (ab27642)] (Cambridge, UK) and polyclonal goat anti-rabbit IgG conjugated with horseradish peroxidase (HRP) from Bio-Rad (Hercules, CA, USA). Rabbit polyclonal Dinitrophenyl-KLH antibody (anti-DNP) were procured from ThermoFisher scientific (Waltham, MA, USA).

3.3. Experimental Conditions and Setup for Two-Dimensional Imaging of Ultra-Weak Photon Emission

A unique design of dark rooms is a prerequisite to avoid any interference by the absence of a photon. In the current study, all of the ultra-weak photon imaging measurements were conducted in an experimental dark room. Further details on the adopted methodology can be found in Prasad and Pospíšil (2013) [27]. The dark room, as well as the measurement setup, is shown in Figure 9. All of the experiments were carried out in three biological replicates, and the representative images have been presented. To study the spectral distribution of the ultra-weak photon emission in the oxidation reactions using Fenton reagents, filter type 644 (Schott and Gen, Jena, Germany), which is a blue-green interference filter with a transmission in the range 340–540 nm, was used and mounted in front of the objective lens of the CCD camera (Figure 1) [27].
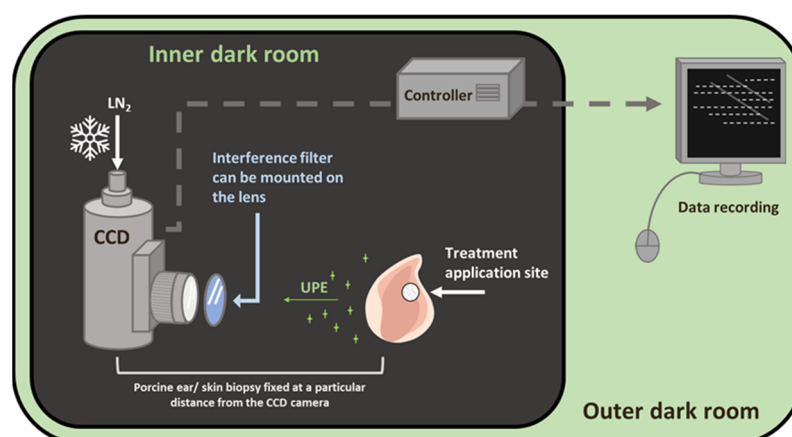

Figure 9. Schematic diagram of the experimental setup for two-dimensional photon emission imaging using a CCD camera. The diagram shows the inner dark room (gray) and the outer control room (green). The filter position for the spectral measurement was positioned in front of the objective lens, as shown.

Two-dimensional photon emission imaging was measured in porcine ear/skin biopsies utilizing a sensitive CCD camera. The skin samples were dark-adapted for 30 min to eradicate any interference by delayed luminescence and treated afterward. The other experimental conditions are as per the procedure described in the listed reference [27]. The VersArray 1300B CCD camera (Princeton Instruments, Trenton, NJ, USA) with a spectral sensitivity of 350–1000 nm and ~90% quantum efficiency was used under the following parameters: scan rate, 100 kHz; gain, 2; accumulation time, 30 min (porcine ear/skin biopsies). The CCD camera was cooled to $-108\ °C$ using a liquid nitrogen cooling system, which helps to reduce the dark current. Before each measurement, the data correction was made by subtracting the background noise from the experimental dataset.

3.4. Protein Immunoblotting

Skin biopsies were prepared through initial washing with physiological solution (0.9% NaCl). First, 0.5 g of the skin biopsies were subjected to the desired treatment (control or Fenton reagent applied topically for 30 min each), followed by rinsing with distilled water. Subsequently, the samples were snap-frozen in liquid N_2. The samples were then homogenized with radioimmunoprecipitation assay (RIPA) buffer (150 mM NaCl, 50 mM Tris (pH 8.0), 0.5% sodium deoxycholate, 0.1% SDS, and 1% NP-40) comprising 1% (*v/v*) protease and phosphatase inhibitor (*v/v*) (three times, 1 min each), followed by sequential centrifugations at 8000 rpm (30 min, 1 time) and 14,000 rpm (45 min, 2 times). The supernatant was collected and quantified with a Pierce BCA protein estimation kit (Thermo Fisher Scientific, Paisley, UK). The detailed sample preparation procedure is presented in Figure 10. Protein samples for Western blotting were prepared with SDS Laemmli sample buffer. The prepared samples were then subjected to electrophoresis and immunoblotting analysis using anti-MDA antibody. For immunoblotting, 2 biological replicates were performed for each measurement.
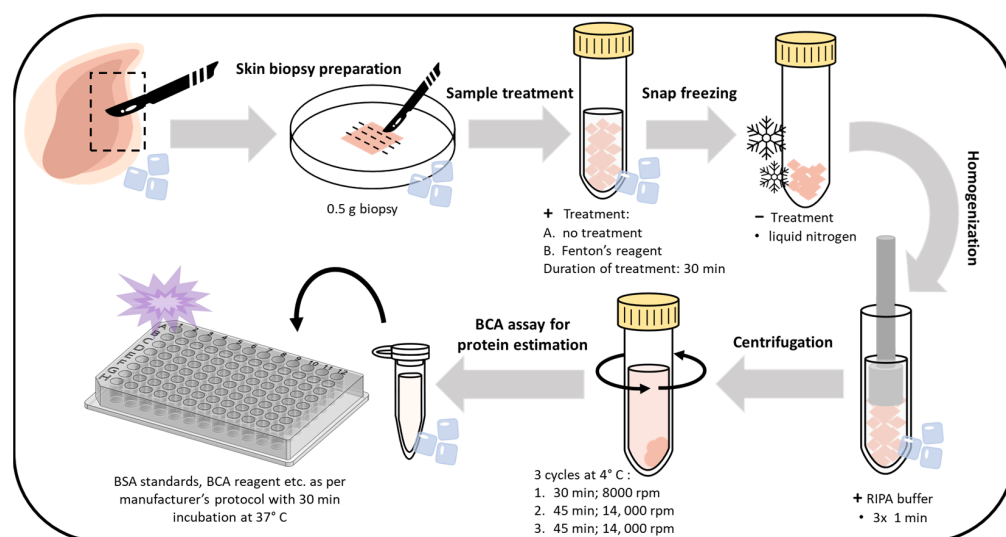
Figure 10. Steps showing the workflow and optimized protocol for whole-skin tissue lysate preparation, isolation, and the BCA assay for protein estimation.

To detect protein carbonyl formation, the collected protein fractions were subjected to derivatization. Carbonyl groups present in the protein side chains were derivatized with 2,4 dinitrophenylhydrazine (DNPH), leading to the formation of stable 2,4 dinitrophenyl-hydrazone (DNP) derivative, which involves the addition of an equal volume of protein and 12% SDS (final concentration at 6%) and subsequent addition of 1X DNPH solution (50 mM solution in 50% sulphuric acid). The mixture was incubated at RT for 30 min and the reactions were neutralized with 2 M Tris base and 30% glycerol ($0.75 \times$ *v/v* of DNPH solution). The resulting protein fractions were centrifuged at 14,000 rpm for 10 min and the supernatants were loaded onto SDS gels for immunoblotting with an anti-DNP antibody.

Whole cell homogenates (10 µg/lane), processed on 10% SDS gel, were then transferred to blotting membranes (nitrocellulose) using a Trans-Blot Turbo transfer system (Bio-Rad, Hercules, CA, USA). The membranes were blocked (BSA in phosphate buffered saline, pH 7.4, containing 0.1% Tween 20) overnight at 4 °C. The blocked membranes were probed for 2 h with an anti-MDA antibody at RT. After 4 cycles of washing with PBST and incubation for 1 h at room temperature with HRP-conjugated anti-rabbit secondary antibody (dilution 1:10,000) and subsequent washing [PBST, $5\times$ (5 min each)], the immunocomplexes were visualized utilizing Immobilon Western Chemiluminescent HRP Substrate (Sigma Aldrich, GmbH, Mannheim, Germany) and imaged using an Amersham 600 imager (GE Healthcare, Amersham, UK). Densitometry analysis of the blots obtained

was generated using Image J 1.53t [public domain software (Bethesda, MD, USA) provided by the National Institute of Mental Health, United States].

4. Conclusions

The skin is the primary interface between the body and environmental aggression and excessive production of reactive species, including ROS, and reactive nitrogen species have been known to form in skin tissues. Oxidative stress and its resulting oxidation products have been reported to be the main cause of ageing. Due to the limitation associated with the use of human skin for research purposes, porcine skin has been used as a model in the present study, with H_2O_2 as an exogenous oxidant. The two-dimensional spatiotemporal images and their spectral analysis confirmed the participation of triplet excited carbonyls and singlet oxygen dimol emission as substantial contributors resulting from oxidative radical reactions in the skin. The resultant oxidatively modified protein adducts and the differences in the band density of the selected proteins in the non-treated and H_2O_2 treated skin tissues were confirmed by blotting analysis. As oxidative stress remains a key factor in distinguishing physiological and pathological conditions, the present study helps to identify the specific protein targets involved in the process of oxidative damage in the skin. In addition, spatiotemporal imaging with a CCD camera, also demonstrated by Abdlaty and co-workers [4], is presented as a powerful tool for non-invasive imaging that has the potential to pave the way for its widespread usage in research and/or clinical trials.

Abbreviations

ROS, reactive oxygen species; UPE, ultra-weak photon emission; RIPA, radio immunoprecipitation assay buffer; DNPH, dinitrophenylhydrazine; MDA, malondialdehyde.

References

1. Zeng, R.J.; Lin, C.Q.; Lin, Z.H.; Chen, H.; Lu, W.Y.; Lin, C.M.; Li, H.H. Approaches to cutaneous wound healing: Basics and future directions. *Cell Tissue Res.* **2018**, *374*, 217–232. [CrossRef]
2. Elias, P.M. The skin barrier as an innate immune element. *Semin. Immunopathol.* **2007**, *29*, 3–14. [CrossRef] [PubMed]
3. Park, S. Biochemical, structural and physical changes in aging human skin, and their relationship. *Biogerontology* **2022**, *23*, 275–288. [CrossRef]
4. Abdlaty, R.; Hayward, J.; Farrell, T.; Fang, Q.Y. Skin erythema and pigmentation: A review of optical assessment techniques. *Photodiagn. Photodyn. Ther.* **2021**, *33*, 102127. [CrossRef] [PubMed]
5. Kong, R.; Bhargava, R. Characterization of porcine skin as a model for human skin studies using infrared spectroscopic imaging. *Analyst* **2011**, *136*, 2359–2366. [CrossRef]

6.   Moniz, T.; Lima, S.C.A.; Reis, S. Human skin models: From healthy to disease-mimetic systems; characteristics and applications. *Br. J. Pharmacol.* **2020**, *177*, 4314–4329. [CrossRef]

7.   Prasad, A.; Balukova, A.; Pospíšil, P. Triplet Excited Carbonyls and Singlet Oxygen Formation During Oxidative Radical Reaction in Skin. *Front. Physiol.* **2018**, *9*, 1109. [CrossRef] [PubMed]

8.   Avon, S.L.; Wood, R.E. Porcine skin as an in-vivo model for ageing of human bite marks. *J. Forensic Odontostomatol.* **2005**, *23*, 30–39.

9.   Haller, H.L.; Blome-Eberwein, S.E.; Branski, L.K.; Carson, J.S.; Crombie, R.E.; Hickerson, W.L.; Kamolz, L.P.; King, B.T.; Nischwitz, S.P.; Popp, D.; et al. Porcine Xenograft and Epidermal Fully Synthetic Skin Substitutes in the Treatment of Partial-Thickness Burns: A Literature Review. *Medicina* **2021**, *57*, 432. [CrossRef]

10.   In, M.K.; Richardson, K.C.; Loewa, A.; Hedtrich, S.; Kaessmeyer, S.; Plendl, J. Histological and functional comparisons of four anatomical regions of porcine skin with human abdominal skin. *Anat. Histol. Embryol.* **2019**, *48*, 207–217. [CrossRef]

11.   Clark, M.; Tilman, D. Comparative analysis of environmental impacts of agricultural production systems, agricultural input efficiency, and food choice. *Environ. Res. Lett.* **2017**, *12*, 064016. [CrossRef]

12.   Debeer, S.; Le Luduec, J.B.; Kaiserlian, D.; Laurent, P.; Nicolas, J.F.; Dubois, B.; Kanitakis, J. Comparative histology and immunohistochemistry of porcine versus human skin. *Eur. J. Dermatol.* **2013**, *23*, 456–466. [CrossRef] [PubMed]

13.   Chen, J.J.; Liu, Y.; Zhao, Z.; Qiu, J. Oxidative stress in the skin: Impact and related protection. *Int. J. Cosmet. Sci.* **2021**, *43*, 495–509. [CrossRef] [PubMed]

14.   Tsuchida, K.; Kobayashi, M. Oxidative stress in human facial skin observed by ultraweak photon emission imaging and its correlation with biophysical properties of skin. *Sci. Rep.* **2020**, *10*, 9626. [CrossRef] [PubMed]

15.   Rinnerthaler, M.; Bischof, J.; Streubel, M.K.; Trost, A.; Richter, K. Oxidative stress in aging human skin. *Biomolecules* **2015**, *5*, 545–589. [CrossRef] [PubMed]

16.   Rinnerthaler, M.; Streubel, M.K.; Bischof, J.; Richter, K. Skin aging, gene expression and calcium. *Exp. Gerontol.* **2015**, *68*, 59–65. [CrossRef] [PubMed]

17.   Papaccio, F.; D'Arino, A.; Caputo, S.; Bellei, B. Focus on the Contribution of Oxidative Stress in Skin Aging. *Antioxidants* **2022**, *11*, 1121. [CrossRef] [PubMed]

18.   Gu, Y.P.; Han, J.X.; Jiang, C.P.; Zhang, Y. Biomarkers, oxidative stress and autophagy in skin aging. *Ageing Res. Rev.* **2020**, *59*, 101036. [CrossRef]

19.   Sies, H. On the history of oxidative stress: Concept and some aspects of current development. *Curr. Opin. Toxicol.* **2018**, *7*, 122–126. [CrossRef]

20.   Sharifi-Rad, M.; Kumar, N.V.A.; Zucca, P.; Varoni, E.M.; Dini, L.; Panzarini, E.; Rajkovic, J.; Fokou, P.V.T.; Azzini, E.; Peluso, I.; et al. Lifestyle, Oxidative Stress, and Antioxidants: Back and Forth in the Pathophysiology of Chronic Diseases. *Front. Physiol.* **2020**, *11*, 694. [CrossRef]

21.   Borgia, F.; Li Pomi, F.; Vaccaro, M.; Alessandrello, C.; Papa, V.; Gangemi, S. Oxidative Stress and Phototherapy in Atopic Dermatitis: Mechanisms, Role, and Future Perspectives. *Biomolecules* **2022**, *12*, 1904. [CrossRef] [PubMed]

22.   Mohideen, K.; Sudhakar, U.; Balakrishnan, T.; Almasri, M.A.; Al-Ahmari, M.M.; Al Dira, H.S.; Suhluli, M.; Dubey, A.; Mujoo, S.; Khurshid, Z.; et al. Malondialdehyde, an Oxidative Stress Marker in Oral Squamous Cell Carcinoma—A Systematic Review and Meta-Analysis. *Curr. Issues Mol. Biol.* **2021**, *43*, 1019–1035. [CrossRef] [PubMed]

23.   Yadav, D.K.; Prasad, A.; Kruk, J.; Pospíšil, P. Evidence for the involvement of loosely bound plastosemiquinones in superoxide anion radical production in photosystem II. *PLoS ONE* **2014**, *9*, e115466. [CrossRef]

24.   Pospíšil, P.; Prasad, A.; Rác, M. Mechanism of the Formation of Electronically Excited Species by Oxidative Metabolic Processes: Role of Reactive Oxygen Species. *Biomolecules* **2019**, *9*, 258. [CrossRef] [PubMed]

25.   Birben, E.; Sahiner, U.M.; Sackesen, C.; Erzurum, S.; Kalayci, O. Oxidative Stress and Antioxidant Defense. *World Allergy Organ. J.* **2012**, *5*, 9–19. [CrossRef] [PubMed]

26.   Chiu, T.; Burd, A. "Xenograft" dressing in the treatment of burns. *Clin. Derm.* **2005**, *23*, 419–423. [CrossRef] [PubMed]

27.   Prasad, A.; Pospíšil, P. Towards the two-dimensional imaging of spontaneous ultra-weak photon emission from microbial, plant and animal cells. *Sci. Rep.* **2013**, *3*, 1211. [CrossRef]

Supplementary data 1

Anti-MDA blot: Porcine samples

M   C1   C2   C3   H1   H2   H3
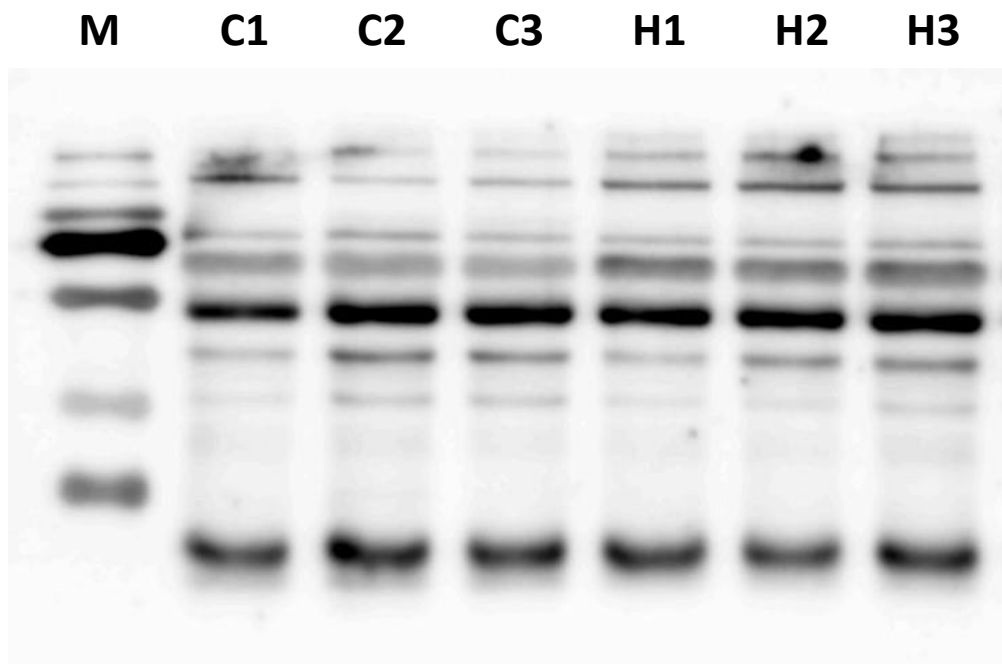
C1-C3: Control samples
H1-H3: H$_2$O$_2$ treated samples

Supplementary data 2

Anti-DNPH blot: Porcine samples

C1-C3: Control samples

H1-H3: H_2O_2 treated samples